AD610615

Best Available Copy

Structural Integrity Department / Research Division

SOLID PROPELLANT STRUCTURAL INTEGRITY INVESTIGATIONS:

DYNAMIC RESPONSE AND FAILURE MECHANISMS

QUARTERLY PROGRESS REPORT NO. 2

TECHNICAL DOCUMENTARY REPORT NO. AFRPL-TR-65-20

COPY 2 OF 3
HARD COPY $. 3
MICROFICHE $. 0.

15 JANUARY 1965

AIR FORCE ROCKET PROPULSION LABORATORY
RESEARCH AND TECHNOLOGY DIVISION
AIR FORCE SYSTEMS COMMAND
EDWARDS, CALIFORNIA

AIR FORCE PROGRAM STRUCTURE NO. 750G
PROJECT NO. 3059

DDC
FEB 8 1965
TISIA E

(Prepared under Contract No. AF 04(611)-9953 by Lockheed Propulsion Company, Redlands, California)

Lockheed Propulsion Company

ARCHIVE COPY 20040702051

SOLID PROPELLANT STRUCTURAL INTEGRITY INVESTIGATIONS: DYNAMIC RESPONSE AND FAILURE MECHANISMS

QUARTERLY PROGRESS REPORT NO. 2

TECHNICAL DOCUMENTARY REPORT NO. AFRPL-TR-65-20

15 January 1965

Contract No. AF 04(611)-9953
Air Force Program Structure No. 750G
Project No. 3059

Prepared for

AIR FORCE ROCKET PROPULSION LABORATORY
RESEARCH AND TECHNOLOGY DIVISION
AIR FORCE SYSTEMS COMMAND
EDWARDS, CALIFORNIA

Prepared by:

D.E. Cantey
Senior Physicist

Approved by:

J. W. Jones, Manager
Structural Integrity

Approved by:

H. Leeming, Supervisor
Structural Integrity Research

J.E. Fitzgerald, Director
Research and Engineering

LOCKHEED PROPULSION COMPANY
P. O. BOX 111
REDLANDS, CALIFORNIA

FOREWORD

This second Technical Documentary Report presents a technical discussion and review of program activity and progress during the period 16 September through 15 December 1964.

(This abstract is unclassified)

ABSTRACT

The results of an investigation of viscoelastic and failure properties of highly filled PbAA and PBAN propellants as a function of solids loading are reported. Failure surface study results are reported, and the results of a limited study of the relationship between crack propagation velocity and propellant physical characteristics are discussed. Propellant dynamic shear and bulk properties were investigated with small deformation piezoelectric devices. An experimental investigation of propellant thermomechanical response to sustained cyclic inertial loading was completed, and the results in agreement with theory are presented. Also discussed are experimental investigations of transient thermoviscoelastic response of propellant under constant cyclic strain amplitude and inertial loading.

TABLE OF CONTENTS

Section		Page
1.	INTRODUCTION AND SUMMARY	1-1
2.	PROPELLANT FORMULATION STUDY -- HIGH SOLIDS LOADING	2-1
	2.1 INTRODUCTION	2-1
	2.2 TEST PLAN	2-2
	2.2.1 Uniaxial Tension	2-4
	2.2.2 Strip Biaxial	2-4
	2.2.3 Diametral Compression	2-4
	2.2.4 Double-Lap Shear	2-5
	2.3 FAILURE PROPERTIES	2-5
	2.4 VISCOELASTIC CHARACTERIZATION AND INVESTIGATION OF NONLINEAR BEHAVIOR	2-17
3.	FRACTURE MECHANICS	3-1
	3.1 GENERAL	3-1
	3.2 FAILURE SURFACE STUDIES	3-1
	3.2.1 Test Analysis	3-2
	3.2.2 Experimental Results	3-6
	3.2.3 Discussion	3-9
	3.3 FRACTURE PROPAGATION STUDIES	3-12
	3.3.1 Analysis	3-12
	3.3.2 Experimental Results	3-15
	3.3.3 Discussion	3-17
4.	DYNAMIC PROPERTIES	4-1
	4.1 INTRODUCTION	4-1

TABLE OF CONTENTS (Continued)

Section		Page
4.2	DYNAMIC VISCOELASTIC CHARACTERIZATION	4-2
4.2.1	Dynamic Shear Modulus	4-2
4.2.2	Dynamic Bulk Modulus	4-5
4.3	LARGE STRAIN DYNAMIC PROPERTIES AND VISCOELASTIC HEATING EFFECTS	4-8
4.3.1	Experimental Techniques	4-8
4.3.2	Dynamic Inertial Loading Tests	4-12
4.3.3	Transient Thermoviscoelastic Response for Constant Cyclic Strain Amplitude and Inertial Loading	4-19
5.	SUBCONTRACT EFFORT	5-1
5.1	PURDUE UNIVERSITY SUBCONTRACT	5-1
5.1.1	Nonlinear Viscoelastic Behavior of Highly Filled Propellants	5-1
5.1.2	Thermomechanical Response Studies of Solid Propellants Subjected to Cyclic and Random Loading	5-2
5.2	UNIVERSITY OF WASHINGTON	5-3
6.	FUTURE PROGRAM	6-1
7	REFERENCES	7-1

LIST OF ILLUSTRATIONS

Figure		Page
2-1	Biaxial Strip Failure Stress and Strain at ICRPG (1963) Failure Point versus Temperature, PBAN, 84% Solids Loading, Bioxidizer	2-9
2-2	Biaxial Strip Failure Stress and Strain at ICRPG (1963) Failure Point versus Temperature, PBAN, 88% Solids Loading, Bioxidizer	2-10
2-3	Biaxial Strip Failure Stress and Strain at ICRPG (1963) Failure Point versus Temperature, Bioxidizer, Uncatalyzed	2-12
2-4	Biaxial Strip Failure Stress and Strain at ICRPG (1963) Failure Point versus Temperature, PBAN, Uncatalyzed	2-13
2-5	Biaxial Strip Failure Stress and Strain at ICRPG (1963) Failure Point versus Temperature, PBAA, Uncatalyzed	2-14
2-6	Biaxial Strip Failure Stress and Strain at ICRPG (1963) Failure Point versus Temperature, PBAA, 88% Loading	2-15
2-7	Biaxial Strip Failure Stress and Strain at ICRPG (1963) Failure Point versus Temperature, PBAN, 88% Loading	2-16
3-1	Test Specimens	3-4
3-2	Dependence of Failure Stress on Stress-State and Solids Loading	3-7
3-3	Dependence of Failure Stresses on Stress-State	3-8
3-4	Failure Surface for PBAN Propellant	3-11
3-5	Stress at Rupture versus Reduced Time at 70°F, LPC-543B Propellant, Batch 4404	3-14
3-6	Master Stress Relaxation Modulus and Shift Factor, Propellant LPC-543B, Batch 4404	3-16
3-7	Crack Extension versus Time	3-18
3-8	Crack Extension versus Reduced Time	3-19
4-1	Dynamic Shear Modulus versus Temperature, PBAA Propellant and Cured Binder, 84% Total Solids Loading	4-3

LIST OF ILLUSTRATIONS (Continued)

Figure		Page
4-2	Dynamic Shear Modulus versus Temperature, PBAN Propellant and Cured Binder, 84% Total Solids Loading	4-4
4-3	Calibration Curve Dynamic Bulk Modulus Apparatus	4-7
4-4	Schematic of Constant Shear-Strain Amplitude Test Device	4-9
4-5	Schematic of Inertial Test Device	4-10
4-6	Vibration Test Apparatus	4-11
4-7	Experimental Displacement Amplitude Ratio, PBAA Propellant, Batch 2916	4-14
4-8	Experimental Steady-State Temperature at Insulated Surface, PBAA Propellant, Batch 2916	4-15
4-9	Experimental Displacement Phase Relationship, PBAA Propellant, Batch 2916	4-16
4-10	Steady-State Displacement Amplitude Ratio for n = 0.30	4-17
4-11	Steady-State Reduced Temperature at Insulated Surface for n = 0.30	4-18
4-12	Propellant Properties versus Vibration History, Measured at 80 RPM and Room Ambient Temperature (Approximately 72°F)	4-21
4-13	Propellant Properties versus Vibration History, Measured at 80 RPM and Room Ambient Temperature (Approximately 72°F)	4-22
4-14	Thermomechanical Response, Constant Strain Amplitude Excitation, Adiabatic Boundary Conditions, PBAA Propellant	4-23
4-15	Thermomechanical Response, Inertial Loading, Adiabatic Boundary Conditions, PBAA Propellant	4-24
4-16	Thermomechanical Response, Constant Strain Amplitude Excitation, Isothermal Boundary Conditions, PBAA Propellant	4-25
4-17	Thermomechanical Response, Inertial Loading, Isothermal Boundary Conditions, PBAA Propellant	4-26

LIST OF TABLES

Table		Page
2-1	PROPELLANT FORMULATION TEST PLAN	2-3
2-2	UNIAXIAL FAILURE STRESS AND STRAIN AT ICRPG (1963) FAILURE POINT, Rate 5%/min	2-6
2-3	DIAMETRAL COMPRESSION HORIZONTAL FAILURE STRESS AND STRAIN AT CENTER, Rate 6.3%/min VERTICAL DIAMETER CHANGE	2-7
2-4	DOUBLE-LAP SHEAR FAILURE STRESS AND STRAIN, Rate 6.7%/min	2-8

Section 1

INTRODUCTION AND SUMMARY

The Structural Integrity Department of Lockheed Propulsion Company is conducting a theoretical and experimental research program to correlate the mechanical behavior and failure properties of solid propellant with the basic characteristics of the propellant and its constituents. This research is supported by the Air Force Rocket Propulsion Laboratory, Research and Technology Division, Air Force Systems Command, Edwards, California, under Contract No. AF 04(611)-9953. The program effort is concentrated on the study of propellant dynamic physical properties, structural failure phenomena, and chemical-physical effects.

In this report, program activities and results for the period 15 September through 15 December 1964 are described and discussed. A section-by-section summary is presented below.

Section 2 — Propellant Formulation Study, High Solids Loading. Failure property investigations in multiaxial stress states were completed for the second group of PBAA and PBAN propellants which include oxidizer modality and burning rate catalyst variations. Little effect on failure properties was observed for the change from optimized trioxidizer to optimized bioxidizer particle size distribution as anticipated from theoretical considerations. Some sensitivity of the failure properties of the PBAA propellants to the liquid burn rate catalyst was observed. Stress relaxation characterization and small strain nonlinear behavior of the first group of formulation variations are discussed along with preliminary correlation of the relaxation data with measured small deformation dynamic response.

Section 3 — Fracture Mechanics. Work during the quarter was concentrated on failure surface definition in orthogonal stress space and studies of crack propagation in biaxial strip test specimens. Studies of test specimens for obtaining failure data in three-dimensional stress states have continued. Results of the failure surface studies are presented. A preliminary estimate has been made of the shape of the failure surface in stress space for an 84 weight-percent solids-loaded PBAN propellant. A maximum tensile stress criterion appears consistent with the limited data for the tensile octant; an internal friction criterion appears generically applicable to the octants where tensions and compressions are combined. Superposed hydrostatic pressure on uniaxial tension caused only small changes in strength and elongation.

The results of the limited studies and experiments that have directed attention to relationships between crack propagation velocity and propellant physical characteristics are described. Good agreement was found between measured and predicted crack extensions.

Section 4 — Dynamic Properties. Experimental investigations of propellant dynamic shear and bulk properties measured with the small deformation piezoelectric devices previously described (Ref. 1) are discussed. Shear moduli of PBAA and PBAN propellant and cured binder are presented and compared with linear thermal expansion measurements of glass transition temperature obtained for similar propellants. Analysis techniques and calibration results are discussed for the dynamic bulk modulus device.

An experimental investigation of propellant thermomechanical response to sustained cyclic inertial loading was completed. Experimental results are presented and it is noted that they are in qualitative agreement with theoretical predictions. In particular, jump instability was experimentally observed to be due to regenerative thermal and mechanical coupling. Also, an experimental investigation of transient thermoviscoelastic response for constant cyclic strain amplitude and inertial loading was completed. Experimental results presented include cyclic degradation observations.

Section 2

PROPELLANT FORMULATION STUDY - HIGH SOLIDS LOADING

2.1 INTRODUCTION

Increasing use is being made of very highly loaded solid propellants in practical motor applications. As the solids loading is increased, the physical properties change and the propellants become more nonlinear in their viscoelastic behavior. For these reasons, research at Lockheed Propulsion Company in the areas of dynamic response and failure mechanisms is presently being concentrated on ballistically feasible propellant formulations approaching the maximum theoretical limit of solids loading. Primary effort during the second quarterly reporting period has been directed towards completion of an experimental parametric study of a series of highly loaded PBAA and PBAN propellants.

Although analysis of the experimental results are so far incomplete, several conclusions concerning the observed effects of high solids loading on propellant physical properties can be made at this time. A systematic degradation of the propellant failure strain capability and an accompanying increase in failure stress are observed as the solids loading is increased, resulting in a net increase in the mechanical energy required to break the specimens. In addition, the viscoelastic properties at small strains are observed to mirror the failure behavior with a general tendency toward higher moduli and increasing nonlinear behavior as the solids loading increases.

Experimental results for the burning rate catalyzed and bimodal oxidizer propellant formulations are presented in the following sections. The results show that changing the oxidizer modality from a trioxidizer to a bioxidizer system has little effect on the failure properties when the particle size distributions for the two modal systems are optimized as discussed in the previous quarterly report.

In general, burning rate catalysts were found to have little effect on failure properties with the single exception that PBAA propellants were found to be softened substantially by the addition of the liquid burning rate catalyst.

2.2 TEST PLAN

Propellants have been prepared consisting of combinations of four propellant formulation variables. These are (1) total weight percent solids loading, (2) binder type, (3) oxidizer particle size distribution, and (4) burning rate catalysts. The total solids loading was varied between 84 and 90 percent. Polybutadiene acrylic acid (PBAA) copolymer and polybutadiene acrylonitrile acrylic acid (PBAN) terpolymer binders were investigated. Two particle size distribution systems were used--a bimodal oxidizer system and a tri-modal oxidizer system, both optimized for minimum processing viscosity. In addition, an assessment of the relative effects of burning rate catalysts, both liquid and solid, on the physical properties and burning rate was planned on a spot-check basis. Formulations which have been cast and prepared for testing are listed in Table 2-1. Formulations will be referred to by the code symbols listed in Table 2-1 throughout this report. All of the propellants are aluminized. The solids particle size distribution is identical for each tri-oxidizer system. Similarly, each bioxidizer system contains an identical solids system, with the exception of the two systems catalyzed with solid catalysts, 84NBCS and 88NBCS. For these systems, a small portion of the fine oxidizer is replaced with an equivalent amount of burning rate catalyst. PBAA binder is cured at a 1.1/1 imine-to-carboxyl ratio level with a trifunctional-to-difunctional curative ratio of 40/60. PBAN binder is cured at a 1.3/1 epoxy-to-carboxyl ratio. Both PBAA and PBAN propellant binders are plasticized. Specific information regarding the formulation of each propellant was presented in Appendix II (Confidential) of LPC Report 667-Q-1 (AFRPL-TR-64-148).

Two 5500-gram batches of each formulation were mixed simultaneously in similar laboratory mixing facilities to provide sufficient propellant for the various specimens and to eliminate batch-to-batch variations as much as possible. The propellants were mixed and cast under vacuum.

The test specimens used in physical property testing were the in situ bonded tab-end type, sawed and milled from bulk casting of propellant. Prior to testing, all specimens were dimensionally inspected and stored in a 70°F desiccated environment.

Experimental data for four stress states are being obtained for the propellant formulations in Table 2-1. Uniaxial tension, strip biaxial, diametral compression, and double-lap shear tests are being performed, using a constant rate of deformation for failure characterization.

The essential characteristics of the specimens and the definitions of failure are discussed in the following subsections.

Table 2-1

PROPELLANT FORMULATION TEST PLAN**

		Total Solids, Weight Percent of Formulation							
		84		86		88		90	
		UC	C	UC	C	UC	C	UC	C
Optimum* Trioxidizer Solids System	PBAA	[illegible]	---	[illegible]	---	[illegible]	88RC X	[illegible]	---
	PBAN	[illegible]	---	[illegible]	---	[illegible]	88NC X	[illegible]	---
Optimum* Bioxidizer Solids System	PBAA	84RB	---	---	---	88RB	88RBC X	---	---
	PBAN	84NB	84NBCS O	---	---	88NB	88NBC 88NBCS OX	---	---

*As determined by bulk density and viscosity measurements
**Data for shaded formulations were reported in first quarterly report (Ref. 1)

UC - Uncatalyzed
C - Burn rate catalyzed
X - Liquid catalyst
O - Solid catalyst

2.2.1 Uniaxial Tension[1]

Tab-end specimens consisting of rectangular bars (4 by 0.3 by 0.3-inches) with wooden tab-ends (bonded in situ to propellant during cure) are being used exclusively for the tensile tests. The stress-strain condition identified as failure is defined by ϵ_m, the so-called strain at maximum stress, as presented in the ICRPG Solid Propellant Mechanical Behavior Manual (Ref. 2). This strain level is usually found to be about 2/3 of the strain level where the load-time record passes through a maximum, and may be associated with the development of extensive dewetting.

2.2.2 Strip Biaxial[1]

Strip biaxial specimens consist of thin plates of propellant with a width much greater than their height. The specimens are prepared by casting propellant into lined wooden boxes of appropriate size and subsequently machining specimens from the box, retaining the wooden tabs along the long sides of the specimens. They are tested at a constant elongation rate applied in a direction normal to the clamped edges. In most instances, strip specimens with a large width-to-height ratio fail by cracking in the central region of the strip where the stress field is reasonably uniform. As in the uniaxial tensile tests, a maximum in the load-time curve sometimes occurs prior to visual crack initiation. Thus, for the sake of uniformity, the stress-strain condition identified as failure in this test is defined in the same manner as for the uniaxial tensile tests. The size of the biaxial strip specimens used is 7.5 by 1.5 by 0.125 inches, and the sheets are filleted from the 0.125-inch thickness to a 3/8-inch thick wooden tab strip.

2.2.3 Diametral Compression[1]

The diametral compression test specimens are 1.5-inch diameter discs, 1/2-inch thick, prepared by machining cast cylinders of propellant. The failure of these specimens is first evidenced by the appearance of fissures at the center, on the surface of the specimens, usually aligned at an angle to the principal stress axes so as to suggest shear failure. Although it is possible that the initiation of failure takes place inside the sample somewhat earlier than is shown by the surface crack, the start of the visible fissuring at the specimen surface defines failure.

[1]These test specimens are described in detail in Reference 21.

2.2.4 Double-Lap Shear

Parallelogram plan-form shear specimens are used for determining propellant failure properties under shear conditions (Ref. 1). With wooden side supports constrained to prevent lateral movement, force applied parallel to the center support results in shear deformation of the propellant and subsequent failure of the propellant in the central region of the specimen. Shear failure surfaces are found to be parallel to the side supports and perpendicular to the free surfaces of the propellant. Visual observation of fracture is difficult, but it is usually observed nearly at the observed peak output force in a constant shear strain rate test. For simplicity, therefore, failure is defined in this test as the peak in the force-time record.

2.3 FAILURE PROPERTIES

Multiaxial failure characteristics of the 10 formulations shown unshaded in Table 2-1 have been investigated. The results show that the absolute magnitudes of the failure stress and strain again vary with stress axiality as anticipated. There is also a consistent change in failure properties with formulation variation for all of the test modes. Thus, because of the large amount of data, unnecessary repetition will be avoided by presenting in graphical form only the strip biaxial test mode results. Failure data for the remaining three test modes are presented in tabular form in Tables 2-2, 2-3, and 2-4.

Figure 2-1 presents comparative biaxial strip failure properties for the 84 weight-percent loaded, bioxidizer, PBAN catalyzed and uncatalyzed formulations 84NBC3 and 84NB, respectively. The solid burn rate catalyzing agent (less than two percent by weight of the total formulation) replaced an equivalent weight of fine-ground ammonium perchlorate to maintain a constant solids loading. Inspection of the data showed a small amount of propellant stiffening due to the solid catalyst resulting in slightly higher failure stresses and lower failure strains. This effect is confirmed by the diametral compression and lap-shear test data.

Similar PBAN, bioxidizer formulations at 88 percent solids loading, with various burning rate catalysts, are compared in Figure 2-2. No significant change in failure properties is apparent from these data as a result of using the burning rate catalysts. The liquid catalyst amounts to less than two percent by weight of the total formulation and replaces an equal quantity of plasticizer so as to keep the total plasticizer-to-polymer ratio constant.

Table 2-2

UNIAXIAL FAILURE STRESS AND STRAIN
AT ICRPG (1963) FAILURE POINT, Rate 5%/min

Failure Stress (psi) / Failure Strain (percent)

Propellant Formulation	Temperature (°F)				
	140	83	10	-50	-85
84 RB	55	79	212	383	635
	5.3	6.0	7.6	5.1	4.81
84 NB	53	76	138	421	850
	19	22.1	12.5	6.2	2.95
88 RB	79	124	294	--	--
	4.1	4.3	5.2	--	--
88 NB	72	96	190	557	773
	13	13.1	12.1	5.3	1.71
84 NBCS	69	91	185	485	802
	18	18.6	12.6	7.1	2.38
88 NBCS	88	108	196	538	882
	14	13.8	11.7	5.6	2.25
88 RC	31	54	167	326	457
	8.2	8.4	8.2	3.08	2.37
88 NC	66	87	181	530	662
	9.2	9.2	9.2	3.20	2.00
88 RBC	40	68	164	326	446
	14.2	12.7	9.7	4.72	2.99
88 NBC	81	107	198	543	--
	10.7	9.7	6.7	3.43	--

Table 2-3

DIAMETRAL COMPRESSION HORIZONTAL FAILURE STRESS AND STRAIN AT CENTER, Rate 6.3%/min VERTICAL DIAMETER CHANGE

Failure Stress (psi) / Failure Strain (percent)

Propellant Formulation	Temperature (°F)		
	140	74	10
84 RB	52.3	102	235
	20.3	27.2	31.2
84 NB	43.6	84.8	211
	37.1	53.6	56.9
88 RB	63.9	127.6	266
	13.1	18.0	20.0
88 NB	54.0	81.7	163
	27.0	30.1	36.2
84 NBCS	53.2	91.7	213
	35.7	44.3	53.7
88 NBCS	69.5	100	170
	24.2	28.2	26.5
88 RC	30.6	102	196
	28.5	30.1	29.1
88 NC	52.3	77.9	170
	25.7	22.0	28.0
88 RBC	38.7	89.6	169
	33.9	31.3	32.9
88 NBC	71.4	112	240
	19.5	25.2	26.6

Table 2-4

DOUBLE-LAP SHEAR FAILURE STRESS AND STRAIN,
Rate 6.7%/min

Failure Stress (psi) / Failure Strain (percent)

Propellant Formulation	Temperature (°F)	
	140	82
84 RB	50.2	80.9
	23.9	25.7
84 NB	40.5	62.1
	41.5	47.8
88 RB	54.0	89.2
	15.1	18.0
88 NB	60.9	80.1
	31.8	34.8
84 NBCS	38.2	66.5
	33.9	37.4
88 NBCS	64.9	104
	31.1	34.1
88 RC	29.2	75.1
	34.1	34.1
88 NC	49.6	88.6
	21.3	31.2
88 RBC	25.9	68.5
	39.4	37.5
88 NBC	65.8	113
	25.1	32.2

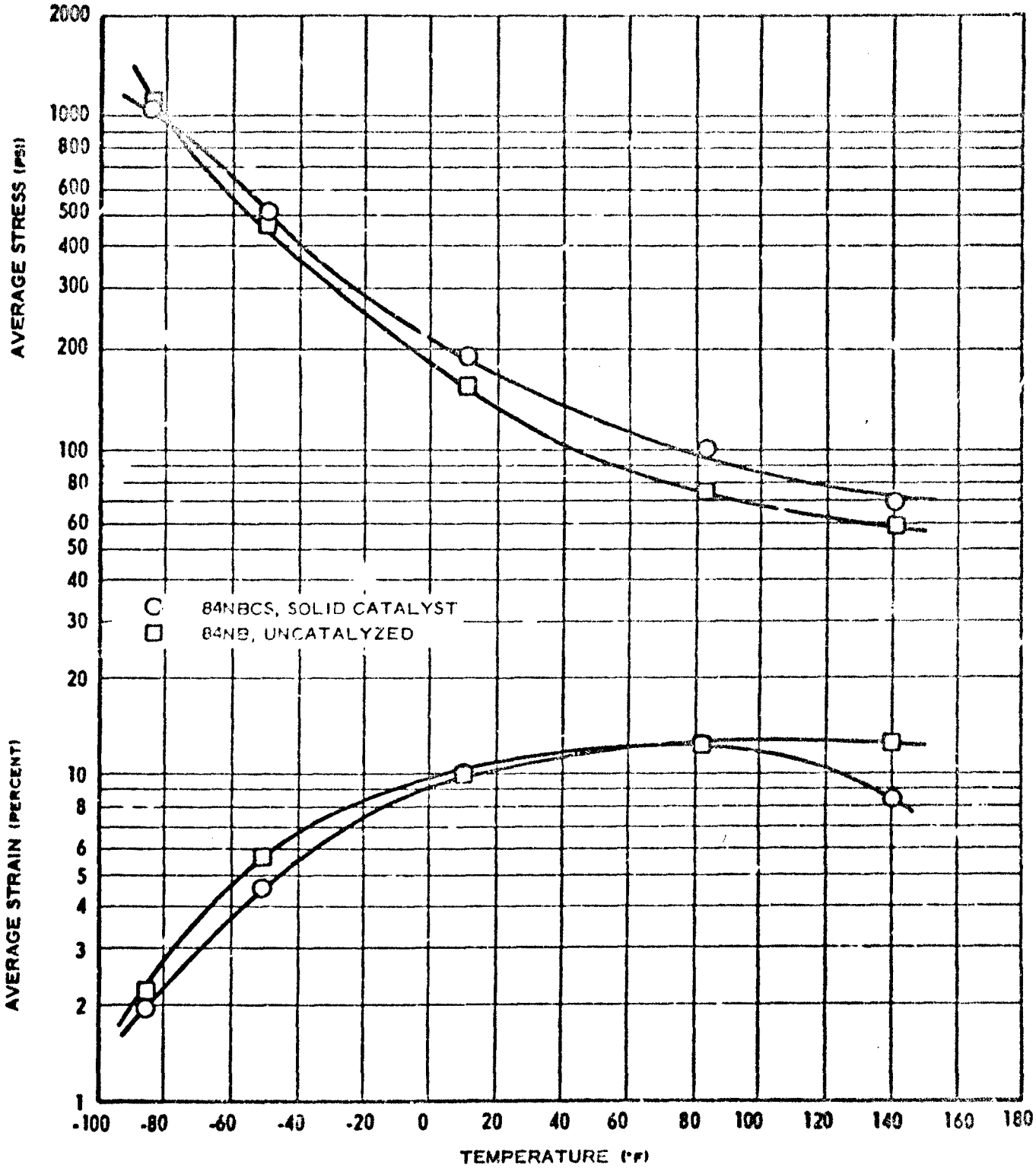

Figure 2-1 Biaxial Strip Failure Stress and Strain at ICRPG (1963) Failure Point versus Temperature, PBAN, 34% Loading, Bioxidizer

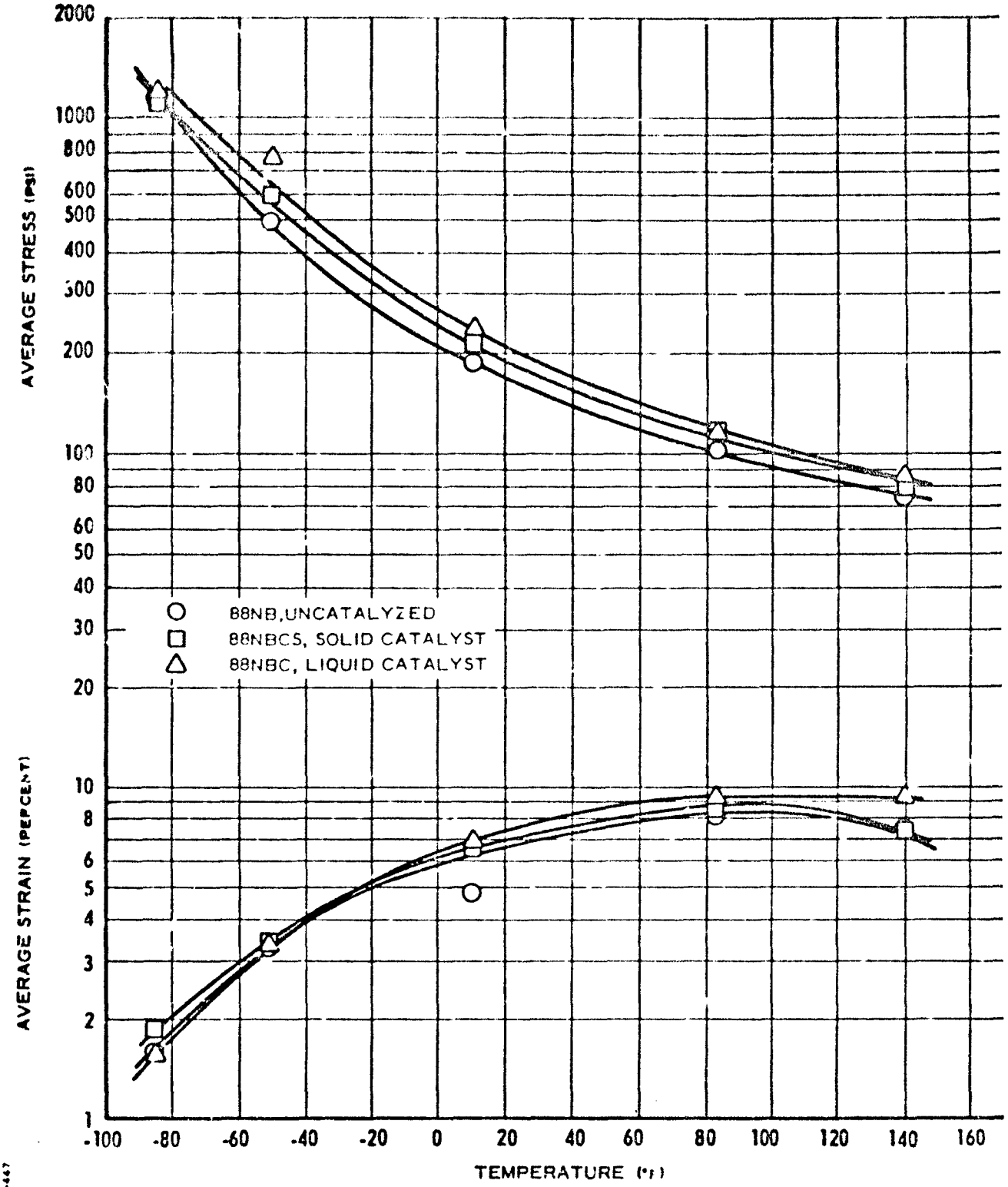

Figure 2-2 Biaxial Strip Failure Stress and Strain at ICRPG (1963) Failure Point versus Temperature, PBAN, 88% Leading, Bioxidizer

In Figure 2-3, the effects of solids loading on the PBAA and PBAN bioxidizer formulations are compared at the 84 and 88 weight-percent solids loading levels. The failure characteristics are similar to the trioxidizer formulations in that increasing solids loading results in increased failure stress and reduced failure strains.

Brittle fracture was obtained with the PBAN propellants when tested at -50 and -85^{0}F. Again it was found that the PBAA propellants have unusually low failure strains and high failure stresses as noted for the uncatalyzed trioxidizer PBAA formulations.

A comparison between the uncatalyzed trioxidizer and bioxidizer formulations is presented in Figures 2-4 and 2-5 for the PBAN and PBAA propellants, respectively. In general, the bioxidizer formulations show slightly superior strain and stress capability for both binder types and solids loading levels. However, this situation is reversed at higher temperatures with the PBAA formulations.

Figures 2-6 and 2-7 illustrate the effect of the liquid burning rate catalyst on the failure properties of the bioxidizer and trioxidizer formulations at 88 percent loading for PBAA and PBAN propellants, respectively. The data for the PBAA binder show a significant softening of the propellant when the liquid burning rate catalyst is added. Failure strain capability is increased by approximately a factor of two at the higher temperatures and the stresses are correspondingly lower. Inspection of Figure 2-7 reveals no such effect for the PBAN binder propellants and in fact a slight stiffening is observed due to the liquid catalyst. The data therefore show a preferential interaction between the liquid burning rate catalyst and the PBAA binder, tending to reduce the effective network crosslinking or otherwise loosen the binder structure. The fact that the biggest effect is obtained at higher temperatures suggests that binder crosslinking structure (or effective chain length) is modified by the catalyst, resulting in a lower modulus in the temperature region where long range interactions are most important.

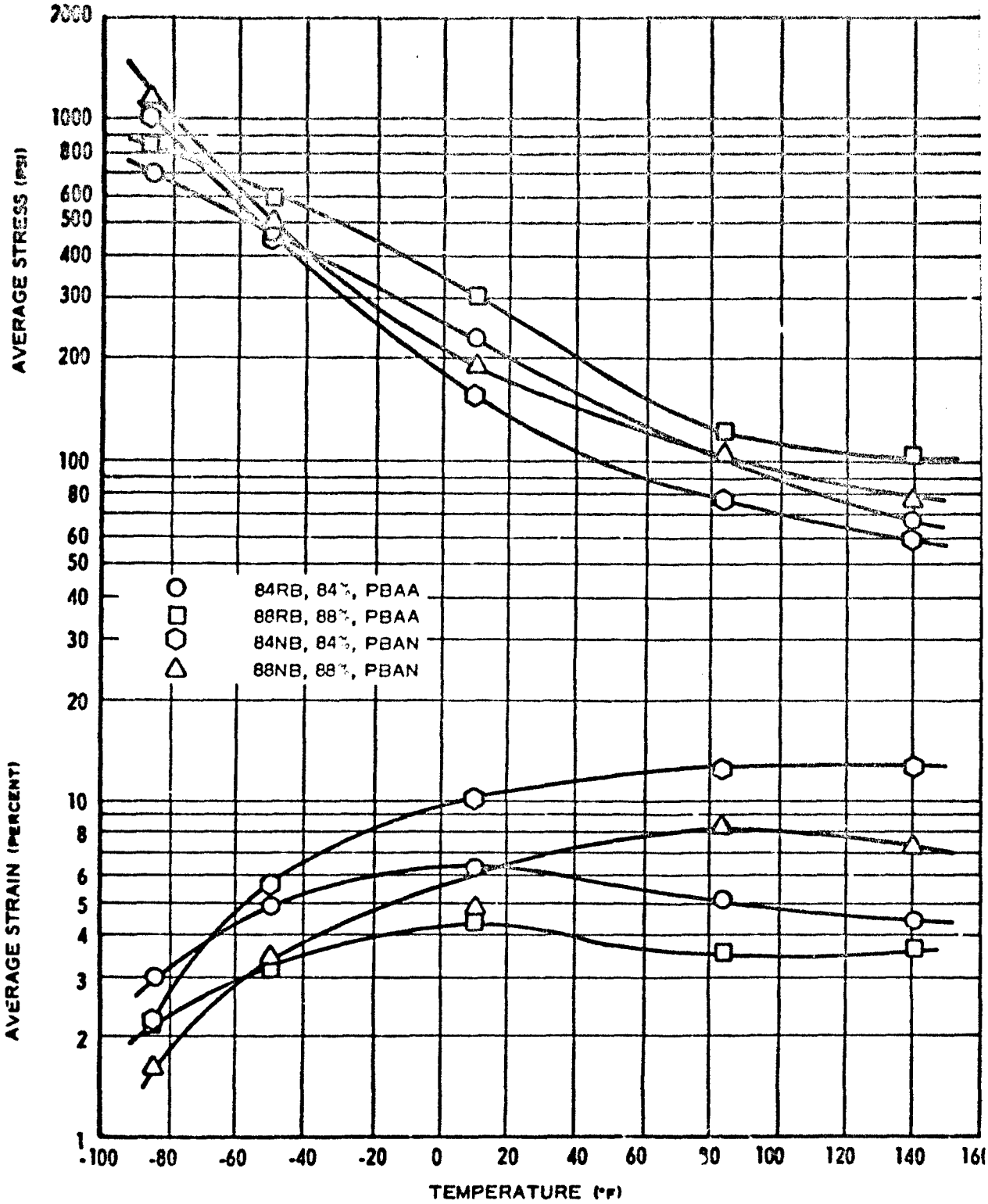

Figure 2-3 Biaxial Strip Failure Stress and Strain at ICRPG (1963) Failure Point versus Temperature, Bioxidizer, Uncatalyzed

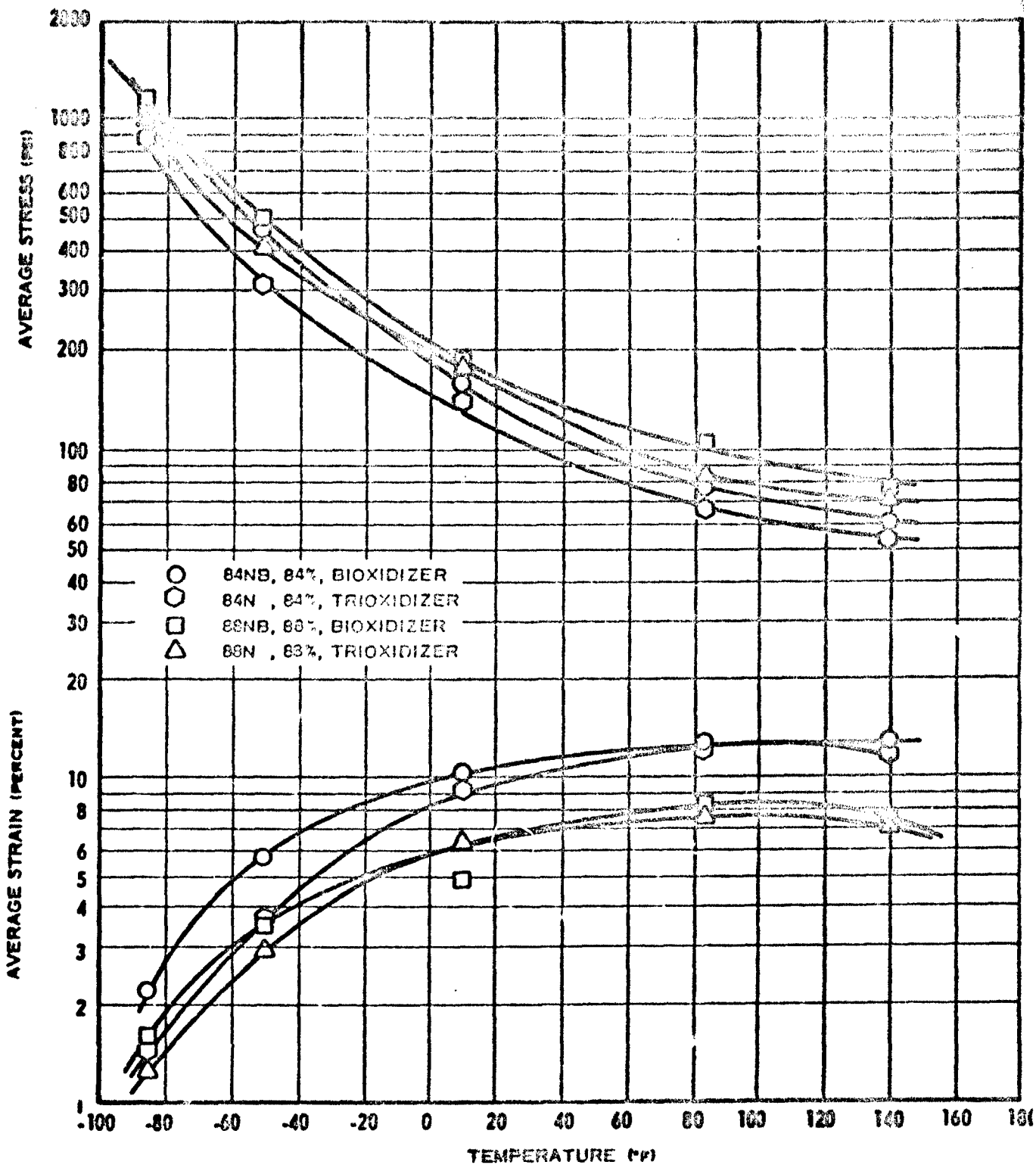

Figure 2-4 Biaxial Strip Failure Stress and Strain at ICRPG (1963) Failure Point versus Temperature, PBAN, Uncatalyzed

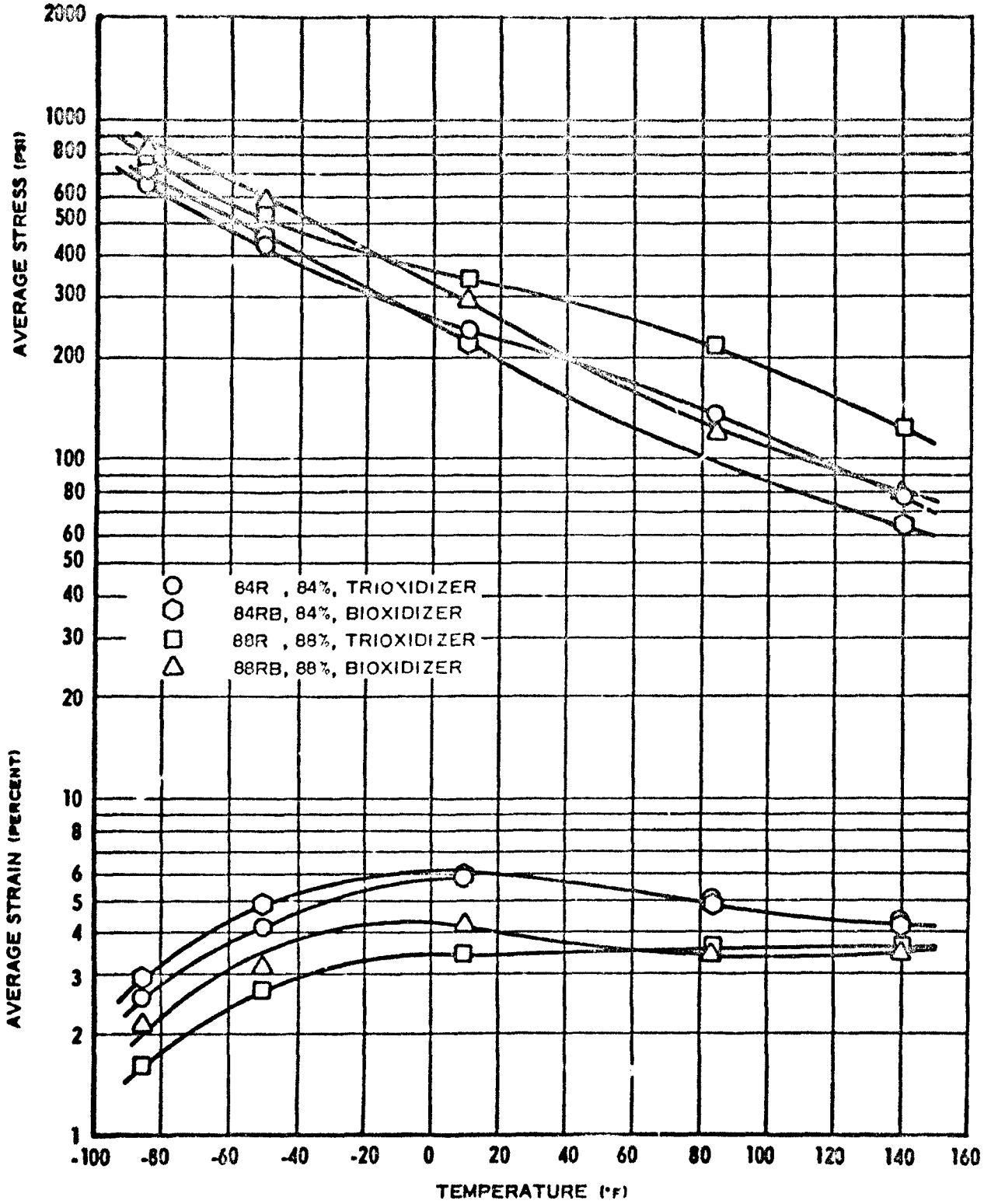

Figure 2-5 Biaxial Strip Failure Stress and Strain at ICRPG (1963) Failure Point versus Temperature, PBAA, Uncatalyzed

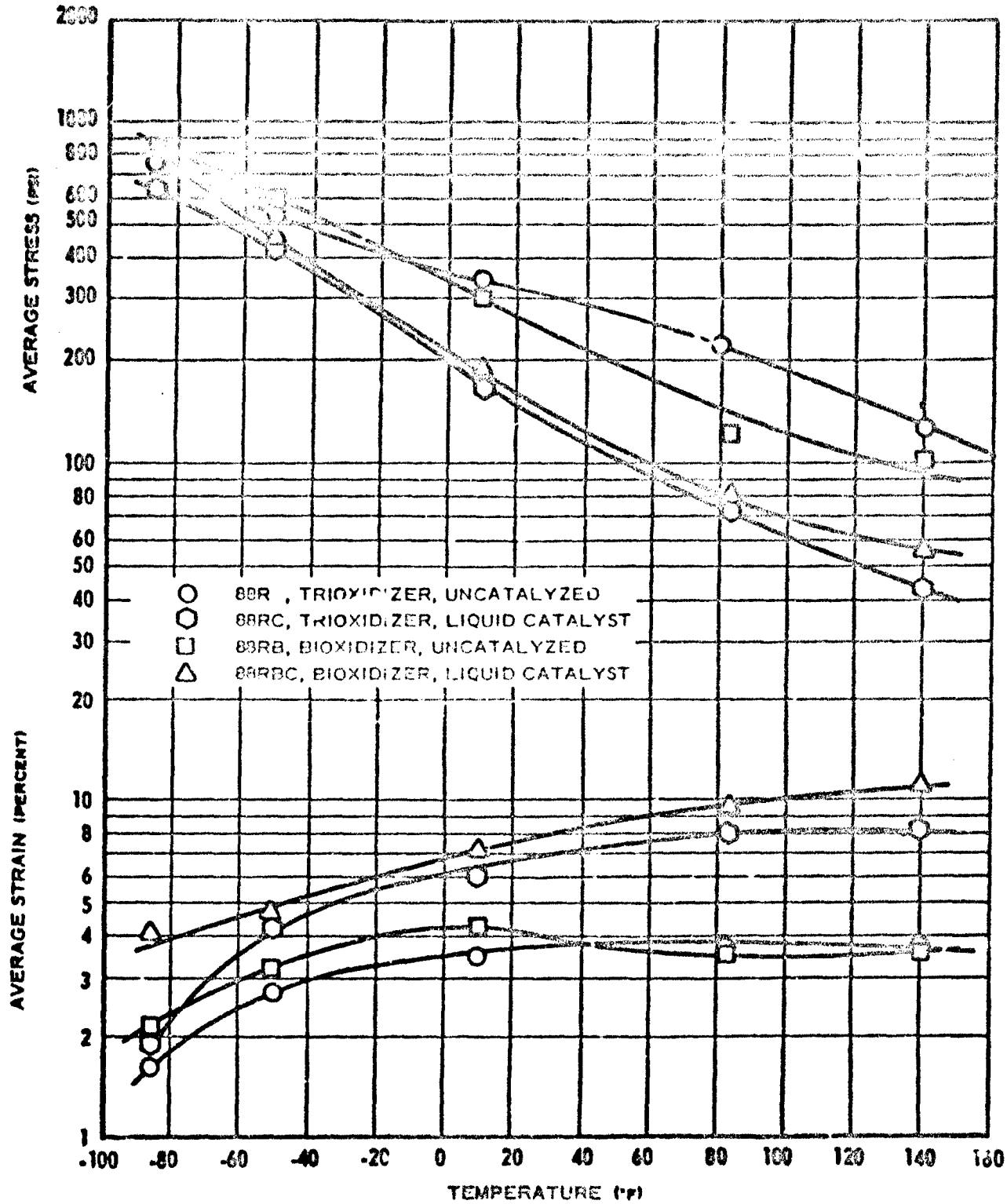

Figure 2-6 Biaxial Strip Failure Stress and Strain at ICRPG (1963) Failure Point versus Temperature, PBAA, 88% Loading

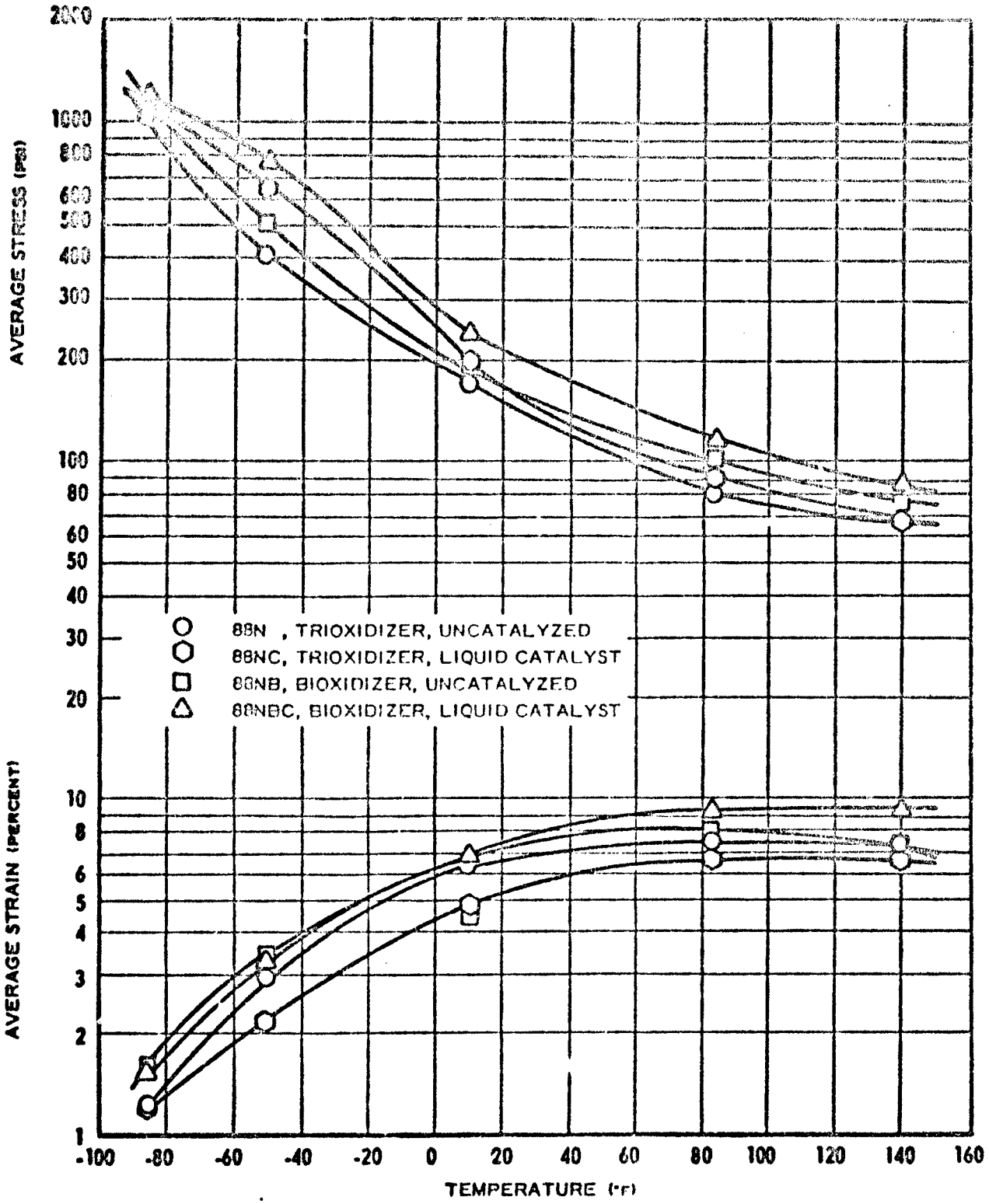

Figure 2-7 Biaxial Strip Failure Stress and Strain at ICRPG (1963) Failure Point versus Temperature, PBAN, 88% Loading

2.4 VISCOELASTIC CHARACTERIZATION AND INVESTIGATION OF NONLINEAR BEHAVIOR

Previous work, given in the first quarterly report, showed that the uniaxial tensile response of the 90 weight-percent loaded formulations was nonlinear at strains of the order of 1 to 5 percent. This nonlinearity was characterized by increasing modulus with increasing strain. Investigation of tensile data for the remaining high solids loaded propellants showed that the relative magnitude of this particular effect increases as the solids loading is increased and as the binder modulus decreases at a constant solids loading.

The study of the tensile relaxation response of the first group of highly loaded propellant formulations has been continued and extended to temperatures ranging from -24^0 F to +174^{0}F. In general, relaxation response was found to be a nonlinear function of strain level in the 1 to 5 percent strain range. In addition, time-temperature superposition of the data was found to be poor. However, mathematical inversion of the reduced relaxation data to complex tensile modulus form was performed and the results were compared with frequency-temperature superposed, experimentally measured dynamic shear data for the same propellants. The dynamic shear tests were performed at very low strains of the order of 6×10^{-3} percent. In general, results which have been analyzed thus far show good agreement between the loss moduli components from the tensile relaxation data and the measured dynamic shear data. However, the storage component curves do not show good agreement. The storage moduli calculated from the tensile relaxation tests are generally larger than the values calculated from the small deformation shear data. The discrepancy increases at lower frequencies or at higher temperatures, resulting in a slope mismatch between the curves of log modulus versus log reduced frequency in the overlap region.

Data reduction and analysis are still in progress and detailed results will be given in subsequent reports.

Section 3

FRACTURE MECHANICS

3.1 GENERAL

Work during the quarter was concentrated on failure surface definition in orthogonal stress space and studies of crack propagation in biaxial strip test specimens. Studies of test specimens for obtaining failure data in three dimensional stress states have continued. Section 3.2 presents the results of the failure surface studies. The information in this section is essentially identical to that contained in AIAA preprint paper No. 65-157. A preliminary estimate has been made of the shape of the failure surface in stress space for an 84 weight-percent solids loaded PBAN propellant. A maximum tensile stress criterion appears consistent with the limited data for the tensile octant; an internal friction criterion appears generically applicable in the octants where tensions and compressions are combined. Superposed hydrostatic pressure on uniaxial tension caused only small changes in strength and elongation.

Section 3.3 describes the results of the limited studies and experiments that have directed attention to relationships between crack propagation velocity and propellant physical characteristics. Good agreement was found between measured and predicted crack extensions.

3.2 FAILURE SURFACE STUDIES

Stress and strain analyses are two fundamental requirements for determining a rocket motor's structural capabilities. The linear theory of viscoelasticity has provided a useful (though not always precise) guide to the stresses and strains in rocket motors. Prediction of failure in solid propellant grains, however, has been dependent upon a much less reliable source. In most instances, failure analyses lean heavily on uniaxial tensile test data. Since a solid propellant grain is subjected to a spectrum of three-dimensional stress states, the applicability of uniaxial tensile data to the prediction of motor failure is questionable. An understanding of how failure properties depend upon the state of stress or stress axiality is required for the proper conduct of a failure analysis.

One descriptive correlation of failure dependence on stress state is the so-called failure surface, defined in a three-dimensional space by the values of the principal stresses at failure. The failure surface and its general topology have been discussed elsewhere (Ref. 3, 4). A major difficulty associated with this type of representation is the fact that the failure properties of solid propellants depend upon their loading history as well as stress axiality. Since a given stress state at failure, in principle, may be reached by an infinite variety of loading histories, a failure surface exists only for specific loading histories. Sharma (Ref. 5), for example, describes traces of the failure surface for those loading histories in which the maximum principal strain rates are identical.

Experimental results on the stress state dependence of filled rubber failure properties have been reported previously by Sharma, Ref. 6) Jones, (Ref. 7) and Majerus, (Ref. 8). In Sharma's paper (Ref. 6), attention was focused upon delineating the failure surface for a viscoelastic material, which, however, was not representative of most propellants. Jones and Majerus made no specific attempt to establish the failure surface.

The following considers the failure surface for a PBAN propellant with a solids loading of between 69 and 80 percent by volume. The mechanics of the test and the reduction of data to a reasonable presentation are emphasized. Representative data for one strain rate and one temperature are presented for a number of multiaxial stress states. While a number of questions remain, particularly with respect to proper stress analysis of the tests, the results of this investigation are encouraging. A first approximation to the failure surface in stress space has been obtained, and its variation with propellant solids loading has been partially explored.

3.2.1 Test Analysis

While linear viscoelastic stress analysis has provided a significant guide to propellant stress analysis, it possesses limitations which are not fully understood, e.g., large deformation effects and the differing responses to compressive and tensile loads. Although it is necessary to consider these effects if an analysis of failure data is to be precise, they cannot be accounted for at the present time in a refined manner. Indeed, their incorporation in test data analysis depends as much upon engineering extrapolation as upon mathematical rigor. As a consequence, the following work has to be viewed more as a step in the proper direction than as an ultimate result.

For the purpose of the present discussion, we shall distinguish between effects of large deformations upon the stress field and the effect of nonlinear material behavior. It can be shown (Ref. 6, 7) that the change in stress values due to consideration of large deformation rarely exceeds the order of the maximum strain value. While deformations at failure in dominantly compressive stress fields may exceed 25 percent, deformations in the tests

reported here are generally of this order or less. The stress analyses of the tests, therefore, are based on the usual assumption of infinitesimal deformations. The effects of bilinear compression-tension moduli are discussed in the following paragraphs appropriate to the particular tests in which they are an important factor.

Seven tests representing a multiplicity of locations in three-dimensional stress space have been used in compiling the data presented herein. Test specimen geometries are shown in Figure 3-1. The tests are listed below, and their principal stress values are shown for the observed sites of failure initiation in terms of applied boundary stresses or loads. The calculation of these stresses is based on the assumptions of material linearity, homogeneity, continuity, and infinitesimal deformation. Arabic subscripts indicate principal stresses, the "1" direction identifies the principal tensile stress in each test.

Strip Biaxial Tension

$$\begin{aligned} \sigma_1 &= \sigma_0 \\ \sigma_2 &= \sigma_1/2 \\ \sigma_3 &= 0 \end{aligned} \tag{1}$$

where σ_0 is the average applied stress for a strip of length at least 5 times its height (Figure 3-1).

Uniaxial Tension

$$\begin{aligned} \sigma_1 &= \sigma_0 \\ \sigma_2 &= \sigma_3 = 0 \end{aligned} \tag{2}$$

where σ_0 is the applied tension.

Uniaxial Compression

$$\begin{aligned} \sigma_1 &= -\sigma_0 \\ \sigma_2 &= \sigma_3 = 0 \end{aligned} \tag{3}$$

where σ_0 is the applied compression.

Strip Biaxial Compression

$$\begin{aligned} \sigma_1 &= -\sigma_0 \\ \sigma_2 &= \sigma_1/2 \\ \sigma_3 &= 0 \end{aligned} \tag{4}$$

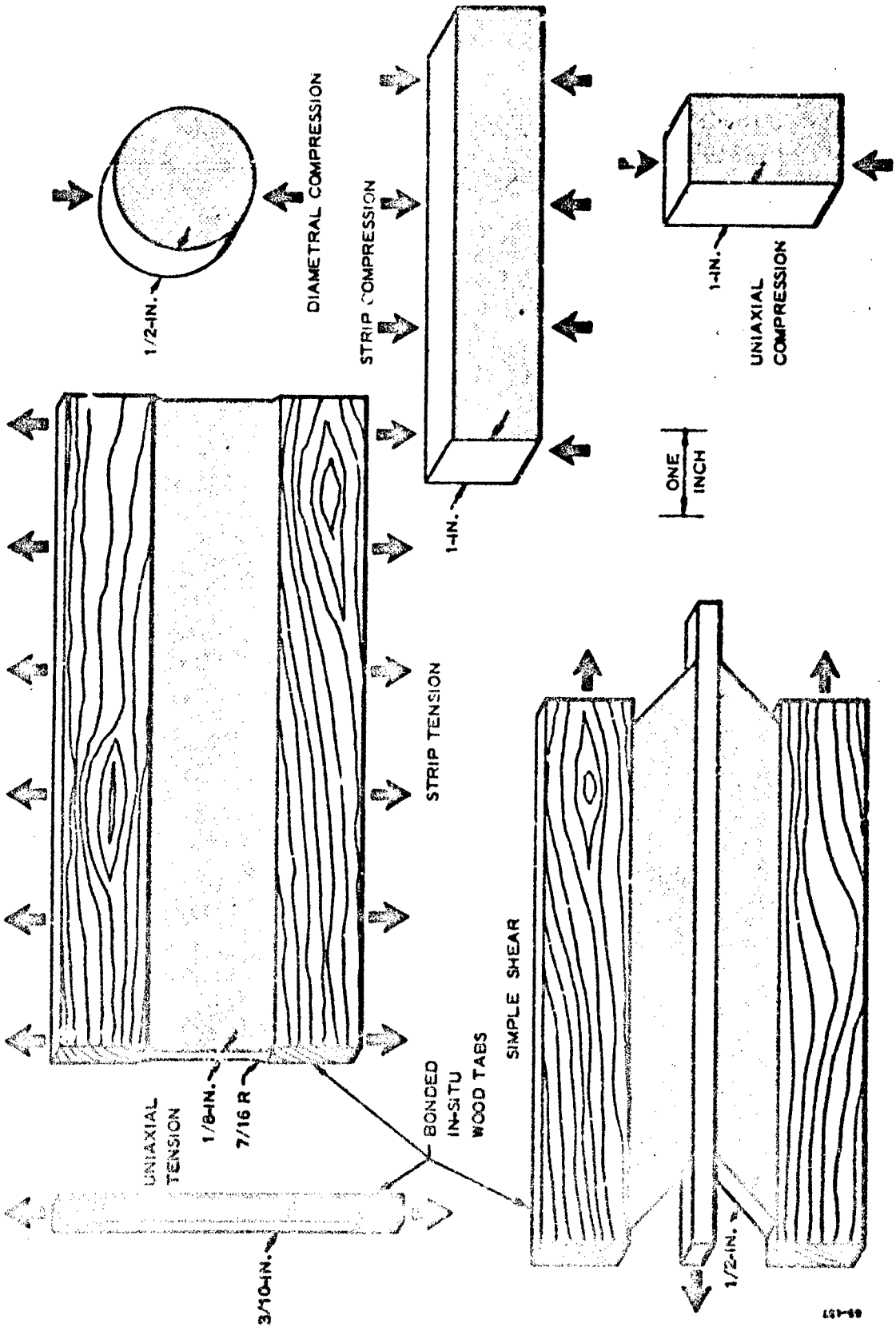

Figure 3-1 Test Specimens

where σ_0 is the applied compression for a strip of length at least 5 times its height.

Diametral Compression

$$\sigma_1 = \frac{F}{\pi d t}$$

$$\sigma_2 = -3\sigma_1 \qquad (5)$$

$$\sigma_3 = 0$$

where

F = applied compression

d = specimen diameter

t = specimen thickness.

Shear

$$\sigma_1 = \tau$$

$$\sigma_2 = -\tau_0 \qquad (6)$$

$$\sigma_3 = 0$$

where τ_0 is the average applied shearing stress in a laterally restrained or "simple" shear geometry (Figure 3-1).

Uniaxial Tension With Superposed Hydrostatic Pressure

$$\sigma_1 = \sigma_0 - \sigma_H$$

$$\sigma_2 = \sigma_3 = -\sigma_H \qquad (7)$$

where $-\sigma_H$ is the applied hydrostatic gas pressure.

The shear test and the diametral compression test require additional considerations. Previously, it was determined that shear strains produce significant stresses normal to the applied shear (Ref. 9) if the outer supports are restrained from lateral motion. Specifically, it was found that the normal stress σ_y across the shear is proportional to the applied shear stress τ_0 and is, approximately,

$$\sigma_y \cong 0.3\,\tau_0 \qquad (8)$$

where τ_0 is the shear force divided by the total area.

Herrmann (Ref. 10) has considered the effect of bilinear material properties on the simple shear test and shows that the normal stress σ_x along the largest dimension is equal to σ_y For a ratio of tensile-to-compressive modulus of 1/2, which is characteristic of propellants with the solids loading* investigated here, the stresses σ_x and σ_y have been found to be approximately 1/3 the shear stress. Therefore, the principal stresses are

$$\begin{aligned} \sigma_1 &= 0.7\,\tau_0 \\ \sigma_2 &= -1.3\,\tau_0 \end{aligned} \qquad (9)$$

whereas linear theory yielded $\sigma_1 = -\sigma_2 = \tau_0$ (Equation 6).

A similarly detailed analysis for the diametral compression test has not been performed, primarily because the stress distribution varies through the body, which significantly complicates the analysis. However, an estimate of the correction can be obtained if one considers the different modulus values in tension and compression. Inasmuch as the compressive modulus is about twice as large as the tensile modulus, one could assume that half of the compressive force is absorbed in the disk without producing transverse stresses and that the remainder of the force gives rise to the tensile stress σ_1. Instead of the 3:1 ratio between the principal compression and tension stresses found in linear analysis (Equation 5), a ratio nearer to 6:1 appears to be more realistic.

It is clear that nonlinear material behavior can influence significantly the evaluation of the test results. While the precision of the analysis is questionable, it is qualitatively correct and reduces the effects due to material nonlinearity.

3.2.2 Experimental Results

Tests were performed on an Instron testing machine. The testing speed was adjusted so that the principal tensile strain rate $\dot{\epsilon}_1$ was equal to 0.07 in./in./min when based on the specimen dimensions before deformation. The occurrence of failure was defined by observed cracking or by the maximum in the load-displacement trace, whichever occurred first.

The test points shown here are representative of a more complete set of failure properties given in Reference 1. For the present purpose of examining the effect of stress axiality on failure, it suffices to consider data derived from one strain rate and at one temperature. Figures 3-2 and 3-3 show failure data for three solid loadings of a PBAN binder at 10°F and 7 percent/min strain rate. The shear and diametral compression test data in Figure 3-3 were reduced according to the bilinear analysis.

* This ratio depends also upon loading, but such detailed consideration has been omitted here.

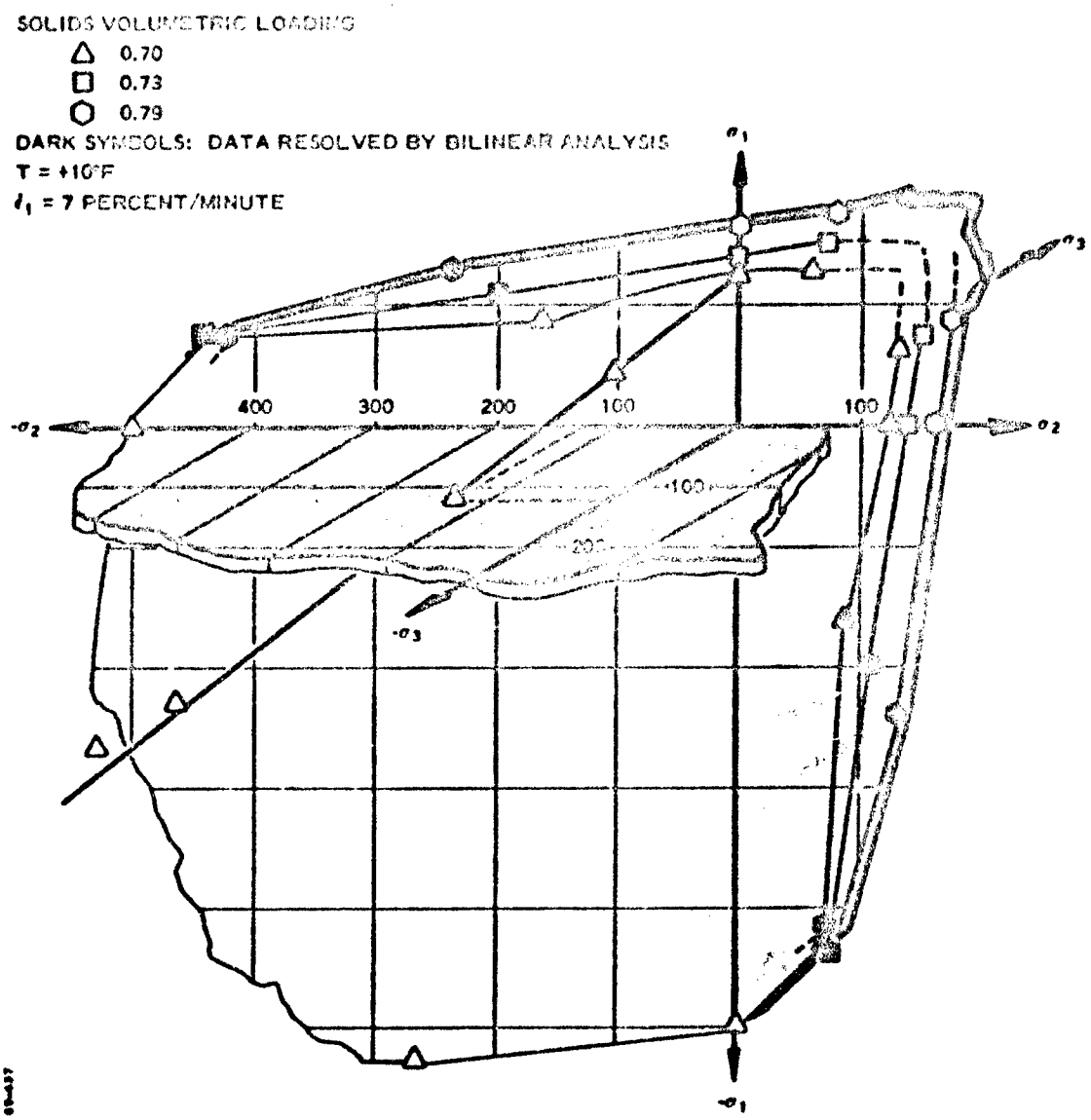

Figure 3-2 Dependence of Failure Stresses on Stress State and Solids Loading

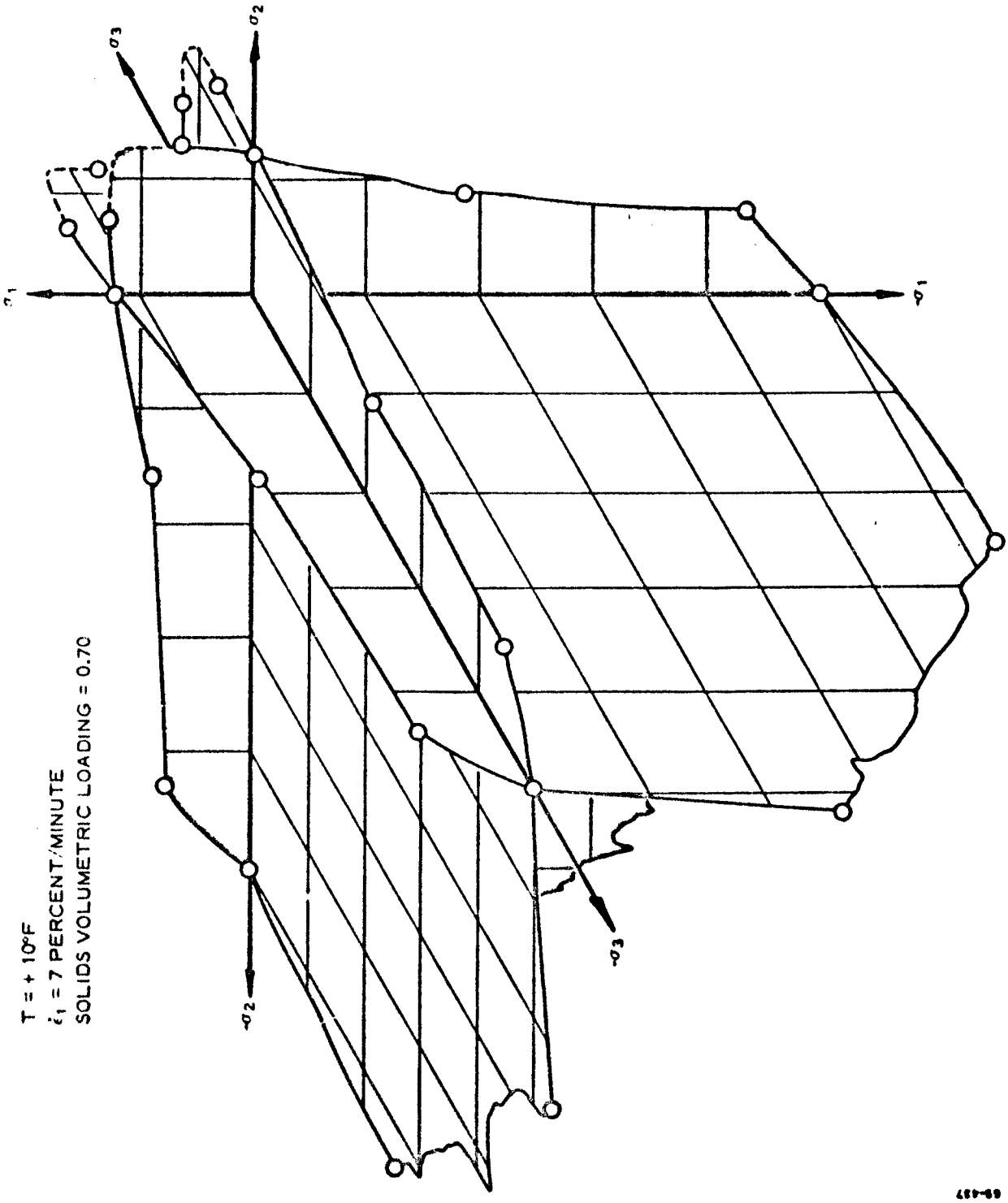

Figure 3-3 Dependence of Failure Stresses on Stress State

3.2.3 Discussion

The modes of failure observed were normal tensile cracking in the strip and uniaxial tensile tests and shear sliding for the remaining tests. Shear failure surfaces were oriented approximately 30°F off the direction of the maximum normal compression stress. An obvious increase in the shear stresses accompanies increases in normal compressions. This is believed to be a consequence of intergranular friction under compression and, of course, is not significant under tensions where the granules tend to be separated by the deformations. In this respect, the general failure behavior of the propellant is similar to that of a water-saturated sandy clay (Ref. 11). Such materials may be characterized by a single value of tensile strength and a shear strength that varies in proportion to the normal stress across the plane of potential shear fracture. This kind of behavior is represented conveniently in the form of a Mohr envelope (e.g., Ref. 12).

Uniaxial data obtained with tension superposed on a hydrostatic (gas) pressure for the 70 percent by volume solids loaded formulation showed that the amount of tension required to cause failure increased only slightly for pressures up to 1000 psi (Figure 3-2). The indicated tensile strength is nominally constant and independent of the pressure, any increment of the latter being carried by neutral pressures in the rubber matrix which fills the voids between particles. These neutral pressures in the rubber naturally do not contribute to an increase of the intergranular frictions or binding forces between the granules and the matrix.

The small increases noted in strength with pressure can be attributed to increases in intergranular friction, interphase friction or increases in the strength of the binder alone under pressure. The size of the effect is such that any of the three phenomena could rationalize the strength changes; as the solids volumetric loading is increased, the interparticle reactions can be expected to dominate in importance.

Since each of the stress states examined in these tests (excepting pressurized tensile tests) lies on one of the coordinate planes* in the principal stress space, an experimental picture of the complete failure surface cannot be constructed. However, in view of the need of failure analysis in solid propellant rocket design, it becomes interesting to sketch a possible extrapolation of the biaxial data to the triaxial stress states. Tests to examine the failure surface in these octants are planned for the future. As a practical example of such need for extrapolation, consider the bond stresses in an unpressurized, axially accelerated motor; in this case, the principal stresses can lie in the ++- or +-- octants, substantially away from any of the coordinate planes. Extrapolation of the data of Figure 3-3 to construct a reasonable surface may be done in various ways. Figure 3-4 illustrates a construction for the part of the surface above the σ_3, σ_2 plane, based on use of the Mohr envelope.

---

*It should be recalled that we are considering engineering stresses only. Due to large deformations, the stress state may be changed such that the test points do not fall exactly on the coordinate planes.

The data obtained in this study do not fit any of the classical analytic failure theories with convincing accuracy. At best, the limited data on the planes in the +++ octant suggest a maximum tensile stress criterion, and the shear and compression data extrapolated into the +-- octant are not in gross disagreement with a linear internal friction criterion. However, agreement with an analytically formulated criterion is valuable but not critical for design purposes and this initial, pragmatic mapping of the surface produces in principle the desired engineering information. With connective theory relating the mechanics of failure to the shape of the failure surface, a confident reduction in engineering detail required for the mapping, in addition to an insight into material strength optimization, would result. This is an ultimate objective of the work in progress.

Experimental tests of PBAA, carboxy-terminated and Nitroplastisol propellants in compression, shear and tension have indicated that the general failure behavior of these propellants is not widely at variance with that depicted in Figures 3-3 and 3-4. Of course, there are differences in stress magnitudes at failure and in the envelopes for different strain rates and temperatures. It is noteworthy that the shape of the failure surface, as well as its spatial location, can change significantly with temperature for a single formulation of the propellant (e.g., Ref. 1, 11).

It should be kept in mind that the above data and their interpolation lack the support of a precise stress analysis. Not withstanding this deficiency, the information as presented exemplifies a better engineering tool for rocket motor evaluation than previously has been available. The obvious limitations of the data emphasize the need for additional experimental points on the failure surface off the coordinate planes and practical stress analysis methods that account for intrinsic and deformational nonlinearities in propellant behavior.

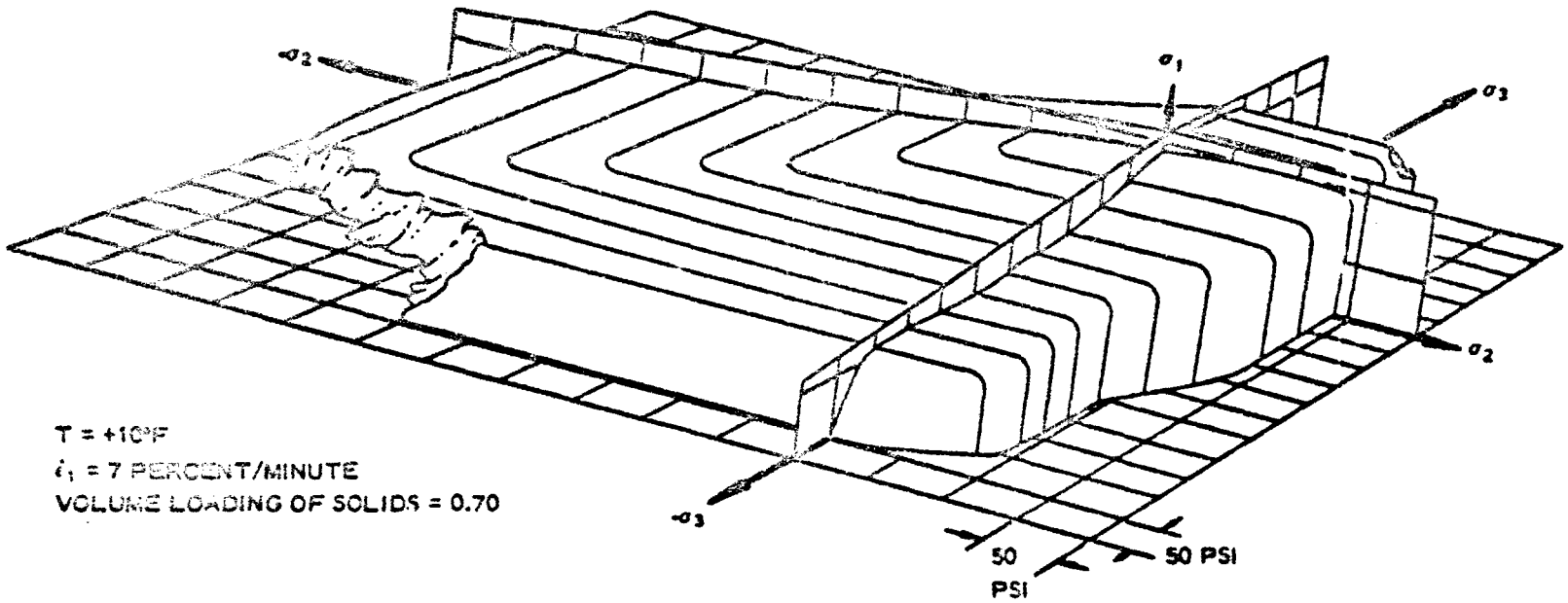

Figure 3-4 Failure Surface for PBAN Propellant

3.3 FRACTURE PROPAGATION STUDIES

Fracture propagation in viscoelastic materials is regulated by their strength, the driving stresses and the energy absorbed in the fracture process. Each of these parameters is time and temperature dependent. This section describes the results of a study of crack propagation in biaxially stressed plates of PBAA propellant.

Current theories of fracture in polymers generally agree that crack extensions occur in discrete jumps of a distance δ which occur in a time t_δ. δ is a fixed dimension characteristic of the material. It is proposed herein that t_δ is a particular function related to the measured failure properties of the propellant and the driving stress. The time dependence of the function at various temperatures is derived and compared with experimental data for crack extension and crack velocity under conditions of time-varying driving stress. Excellent agreement between measured and predicted crack extensions was observed.

3.3.1 Analysis

The first criterion for the elastic fracture of rubbery materials resulted from an extension of the Griffith brittle fracture theory (Ref. 13) by Rivlin and Thomas (Ref. 14). Greensmith and Thomas (Refs. 15, 16, 17, 18) observed that, under equilibrium conditions, the energy absorbed by fracture could be approximated by

$$T = W_d d \tag{1}$$

where W_d is the critical strain energy density for failure in an initially uncracked specimen and d is twice the radius of curvature of the crack tip, Williams (Refs. 19, 20) applied the concept of the Griffith criterion to prediction of crack initiation and propagation in rubbery materials along similar lines of inquiry.

Williams' model of the crack postulated that the crack extended in discrete jumps of distance δ. In an infinite sheet stressed biaxially in tension, the stress at the tip of a crack of initial length 2b in the sheet is given by

$$\sigma_c \approx 2\sigma_0 \sqrt{\frac{b + m\delta}{2\delta}} \tag{2}$$

where σ_0 is the stress normal to the crack's axis at a distance and m is the number of jumps by which the crack has extended. The crack tip radius of curvature d/2 is identified in Equation (2) as δ. According to this relationship, the stress increases with crack length $b+m\delta$ and the crack velocity may

be expected to increase with its extension. Applying linear theory to the crack in a viscoelastic medium, Williams (Ref. 20) found expressions for crack velocity and extension with time. These expressions were based on the assumption of a maximum strain rupture criterion.

Recent work at LPC (Refs. 21, 1, 22) has shown that gross failure in propellant conforms to a maximum tensile stress failure criterion. Application of the stress criterion to the crack extension problem is, therefore, appropriate.

Only a special case of crack extension will be treated here: namely, when the crack tip stresses are not a function of crack length. Equation (2) above describes the stresses at the crack tip when the crack is small with respect to the size of the plate and far removed from its boundaries. When the crack is long with respect to the sheet width (perpendicular to the crack), the crack tip stresses do not change materially with extension. In practice this condition is achieved by clamping a long plate between rigid boundaries and slitting it a distance about equal to its height (or gage length). The slitted specimen is then extended normal to the slit, which can be considered to be an initial static crack. The critical dimensions of the crack influencing its propagation under these boundary conditions are its tip radius and the jump distance δ.

The crack extension model to be considered here follows that proposed by Rivlin, Thomas, Williams, et al, in that extension of the crack occurs in discrete jumps of distance δ. When the extension δ occurs in a time t_δ, the crack velocity $\dot{S}$ is given by the identity

$$\dot{S} \approx \frac{\delta}{t_\delta} \tag{3}$$

The variation of $\dot{S}$ with material properties and crack driving stress is specified by the variation of t_δ with these properties. δ is a constant characteristic dimension for the material thought to be related to its microstructure.

Extending consideration of Equation (3) for the viscoelastic case, we postulate that $\dot{S}(t)$ is proportional to the time to failure observed in tests of the material and inversely proportional to the driving stress. The particular test mode of interest herein is constant strain rate. When measured at constant strain rate, the rupture stress in propellant varies with the time to rupture of the sample as shown in Figure 3-5. The observed relationship may be approximated analytically by

$$\sigma_r(t) \approx B(1/t)^m \tag{4}$$

over wide ranges of time. Assuming gross rupture behavior varies identically with the microscopic fracture, the variation of $t_\delta(t)$ with time may be expressed as

$$t_\delta(t) \approx \frac{B}{k_1}(1/t)^m \tag{5}$$

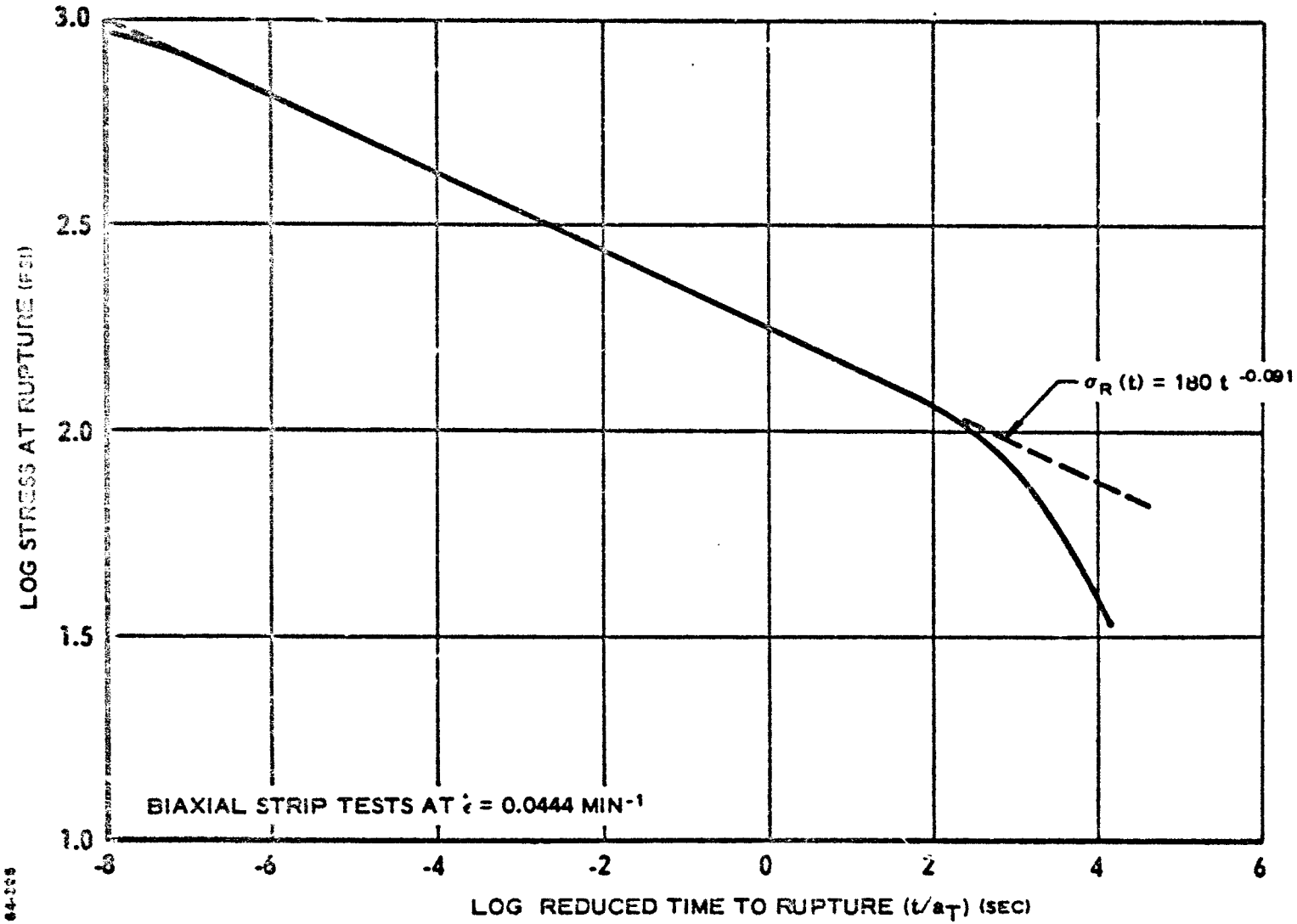

Figure 3-5 Stress at Rupture versus Reduced Time at 70°F, LPC-543B Propellant, Batch 4404

where k_1 is an undetermined constant. The driving stress in the sheet under constant strain rate conditions may be approximated by

$$\sigma_0(t) \approx \frac{A\dot{\epsilon}}{1-n} t^{1-n} \tag{6}$$

when the relaxation modulus is linear with time in log-log coordinates. n is the slope of the log modulus curve, A is its intercept at t = 1, and $\dot{\epsilon}$ the strain rate. The relaxation modulus for the propellant used in these experiments is shown in Figure 3-6.

Postulating that

$$t\delta(t) \approx \frac{B(1/t)^{-m}}{k_1 \frac{A\dot{\epsilon}}{1-n} t^{1-n}} \tag{7}$$

it follows that

$$\dot{S}(t) \approx \frac{k_1 \delta A\dot{\epsilon}}{B(1-n)} t^{1-(m+n)} \tag{8}$$

and, integrating

$$S(t) \approx \frac{k_1 \delta A\dot{\epsilon}}{B(1-n)(2-m-n)} t^{2-(m+n)} - c \tag{9}$$

S(t) plotted versus $t^{2-(m+n)}$ should yield a linear relationship for the crack propagation model described by Equation (9). The crack extension with time is an experimental observable.

According to the work of Williams (Ref. 20), the dimension δ may be estimated as the critical radius of the crack tip. The measured critical crack tip diameter is approximately 0.02 inch and, hence, $\delta \approx 0.01$ inch. The value of δ for gum rubbers was estimated to be of this order by Thomas (Ref. 17). The constants k_1 and c are, therefore, the only undetermined constants.

3.3.2 Experimental Results

Fracture extension experiments were made using biaxial strip test specimens of PBAA propellant (LPC-543B, Batch 4404). The specimens were machined plates (10 x 2.25 x 0.13 inches) with in situ bonded wooden restraints along the long edges. Fracture specimens were slit with a razor blade along their midlines a distance of 2.4 inches from one edge. The specimens were tested in an Instron tester at a crosshead speed of 0.1 inch/minute to obtain a strain

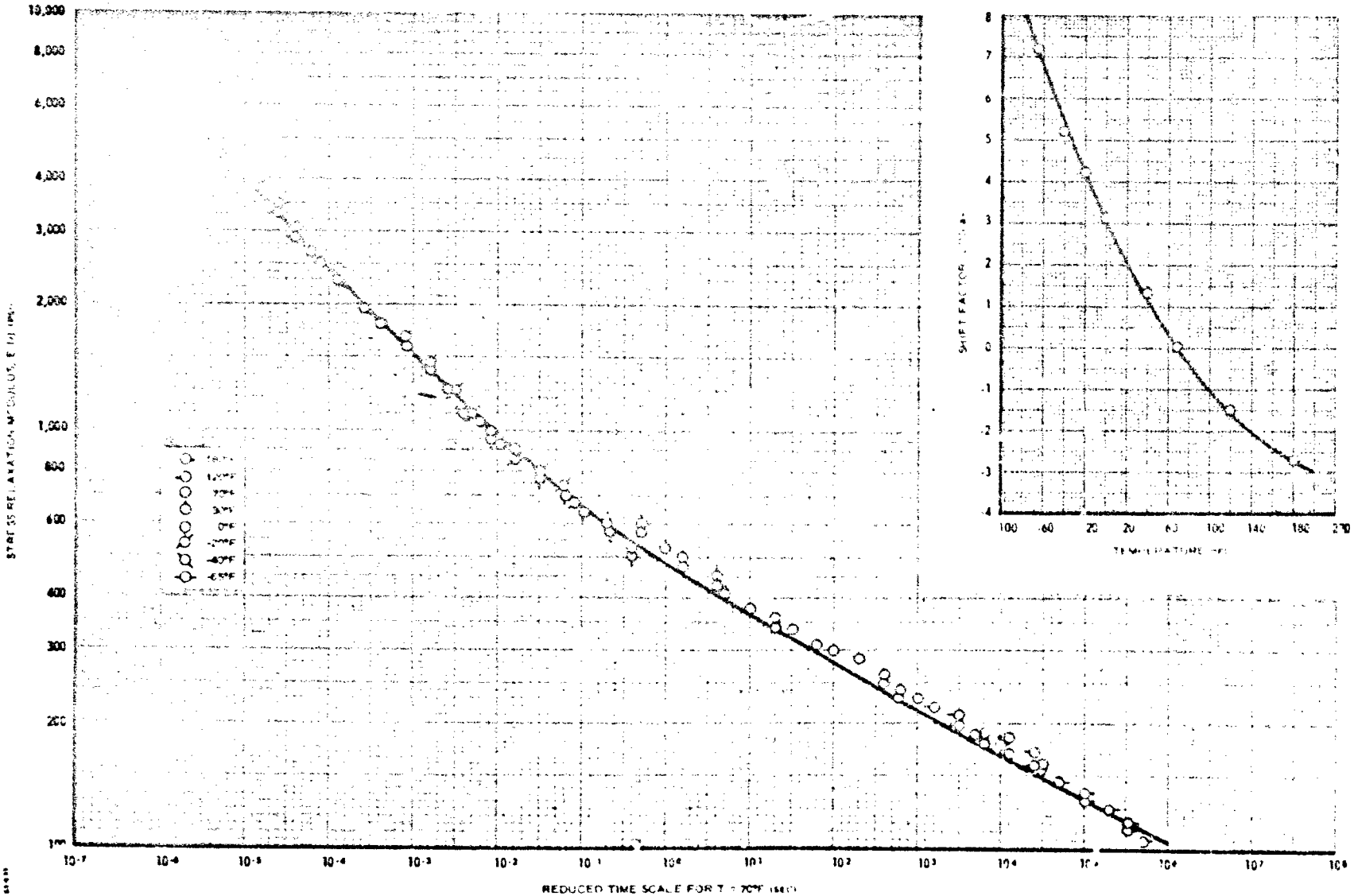

Figure 3-6 Master Stress Relaxation Modulus and Shift Factor, Propellant LPC-543B (Batch 4404)

rate of 0.0444 min^{-1} in the body of plate. The ultimate property data shown in Figure 3-5 were obtained in tests of identical but unslit specimens at the same strain rate. The stress relaxation modulus data shown in Figure 3-6 were obtained in tests of uniaxial wooden tab-end tensile specimens tested in accordance with the ICRPG test procedure (CPIA No. 21, 1963). The data of Figures 3-5 and 3-6 are presented in reduced variable form, using the shift factor shown on Figure 3-6.

Crack extensions were measured at 0.1 inch intervals by visual observation of the crack through a magnifying glass. Typical data are shown in Figure 3-7. Measured crack extensions are shown plotted versus $t^{2-(m+n)}$ in Figure 3-8. The exponents n and m were measured from shifted data. The slopes were taken in the time region within which the experiment was done and the intercepts at various temperatures determined graphically.

3.3.3 Discussion

The data of Figure 3-8 show excellent agreement with the postulated time variation of crack extension. Taking the constant of integration in Equation (9) as

$$-c = \frac{\xi A \dot{\epsilon} \, t_i^{2-(m+n)}}{k_1 B(1-n)(2-n-m)}$$

where t_i is the time of crack initiation and $\xi = 0.01$, the undetermined constant k_1 is found to be 165 for the data presented. Crack velocities predicted by Equation (8) are of the order of 1.0 to 2.5 inches per minute, depending on crack length and test temperature, in excellent agreement with the experimental observations.

The agreement between the crack velocity and extension relationships, Equations (8) and (9), apply only to the constant strain rate test mode for initially quite long cracks. Further analysis is required for this test mode for cracks initially small with respect to plate dimensions. Small cracks can be expected to accelerate rather rapidly with time, because of the high stress concentrations at their tips (cf. Equation 2).

The failure properties of propellant (i.e., those shown in Figure 3-5) do not shift linearly with varying strain rate. Extension of $\dot{S}(t)$ and $S(t)$ relationships to consideration of crack extension at varying strain rate requires, therefore, measurement of the failure properties at various strain rates.

Crack propagation under other conditions of time varying stress is a matter of both general and specific interest. The observed slopes of rupture stress versus time curves for constant stress and constant strain tests of the propellant used in these tests is approximately the same as the slope of the curve shown in Figure 3-5. The analysis for $S(t)$ appropriate to the constant

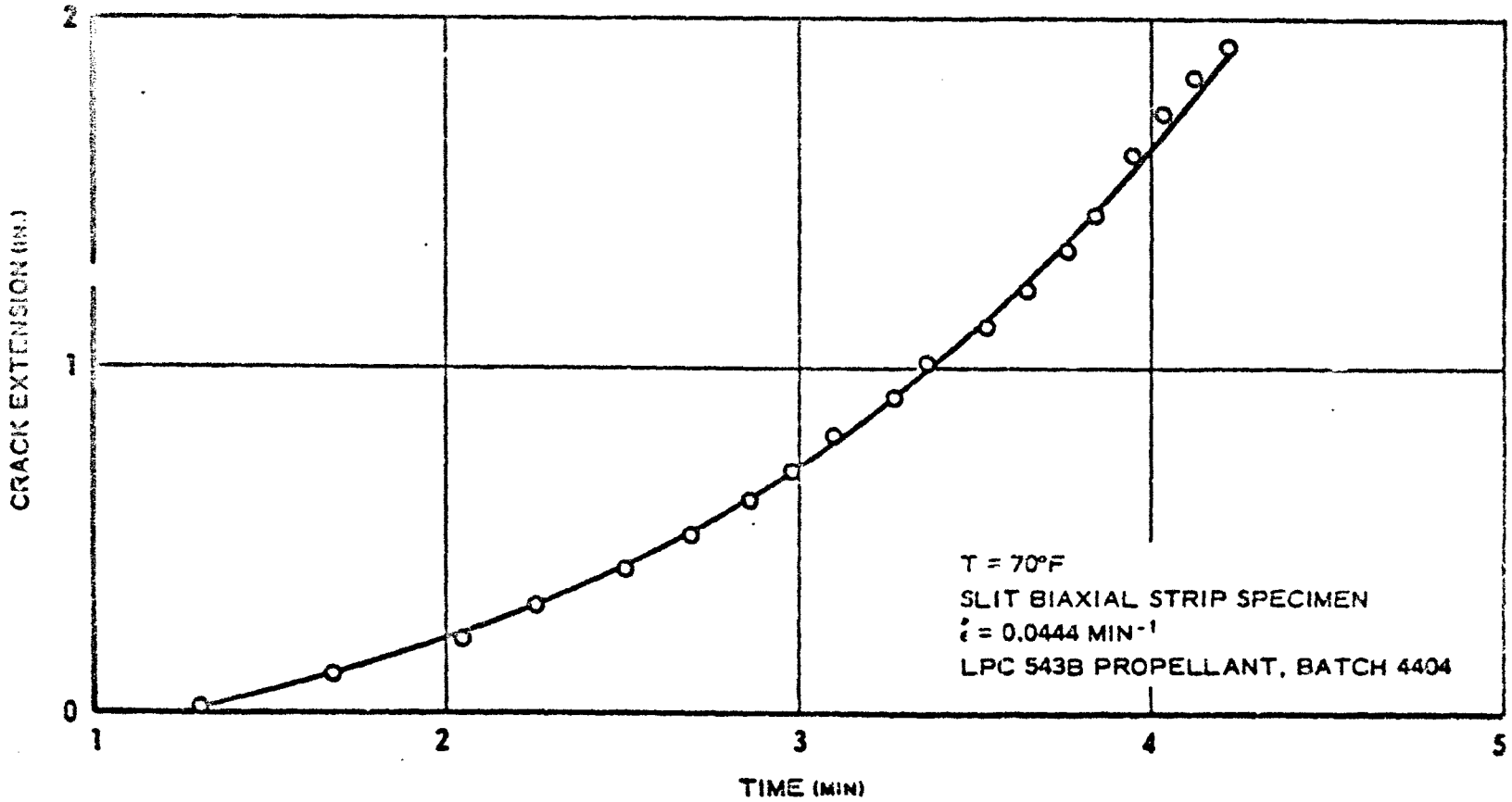

Figure 3-7 Crack Extension versus Time

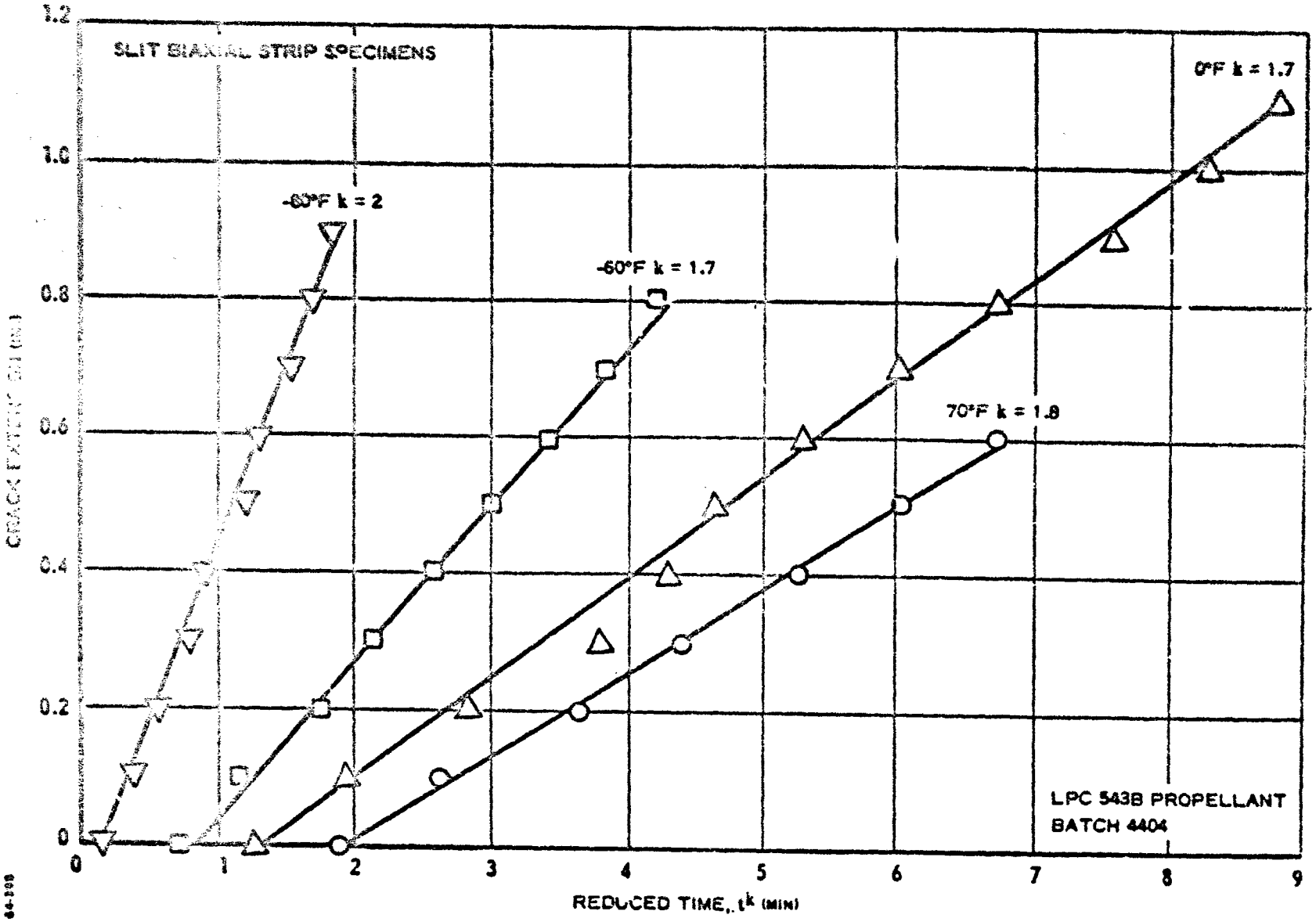

Figure 3-8 Crack Extension versus Reduced Time

stress test condition predicts that the cracks propagate at a nearly uniform velocity. Under constant strain conditions, a crack started by the initial straining should decelerate and stop. Both predictions are in accord with data obtained in single tests. Further analysis and experimentation defining such behavior is recommended.

The agreement between the analytical predictions and experimental observations is considered excellent. Extended efforts with greater attention to rigorous theoretical development of the analysis is recommended. Future engineering applications of fracture mechanics analysis include, for example, rocket grain defect analysis and prediction of threshold conditions for catastrophic grain cracking. Extension of fracture mechanics analysis to the energetics of fracture extension is also a potentially fruitful method for studying the relationships among binder molecular structure, interphase adhesions, solids particulate properties, and intrinsic propellant strength.

Section 4

DYNAMIC PROPERTIES

4.1 INTRODUCTION

Current areas of interest are as follows:

- Determination of viscoelastic and thermoelastic properties of propellant and associated materials, using cyclic techniques
- Investigation of propellant mechanical and thermal response to sustained cyclic loading
- Determination of vibration failure modes in solid propellants and correlation of propellant microstructure with vibration failure resistance

Previous work at LPC (Ref. 21) has demonstrated the equivalence of transient and dynamic physical property characterization techniques for practical propellants. The problems introduced by the nonlinear viscoelastic behavior of highly loaded propellant systems (e.g., strain-induced nonlinearity and thermal degradation) were examined by means of large deformation dynamic tests. In addition, viscoelastic heating effects were studied; and the possibility of regenerative heating, leading to thermal and mechanical instability in solid propellant systems subjected to sustained cyclic loading, was deduced on theoretical grounds. The current work is directed at the extension and amplification of these results.

Experimental investigations are discussed in which propellant dynamic shear and bulk properties were measured with the small deformation piezoelectric devices previously described (Ref. 1). Shear moduli of PBAA and PBAN propellant and cured binder are presented and compared with linear thermal expansion measurements of glass transition temperature obtained for similar propellants. Analysis techniques and calibration results are discussed for the dynamic bulk modulus device.

An experimental investigation of propellant thermomechanical response to sustained cyclic inertial loading was completed. Experimental results are presented, noting that they are in qualitative agreement with theoretical predictions. In particular, jump instability caused by regenerative thermal and mechanical coupling was obtained experimentally. Also completed were experimental investigations of the transient thermoviscoelastic response under constant cyclic strain amplitude (fixed output) loading and with inertial loading. Experimental results are given including an investigation of cyclic degradation effects.

4.2 DYNAMIC VISCOELASTIC CHARACTERIZATION

4.2.1 Dynamic Shear Modulus

An apparatus for measuring viscoelastic response in shear and tension-compression modes at very small strains over a wide range of temperature and frequency was described in the first quarterly report (Ref.). Briefly, the device consists of a piezoelectric driver arranged to dynamically strain solid or liquid specimens with deformations of the order of 1 to 10 micro-inches. The specimen output force and phase relationship to the driving deformation are measured and are used, together with the measured specimen dimensions, to calculate dynamic viscoelastic properties of the specimen. The apparatus is presently being used to viscoelastically characterize a wide variety of propellants, binders and associated rocket motor materials.

Dynamic shear moduli of PBAA and PBAN propellants and cured binders have been obtained over a wide range of temperature and at frequencies from 20 to 1000 cycles per second. Storage and loss moduli (G' and G", respectively) are shown plotted versus temperature at several frequencies in Figures 4-1 and 4-2 for both the 84 percent solids loaded propellants and the cured binders. In addition, the "glass transition temperature region" as measured by linear thermal expansion coefficient techniques on similar propellant formulations is shown on each graph. Correlation of this temperature with the temperature region where the propellant dynamic properties become relatively independent of temperature and frequency was observed for Nitroplastisol propellant and binder in addition to the rubber-base propellants shown.

The data show the generally anticipated effect of the addition of solid filler to an elastomer. The viscoelastic transition region is significantly broadened and the moduli are increased particularly at higher temperatures. Characteristic regions, such as the loss moduli peaks and the low temperature limit where the response becomes frequency independent, are observed to shift slightly to higher temperatures with the addition of filler. This effect also occurs for the Nitroplastisol propellant and binder where the magnitude of the shift appears to be much more significant. The anticipated shift of the response curve to higher temperatures as the excitation frequency is increased is clearly evident for both sets of data. The generally lower characteristic temperatures for the PBAA as compared with the PBAN materials correlates well with the better low temperature physical property capability observed for PBAA propellants.

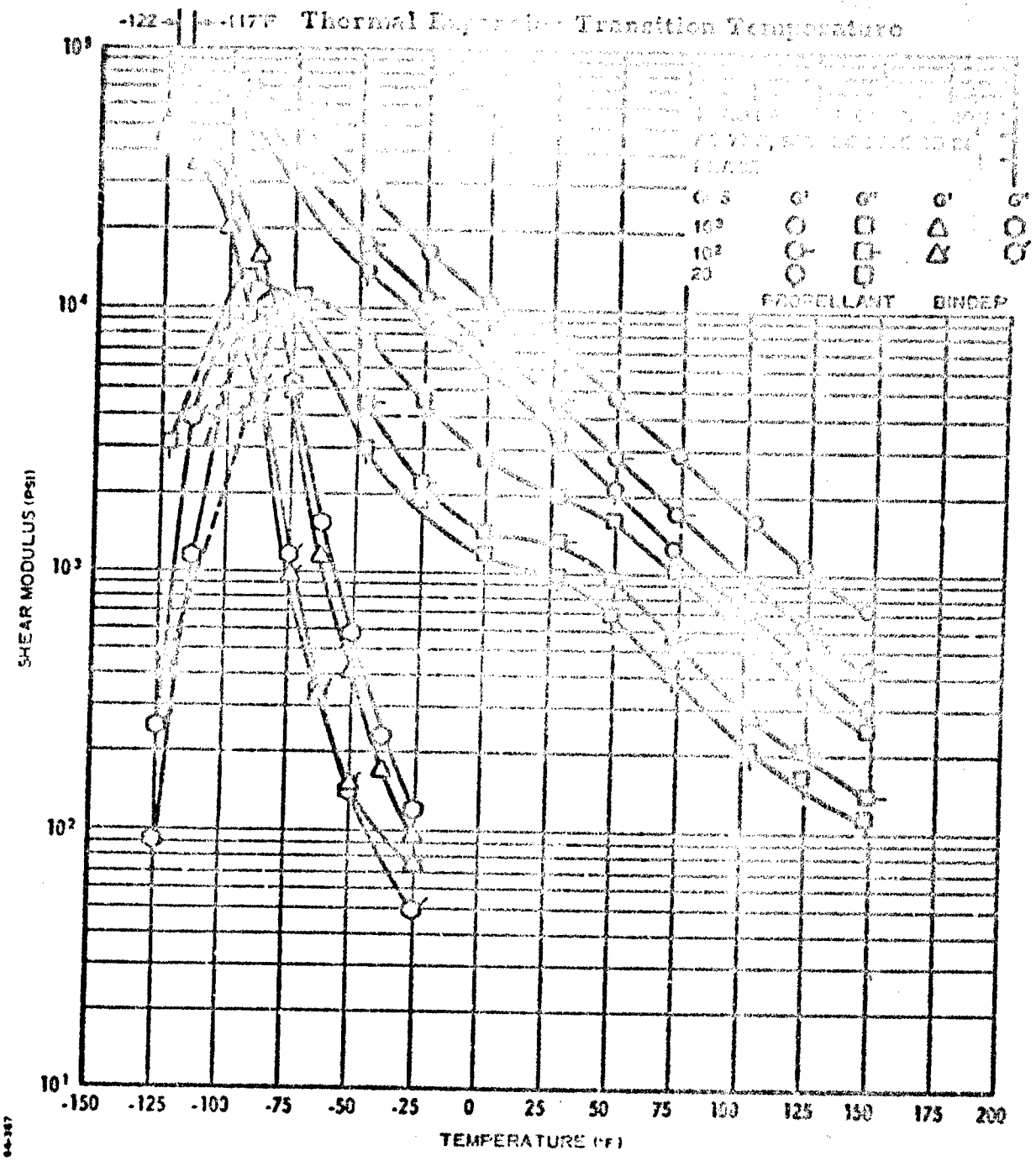

Figure 4-1 Dynamic Shear Modulus versus Temperature, PBAA Propellant and Cured Binder, 84% Total Solids Loading

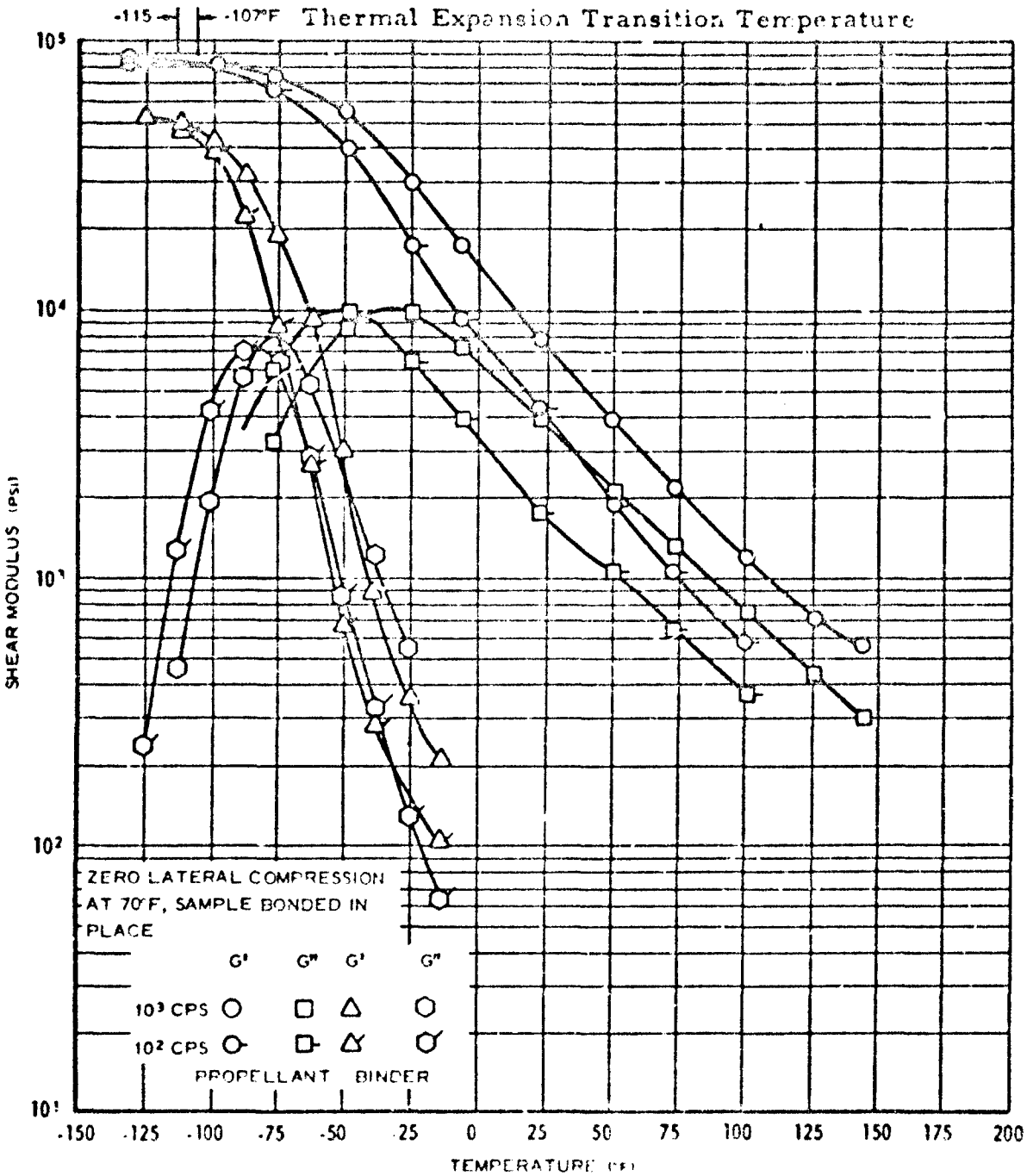

Figure 4-2 Dynamic Shear Modulus versus Temperature, PBAN Propellant and Cured Binder, 84% Total Solids Loading

4.2.2 Dynamic Bulk Modulus

An apparatus, similar to the dynamic shear modulus device (described in the last section) but designed to measure the dynamic bulk moduli of materials, is currently being evaluated. The apparatus contains a pressure cavity within which the specimen material is placed. The specimen is hydrostatically pressurized and a small sinusoidal pressure is superposed on the hydrostatic component by sinusoidally varying the volume of the cavity by means of a piezoelectric driver and piston arrangement (Ref. 1). The resulting sinusoidal pressure is measured and compared with the input volume change to compute bulk modulus properties of the confined material.

The device is presently being calibrated with standard fluids for eventual measurement of propellant properties. The calibration technique is as follows. The bulk modulus (K) is defined as

$$K = \Delta P / \frac{\Delta V}{V} \tag{1}$$

where V is the nominal cavity volume, ΔV is the dynamic volume change and ΔP is the resulting dynamic cavity pressure. Of major concern in the calibration process, particularly for high bulk modulus materials, is the effective bulk modulus or compliance of the constraining cavity. Clearly, for a real cavity with finite compliance, the input volume change will equal the sum of the sample volume change ΔF_ℓ and the cavity volume change ΔV_o, that is:

$$\Delta V = \Delta V_\ell + \Delta V_o \tag{2}$$

Since both the cavity walls and the constrained sample experience the same pressure variation ΔP (assuming that measurement frequencies are low enough to make pressure wave propagation effects negligible) we can define the sample bulk modulus K_ℓ and the effective cavity bulk modulus K_o as follows:

$$K_\ell = \Delta P / \frac{\Delta V_\ell}{V} \quad , \quad K_o = \Delta P / \frac{\Delta V_o}{V} \tag{3}$$

Combining these definitions with the volume relationship, Equation (2), results in

$$B_\ell + B_o = \frac{1}{\Delta P} \frac{\Delta V}{V} = B \tag{4}$$

where B_ℓ and B_o are the sample and cavity compliances, defined as reciprocals of the respective bulk moduli and B is the total measured compliance, the reciprocal of K in Equation (1). The output dynamic pressure ΔP and input dynamic volume change are linearly related to the apparatus output and input transducer voltages v_o and v_i as follows:

$$\Delta P = C_1 v_o \quad , \quad \Delta V = C_2 v_i$$

Thus, Equation (4) becomes

$$B_{\ell} + B_o = \left(\frac{C_2 v_1}{C_1 V}\right) \frac{1}{v_o} \tag{5}$$

Therefore, for constant input voltage, v_1, and constant cavity compliance, B_o, the sample compliance is linearly related to the reciprocal of the measured output voltage. Thus for a constant cavity compliance, the apparatus can be calibrated by defining the linear relationship of Equation (5) from measurements of samples with known bulk compliance.

A typical calibration curve is shown in Figure 4-3 for a single temperature and hydrostatic pressure. In general, the calibration curve will be a function of both temperature and hydrostatic pressure, the temperature dependence associated primarily with the input and output transducer coefficients and the pressure dependence associated primarily with a reduction of mechanical slack in the system as the hydrostatic pressure is increased.

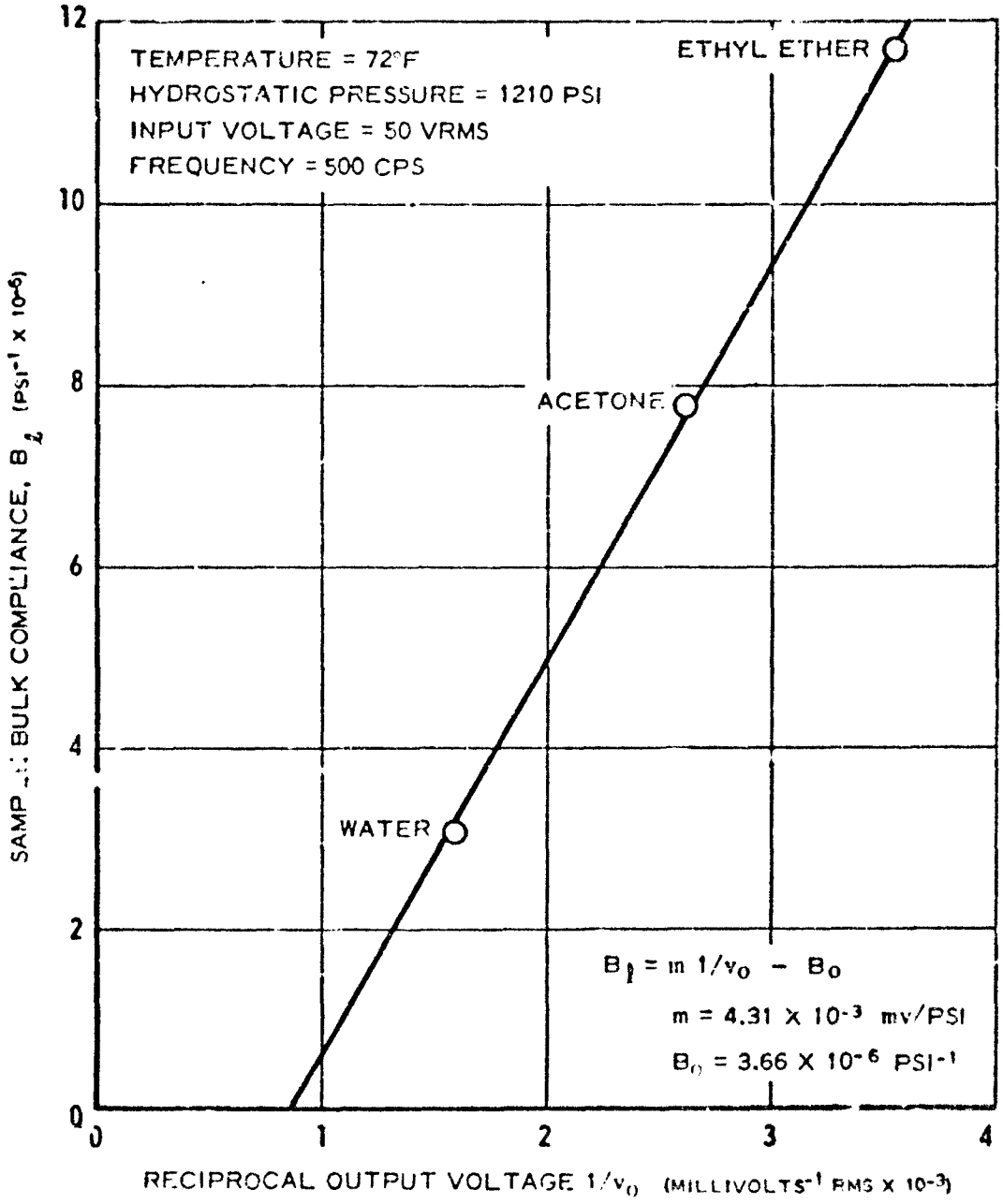

Figure 4-3 Calibration Curve Dynamic Bulk Modulus Apparatus

4.3 LARGE STRAIN DYNAMIC PROPERTIES AND VISCOELASTIC HEATING EFFECTS

Earlier work at LPC in this area consisted of analytical studies of the physical and thermal response of propellant to dynamic loading and experimental measurements of the dynamic response of propellants to large cyclic deformations (Refs. 21, 1). These investigations showed that a large temperature rise could be obtained and certain types of nonlinearities and degradation effects were found to be significant in the response of an 84 percent total solids-loaded propellant at strain levels of only a few percent.

Present work is examining the validity of using linear viscoelastic theory to predict the thermo-mechanical response of highly filled propellants. The ultimate aim is to develop engineering methods for the prediction of dynamic behavior and heating effects in real motor situations.

Additional experimental data are given from constant strain amplitude and inertial loading experiments on propellant. Regenerative coupling between generated heat and viscoelastic properties was obtained under inertial loading conditions and resulted in jump-instability, as predicted theoretically.

Further experimental data are presented from tests in which transient, dynamic thermoviscoelastic response, and degradation effects were studied under two types of thermal boundary conditions: (a) approximately adiabatic and (b), unidirectional heat flow to a constant temperature boundary.

4.3.1 Experimental Techniques

Propellant specimens were subjected to steady-state sinusoidal shear displacements, as shown in Figures 4-4 and 4-5. Two loading conditions were investigated: (1) output rigidly connected to force transducer (fixed output), and (2) output inertially loaded by large mass.

For the first loading condition, the input strain and the output force were measured together with the phase relationship between them. From these data, the dynamic shear storage and loss moduli were then obtained as previously described (Ref. 1). When an inertial loading test was made, the input strain amplitude (V_1) and the amplitude of the mass (V_m) were measured and also the phase difference (α) between them.

In both test modes, the specimen is driven at a constant sinusoidal displacement by means of a mechanical cam-drive arrangement. This is shown pictorially in Figure 4-6, arranged for an inertial loading test. The milling machine, shown at the right of the photograph, actuates a cam and cam-follower arrangement to drive the propellant shear specimen shown in the center of the photograph. Return force for the cam-follower is supplied by the compression

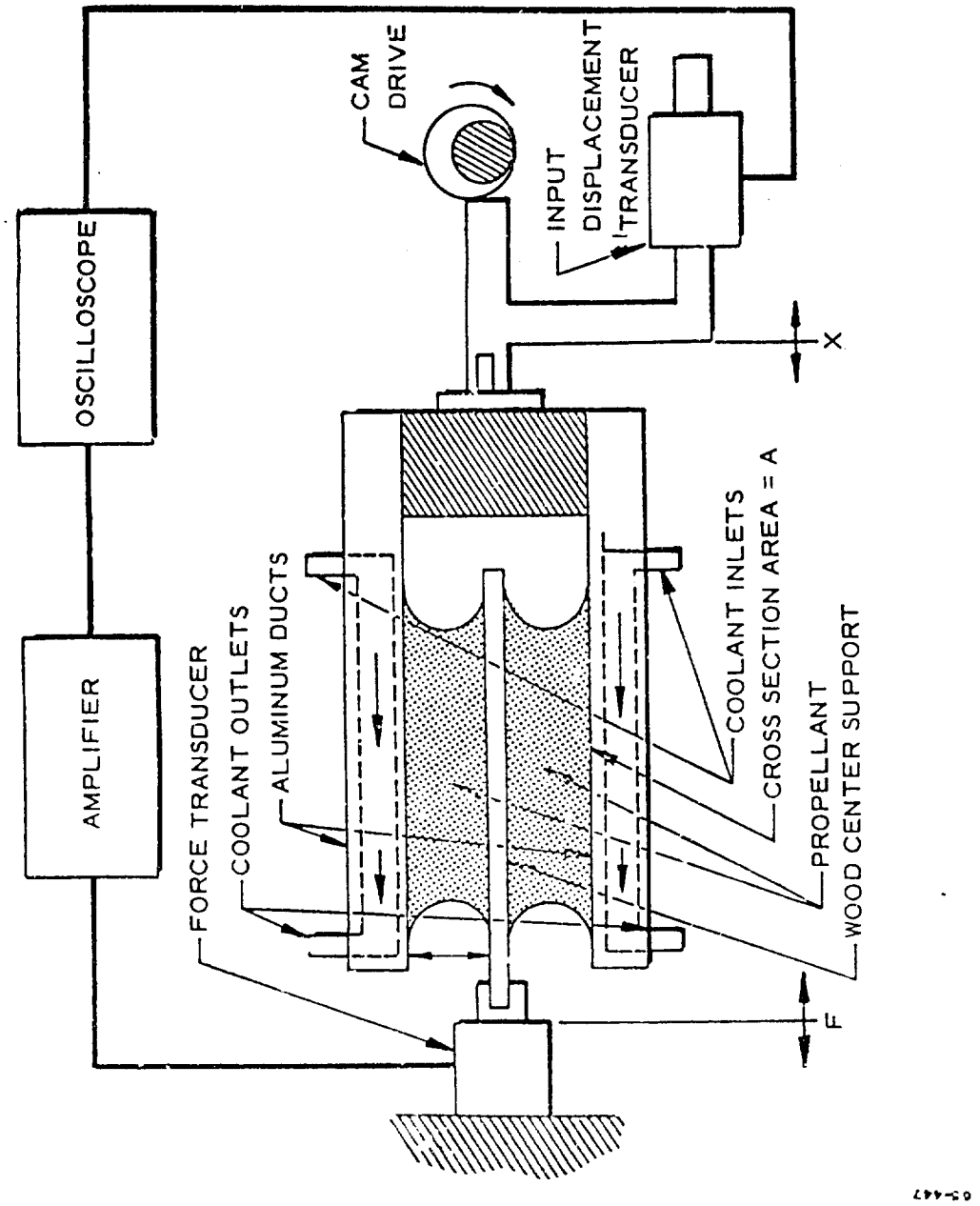

Figure 4-4 Schematic of Constant Shear-Strain Amplitude Test Device

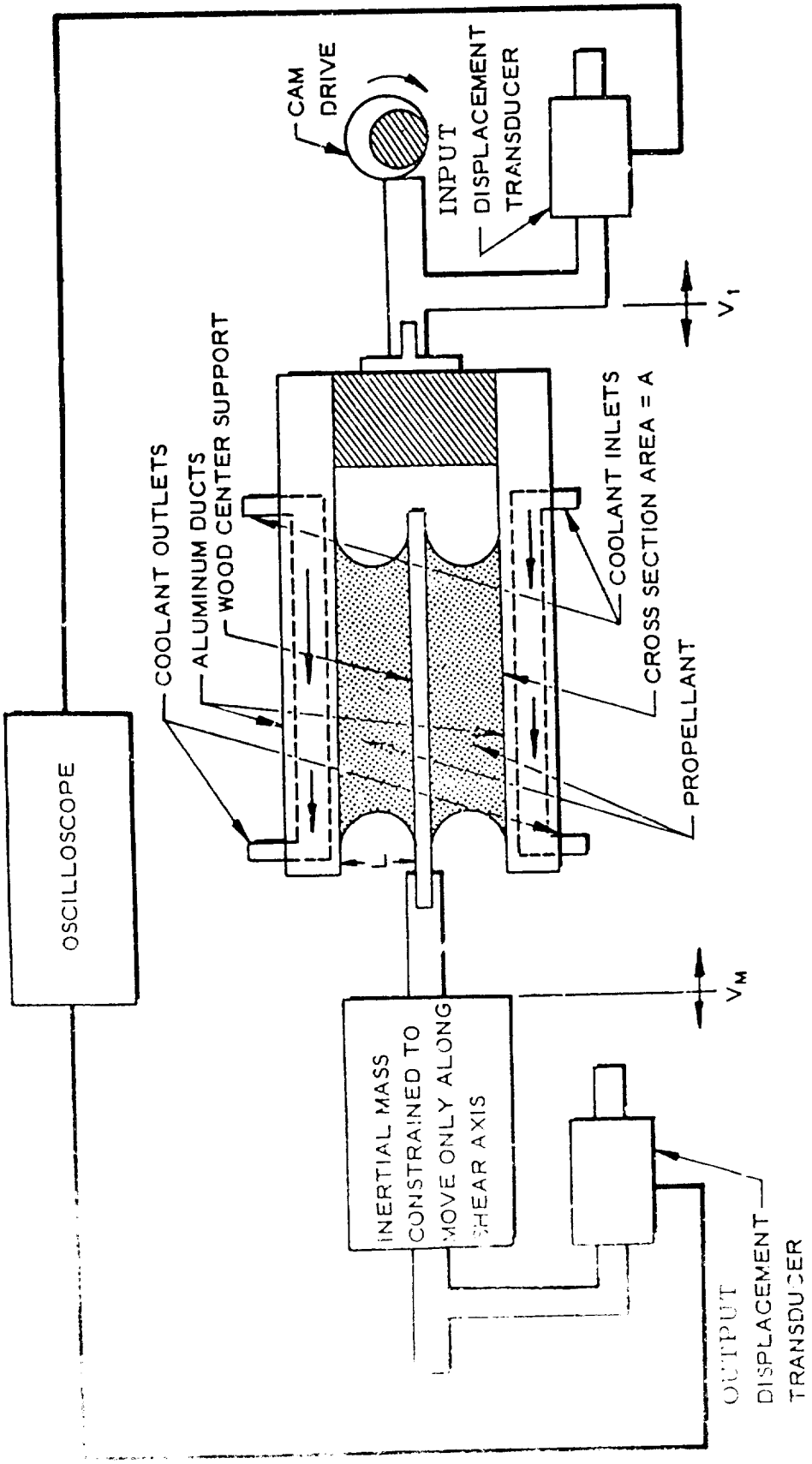

Figure 4-5 Schematic of Inertial Test Device

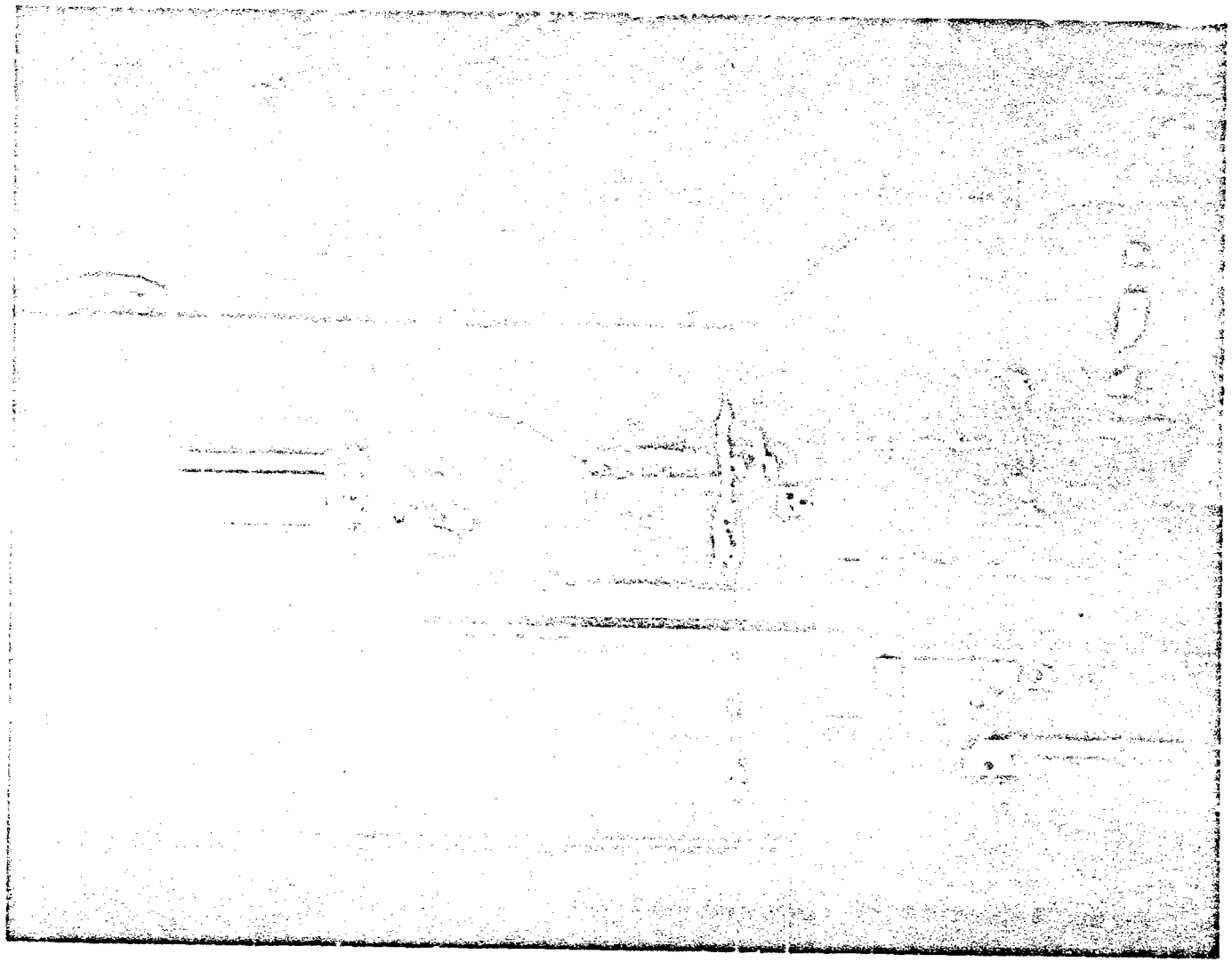

Figure 4 -6 Vibration Test Apparatus

LOCKHEED PROPULSION COMPANY

spring between the driver shaft guides. Input motion is measured at the sample supports by a potentiometer-type linear motion transducer. The center support of the double-lap shear specimen is attached to a loading shaft constrained to move only along the axis of shear by a set of rectangular linear motion bearings. The inertial mass is clamped to the loading shaft and is adjusted by addition or removal of weights. The sliding friction of the arrangement when fully loaded is only a few ounces. Output motion is measured at the sample support by another potentiometer-type linear motion transducer.

For the fixed output test, the inertial loading system is replaced by a rigid force-measuring cell to which the specimen is attached (Ref. 21).

The excitation frequency is changed by varying the cam revolution speed in discrete steps from 1.3 to 45 cycles per second. The input displacement amplitudes are controlled by interchanging driver cams.

Specimens were prepared by bonding milled propellant bars to the support members with epoxy adhesive. The semicircular fillets shown in the figures (4-4 and 4-5) were machined into the propellant bars to prevent specimen cracking in the regions of high stress at the specimen corners. All tests were performed with the outer supports constrained to prevent lateral strain and standardize the test geometry.

Two thermal boundary conditions were investigated. The first was an approximation to unidirectional heat flow laterally outward from the double-lap shear center support, and the second was an approximation to adiabatic conditions. Figures 4-4 through 4-5 illustrate the unidirectional heat flow experimental arrangement. In application, all exposed propellant surfaces were thermally insulated with a soft foam-rubber material so that the majority of the heat generated in the propellant was conducted laterally away from the low thermal conductivity center support member to the metal side supports which were maintained at constant temperature by circulating fluid. An approximation to adiabatic conditions was achieved by replacing the conductive metal outer supports with wood, a relatively low-conductivity material, and insulating all surfaces with foam-rubber material. The temperature distributions throughout the specimens were monitored with small thermocouples imbedded directly in the propellant or support material.

4.3.2 Dynamic Inertial Loading Tests

An interesting prediction obtained from the analysis of the inertial loading problem was that regenerative coupling between the temperature-dependent properties and the generated heat could lead to an instability with a consequent large increase in temperature and output amplitude, and a possible propellant failure. This analysis and the calculated response curves were given in the previous quarterly report.

Experimental data confirming the existence of this response instability were obtained during the present reporting period. Typical experimental results are presented in Figures 4-7, 4-8, and 4-9. The data represent response parameters at each frequency immediately after vibration is started and before significant heating has occurred (isothermal response) and also the response after sufficient time to attain thermal equilibrium in the shear specimen with isothermal boundaries (equilibrium response). The theoretical response curves for the steady-state amplitude ratio and insulated surface temperature are reprinted in Figures 4-10 and 4-11 from the first quarterly technical report (Ref. 1) for qualitative comparison. The theoretical curves predict response for a hypothetical propellant with an isothermal complex shear modulus log-log slope of 0.30. Quantitative comparison of the experimental data with theoretical prediction based on measured propellant properties has been completed (with reasonably good agreement found) and will be presented in a subsequent report.

Interpolation between the experimental data points presented in Figures 4-7 through 4-9 are based upon the theoretical predictions. The experimental frequencies which can be used are limited by the belt-gear drive mechanism of the milling machine used for the vibration tests.

Of particular interest is the double-valued response observed in the steady-state equilibrium response at 660 rpm for the 0.050-inch peak input displacement. It should be emphasized that each equilibrium data point represents the sample response or temperature after equilibrium has been attained at the particular vibration frequency. This vibration time can vary from 20 minutes to over one hour for the test configuration used. For example, the test sequence for the 0.050-inch peak displacement, equilibrium tests was as follows.

With the sample initially at room ambient temperature, vibration was begun at 210 rpm and continued until thermal (and mechanical response) equilibrium was attained. The excitation frequency was then immediately raised to 325 rpm and maintained until a new equilibrium was established and so forth, monotonically increasing the excitation frequency in steps and allowing the specimen time to reach equilibrium at each frequency. After the maximum frequency equilibrium, the frequency was monotonically decreased in steps, again allowing equilibrium to be attained at each frequency. During the increasing frequency sequence, the response parameters reached equilibrium at the lower 660 rpm data point for amplitude ratio, insulated surface temperature and phase angle. However, the system attained equilibrium at the upper branch point for the decreasing frequency sequence. Prolonged equilibrium vibration at this upper branch point resulted in eventual specimen failure in the form of a crack propagating along the direction of shear and at the insulated surface. Inspection of the failure indicated that the crack initiated in the specimen center (the highest temperature region) and propagated outward toward the semicircular end fillets.

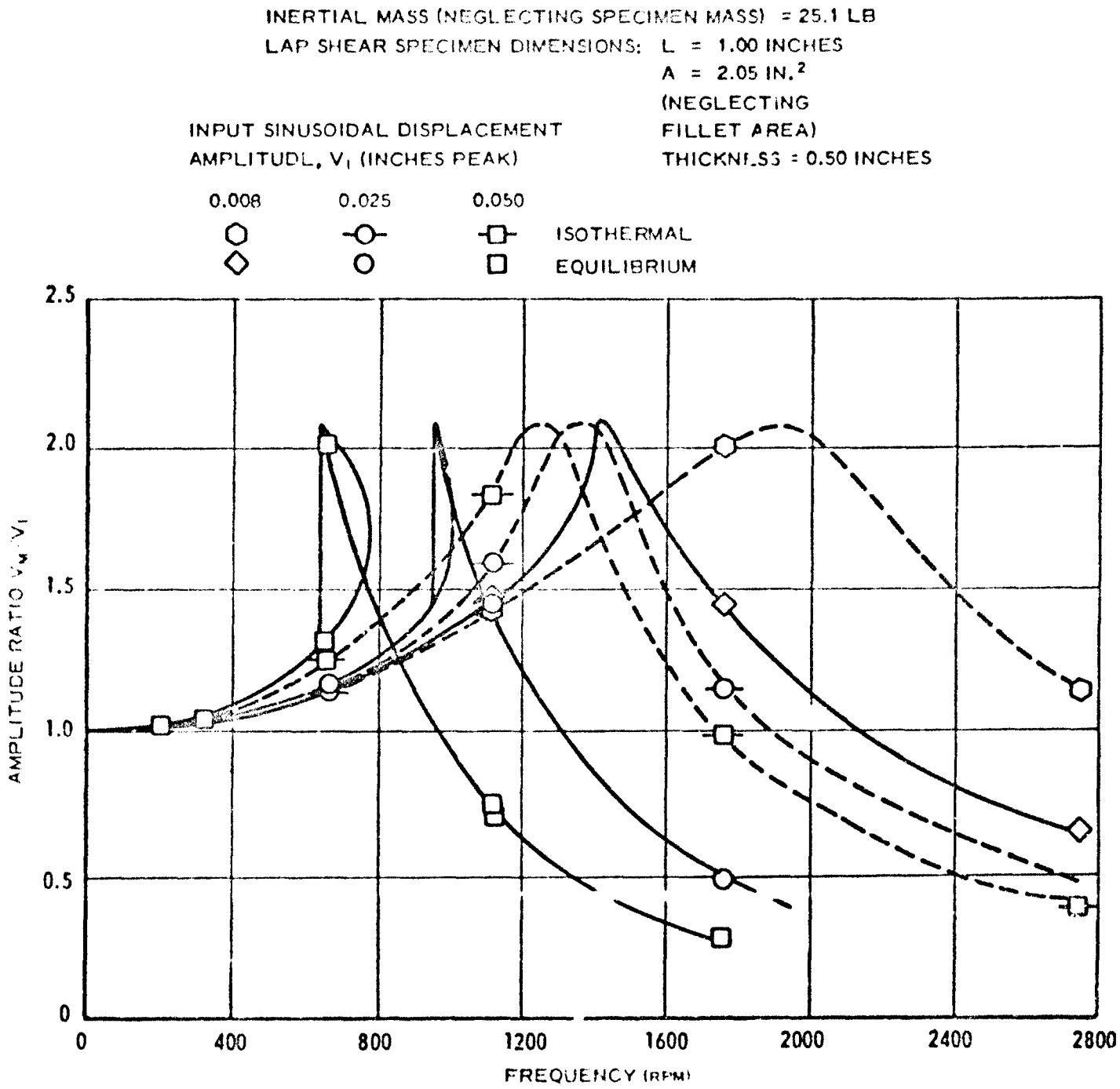

Figure 4-7 Experimental Displacement Amplitude Ratio, PBAA Propellant, Batch 2916

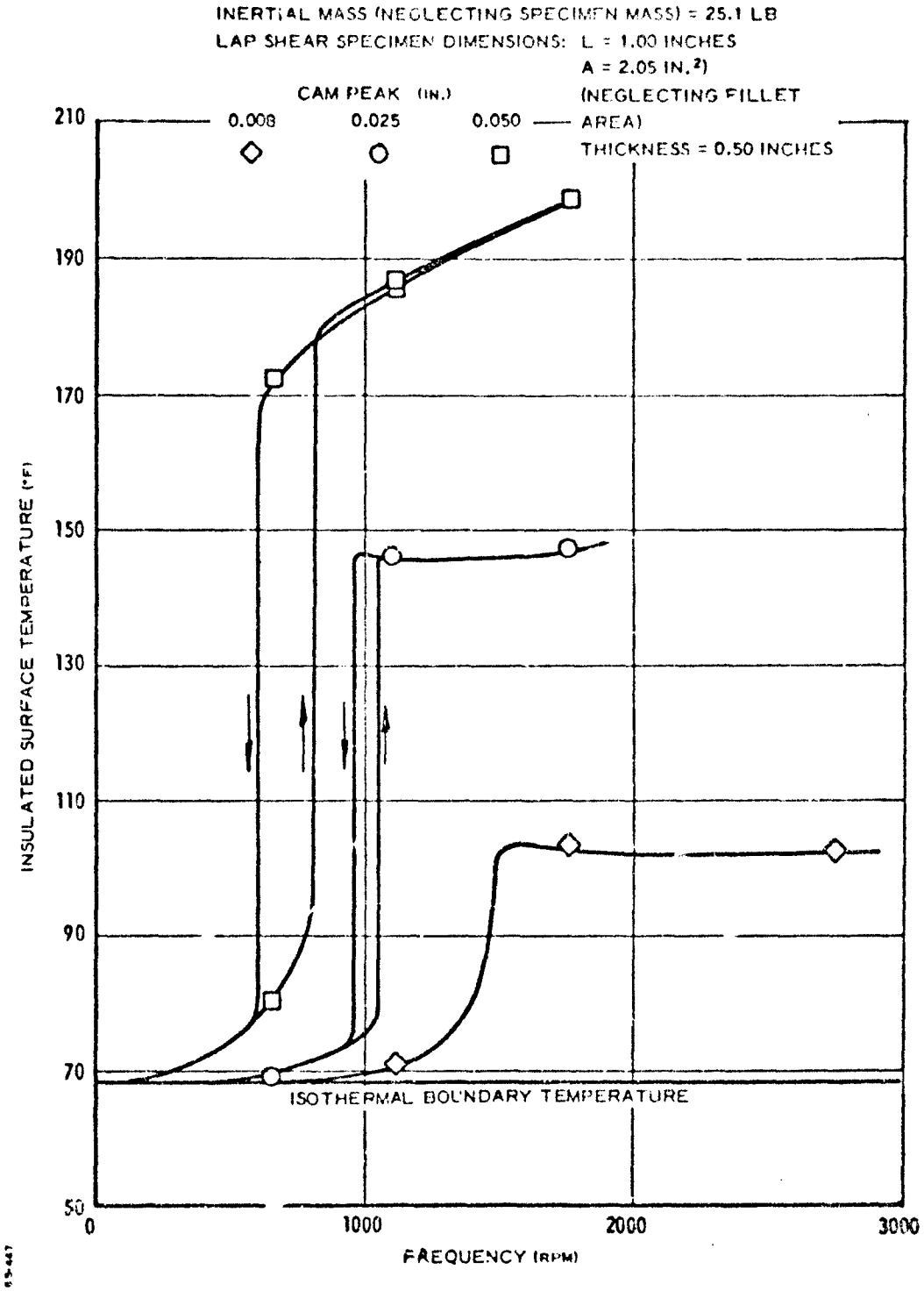

Figure 4-8 Experimental Steady-State Temperature at Insulated Surface, PBAA Propellant, Batch 2916

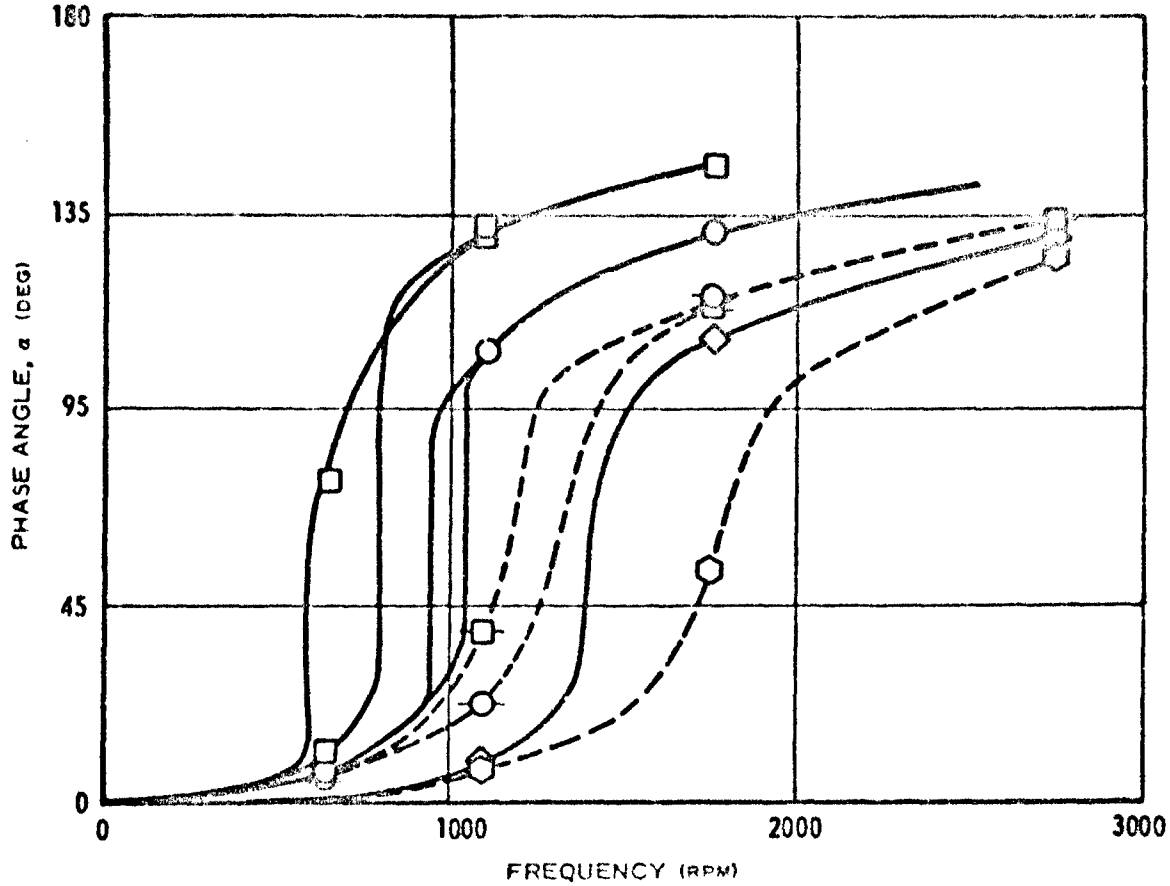

INERTIAL MASS (NEGLECTING SPECIMEN MASS) = 25.1 LB
LAP SHEAR SPECIMEN DIMENSIONS: L = 1.00 INCHES
A = 2.05 IN.^{2}
(NEGLECTING FILLET AREA)
THICKNESS = 0.50 INCHES

INPUT SINUSOIDAL DISPLACEMENT AMPLITUDE, V_I (INCHES PEAK)

0.008	0.025	0.050	
⬡	-○-	-□-	ISOTHERMAL
◇	○	□	EQUILIBRIUM

Figure 4-9 Experimental Displacement Phase Relationship, PBAA Propellant, Batch 2916

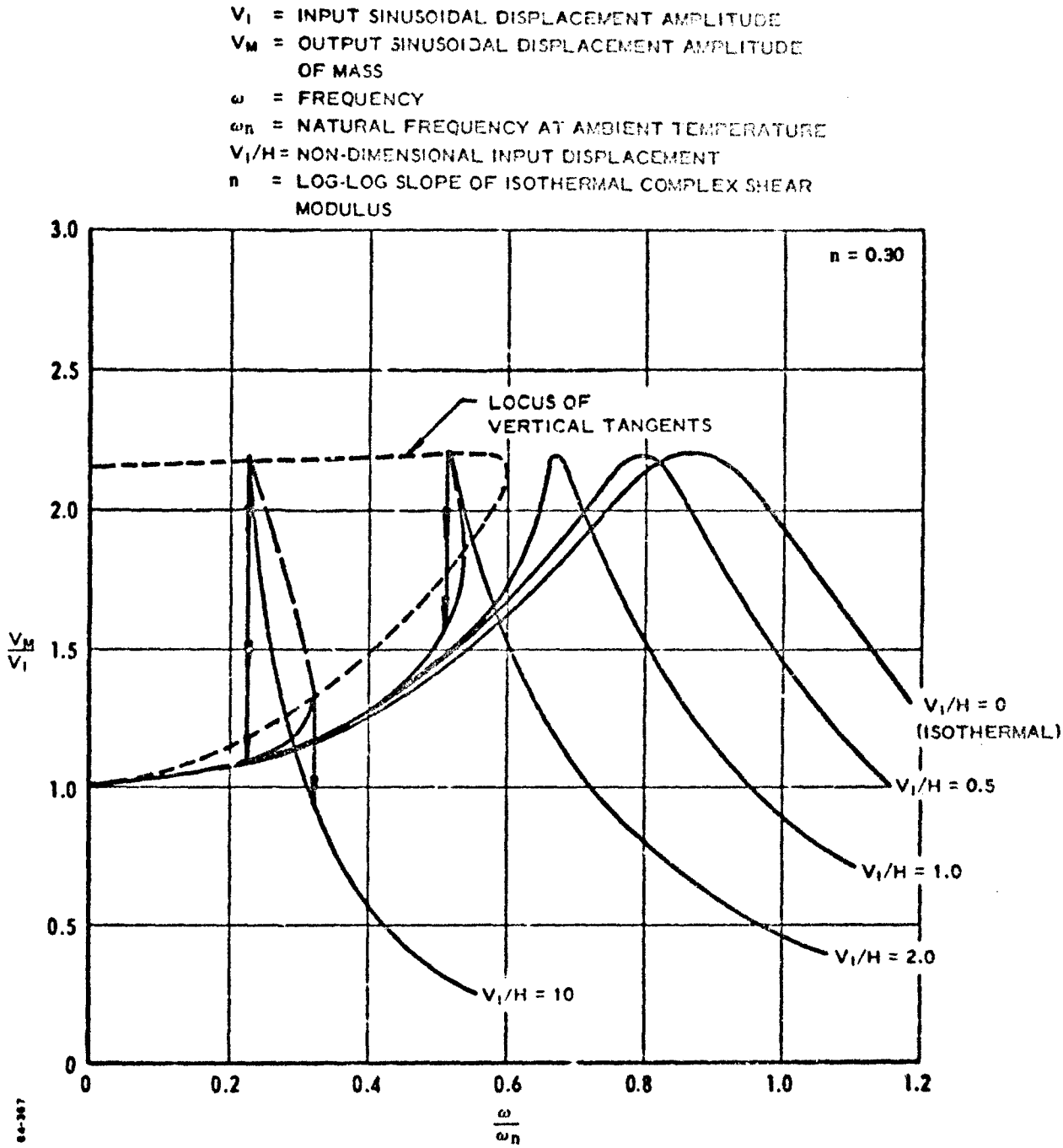

Figure 4-10 Steady-State Displacement Amplitude Ratio for n = 0.30

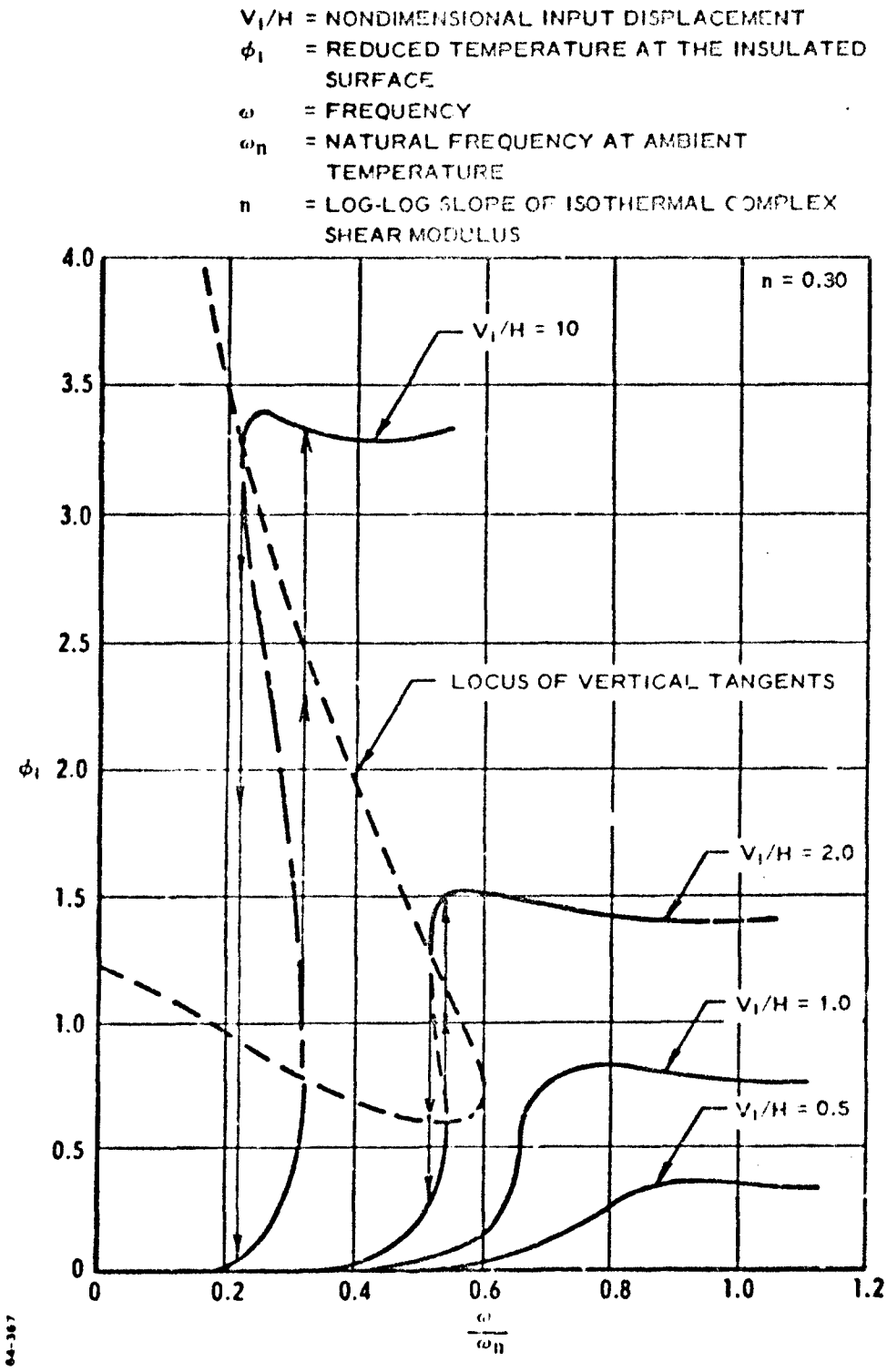

Figure 4-11 Steady-State Reduced Temperature at Insulated Surface for n = 0.30

As a practical result of these investigations, it is clear that rocket motor vibration response and analysis will be severely complicated by thermo-mechanical coupling effects if the motor configuration and vibration environment result in appreciable inertial loading of the propellant grain as a whole, or in localized areas within the grain (such as at the base of a slender star point). In addition to the usual frequency, ambient temperature and vibration time parameters, it is clear that the thermal and vibration environmental history of the motor must be considered in order to specify and define the motor requirements and vibration response characteristics. It would seem that the length of time which must be considered in predicting response will be of the same order as the thermal time constant in the critical region within the motor grain.

The experimental and theoretical results show the multiple-valued equilibrium response region to occur in a very narrow frequency range which is dependent on the vibration loading level, the natural frequency of the system at the reference temperature, the thermal boundary conditions, and the propellant visco-elastic properties. For a given vibration loading level, the most stringent loading conditions are applied to the propellant along the upper branch of the instability response region. This is where the amplitude ratio is a maximum and the phase angle is approximately 90 degrees, resulting in large strain amplitudes in the propellant as well as high equilibrium temperatures. At frequencies above this narrow region, the amplitude ratio decreases rapidly, resulting in lower strains even though the phase difference continues to increase. Below the instability region, propellant strain and temperature are both low. Both lap-shear propellant specimens used for the investigation of the jump-instability response failed on the upper branch of the 0.05-inch peak input displacement instability region at 660 rpm, as described previously. For the one-inch shear specimen gage length and roughly 90-degree phase shift at that point, the specimen was subjected to peak strains between 5 and 10 percent, consistent with vibration failure strain levels observed previously for constant strain amplitude loading conditions (Ref. 1).

4.3.3 Transient Thermoviscoelastic Response for Constant Cyclic Strain Amplitude and Inertial Loading

The preceding discussion of equilibrium cyclic inertial loading considered only the material response immediately after the initiation of vibration (isothermal response) and at thermal mechanical steady-state response (equilibrium response). Transient thermal and mechanical response of the inertially-loaded system is very difficult to calculate analytically, particularly in the region of instability where the mechanical response sweeps through the resonance region as the temperature changes.

To investigate the effect of various loading and thermal boundary conditions on this transient response, a series of experimental tests were performed on samples identical to those used for the previous equilibrium tests.

Two double-lap shear propellant specimens were prepared from PBAA propellant bars milled from the same bulk casting (P2916). One sample was prepared with wooden support members and completely insulated to approximate adiabatic conditions; the other was prepared with liquid-cooled metal side supports and a low-conductivity center support to approximate unidirectional heat flow. Each specimen was subjected to a series of four vibration runs -- two runs with constant strain amplitude loading at 2720 rpm and 2.47 percent peak strain, and then two runs with inertial loading at 1115 rpm and 0.0247-inch peak input displacement amplitude. The multiple runs were performed to monitor degradation effects due to the combined thermal-mechanical environment. Material properties were measured before and after each vibration run at a frequency of 80 rpm, room ambient temperature and 2.48 percent peak strain amplitude. The results of these single frequency check runs, plotted as a function of total vibration cycles, are presented in Figures 4-12 and 4-13 for the adiabatic and isothermal boundary conditions, respectively. Appreciable propellant degradation was obtained during the vibration sequence as evidenced by decreasing storage and loss moduli. The rate of degradation is seen to increase during the inertial loading sequence due to the larger transient strain amplitudes experienced by the samples.

Figures 4-14 and 4-15 present the transient mechanical and thermal response for vibrations runs 2 and 4, referred to in Figure 4-12, for the adiabatic boundary conditions. Similarly, Figures 4-16 and 4-17 present the same information for vibration runs 2 and 4 referred to in Figure 4-13 for the isothermal boundary conditions.

The storage modulus, loss modulus and loss tangent data presented here were calculated using an average phase angle, due to the nonlinearity of the Lissajous pattern ellipse discussed in the first quarterly report (Ref. 1, page 4-24, Figure 4-18). The tangent of the angle as calculated from the vertical (force) intercepts was averaged with the tangent calculated from the horizontal (displacement) intercepts. This average value appears to correspond most closely with the effective loss tangent as calculated from the measured area of the Lissajous or hysteresis pattern.

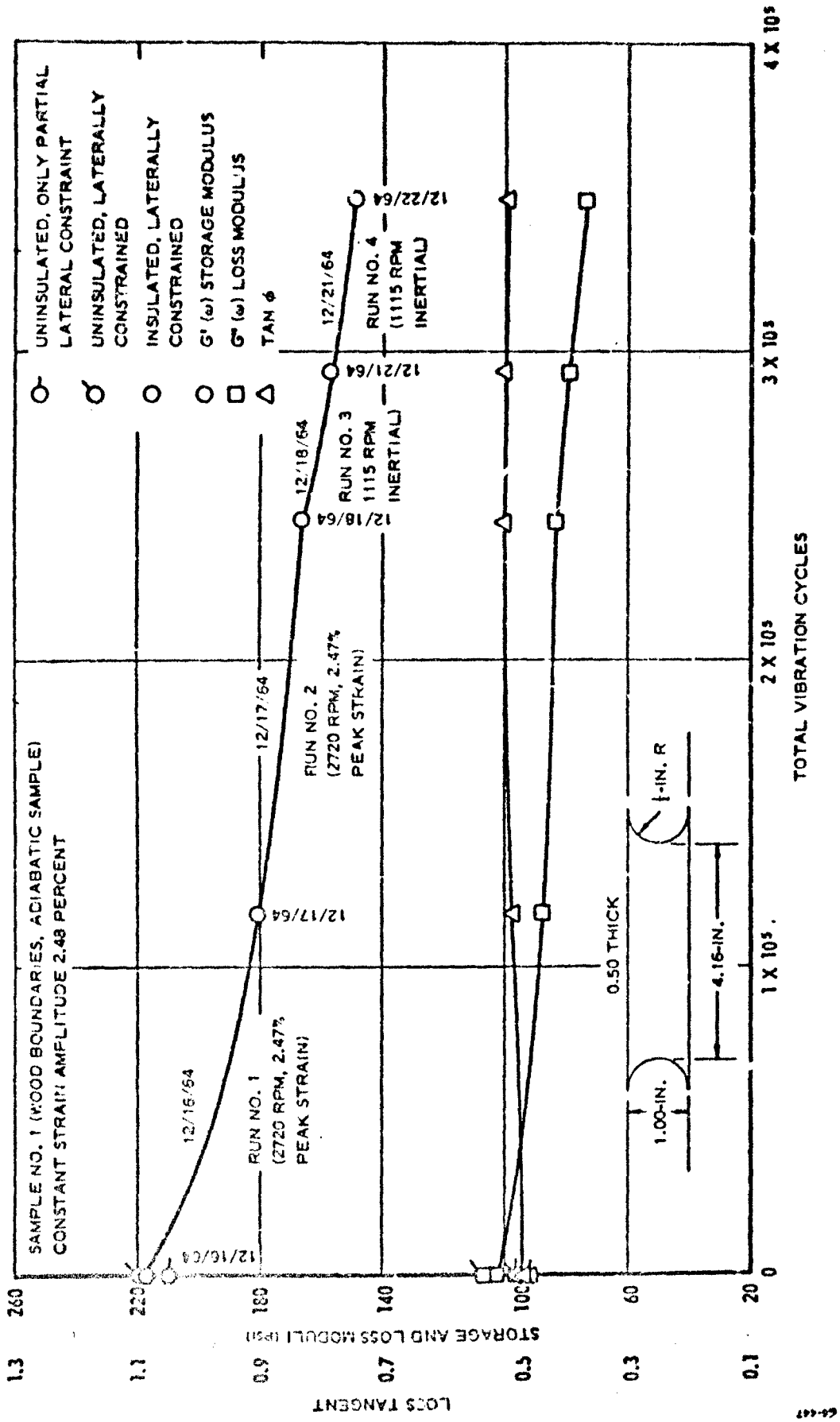

Figure 4-12 Propellant Properties versus Vibration History, Measured at 80 RPM and Room Ambient Temperature (Approximately 72°F)

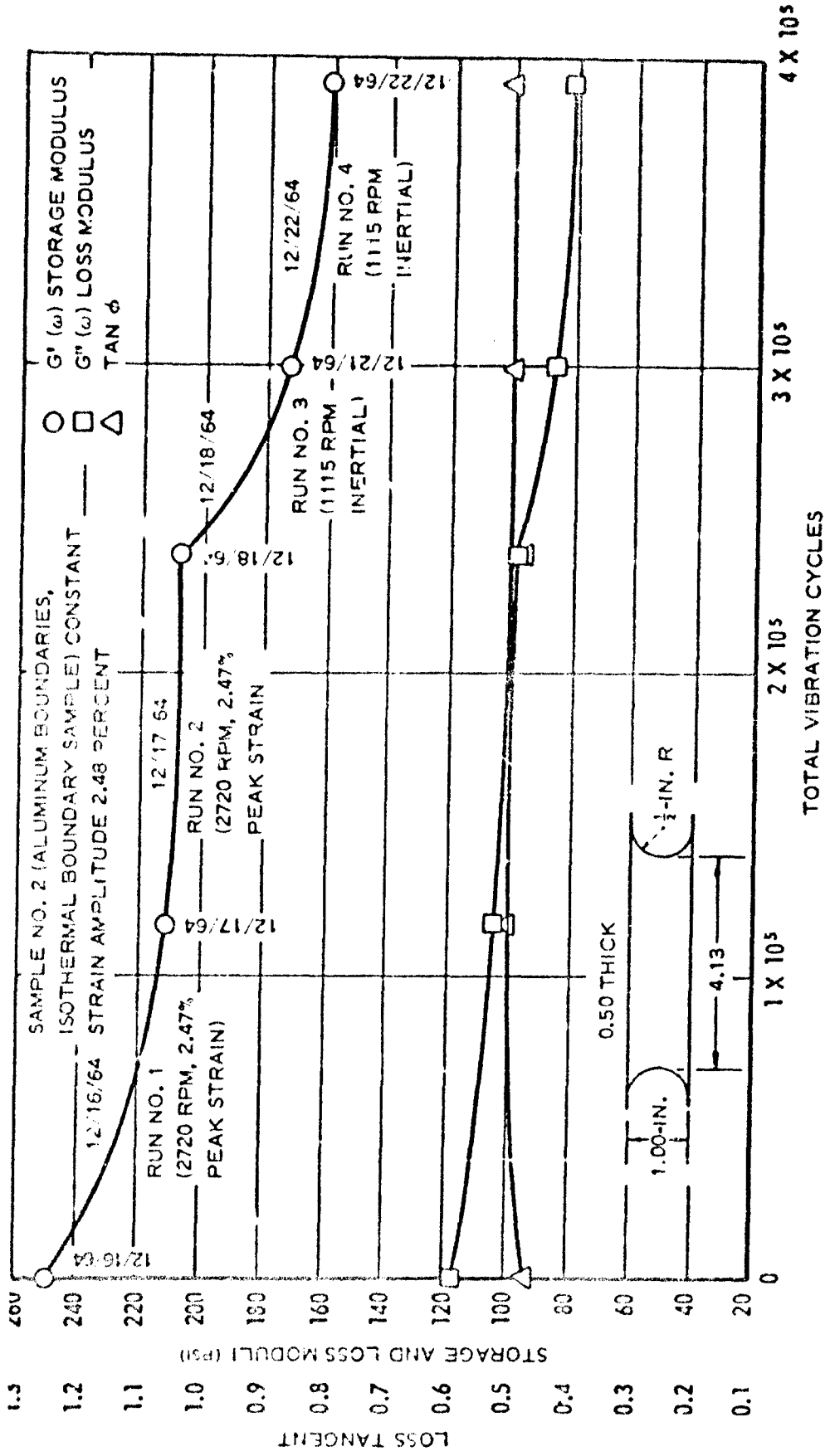

Figure 4-15 Propellant Properties versus Vibration History, Measured at 80 RPM and Room Ambient Temperature (Approximately 72°F)

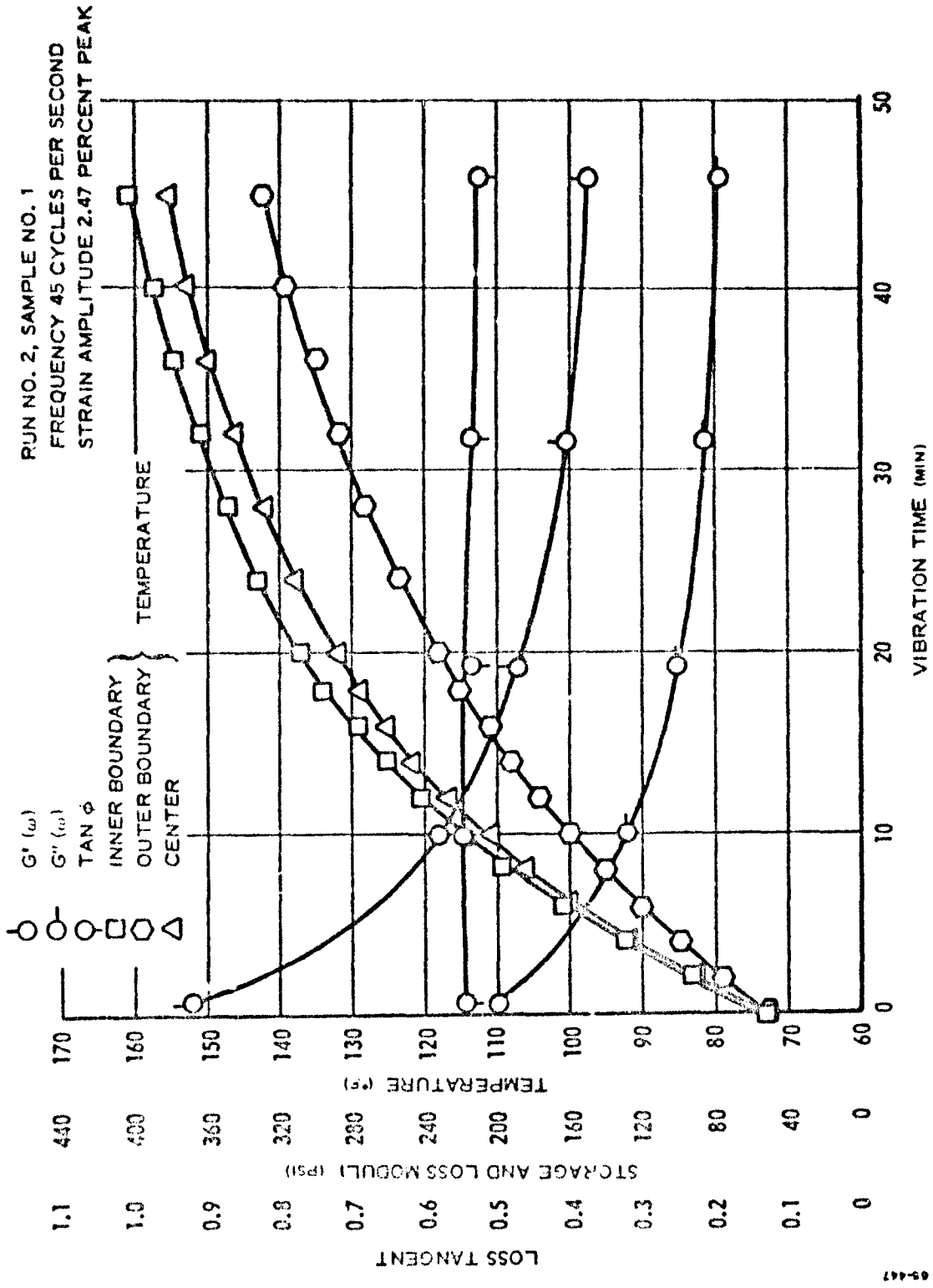

Figure 4-14 Thermomechanical Response, Constant Strain Amplitude Excitation, Adiabatic Boundary Conditions, PBAA Propellant

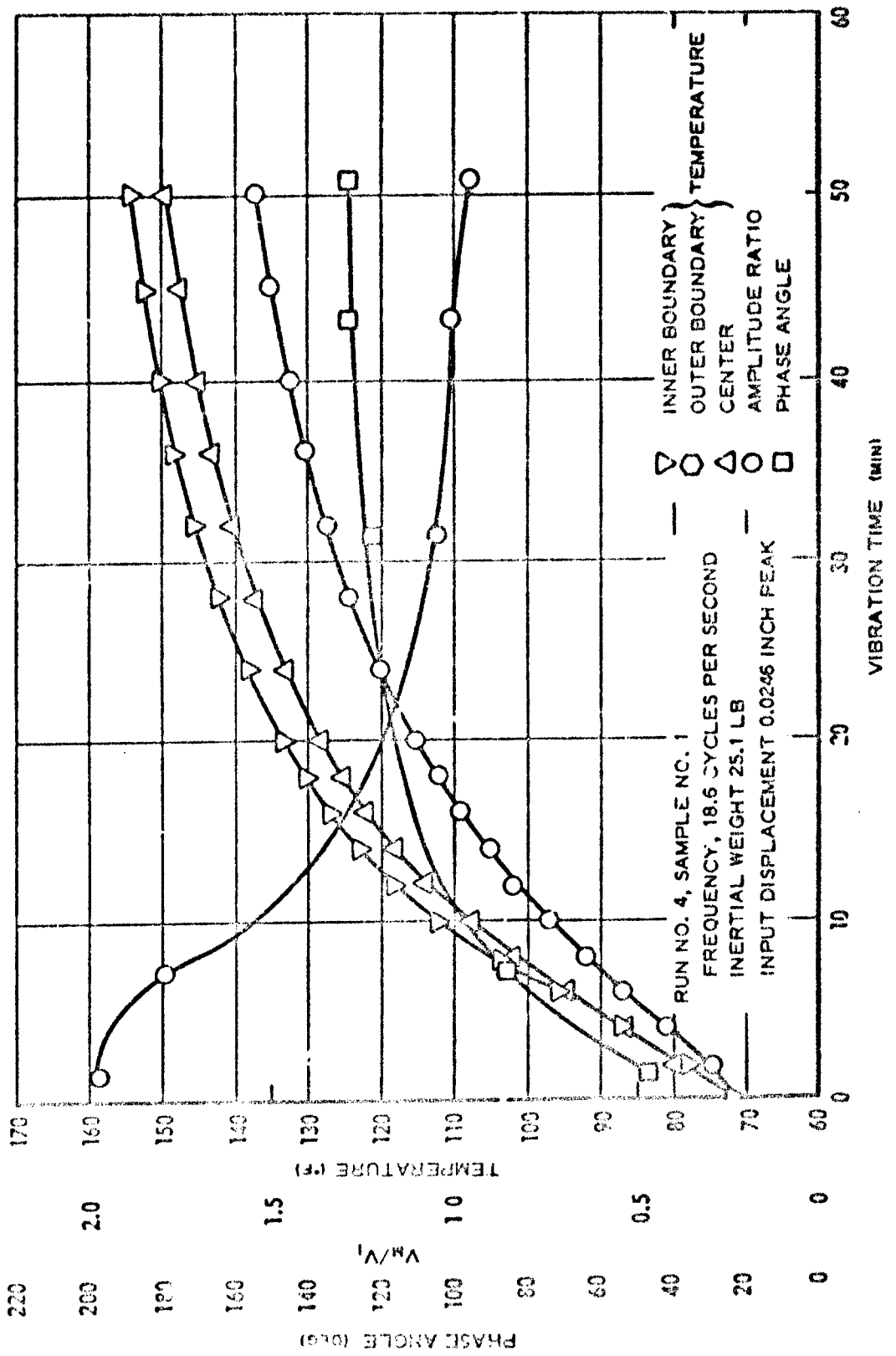

Figure 4-15 Thermomechanical Response, Inertial Loading, Adiabatic Boundary Conditions, PBAA Propellant

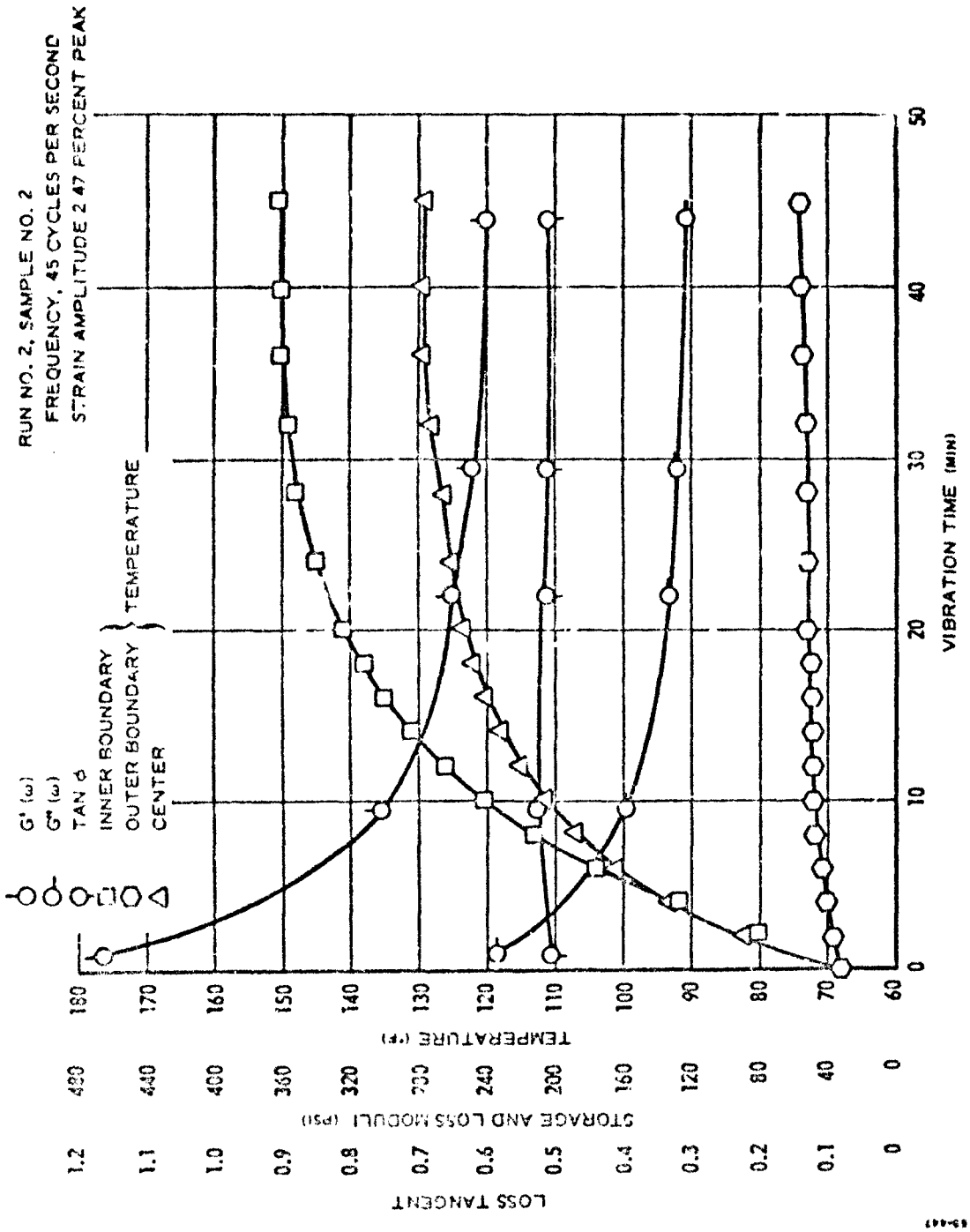

Figure 4-16 Thermomechanical Response, Constant Strain Amplitude Excitation, Isothermal Boundary Conditions, PBAA Propellant

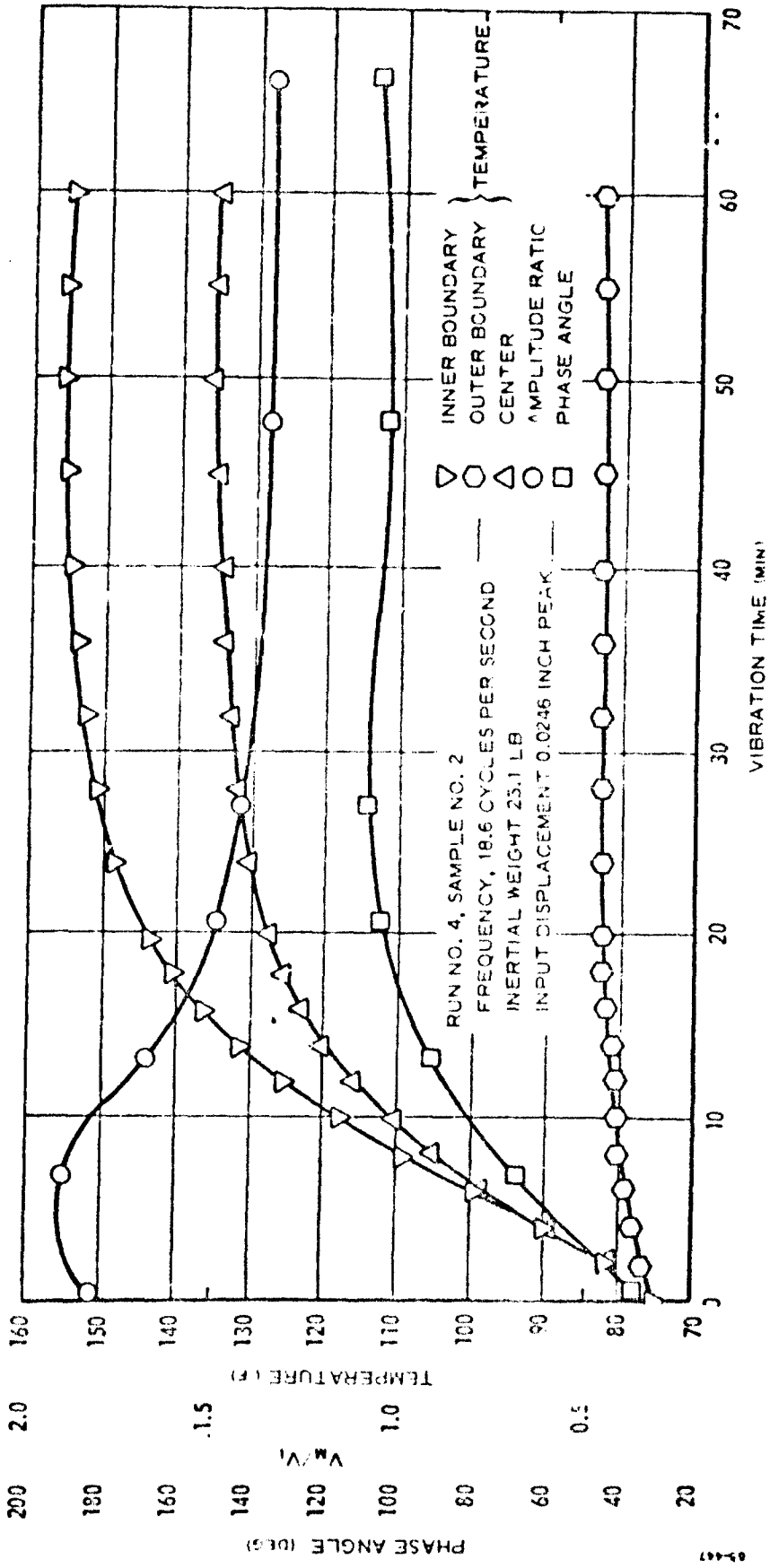

Figure 4-17 Thermomechanical Response, Inertial Loading, Isothermal Boundary Conditions, PBAA Propellant

Section 5

SUBCONTRACT EFFORT

5.1 PURDUE UNIVERSITY SUBCONTRACT (Quarterly Summary Report to Lockheed Propulsion Company, September 21 - December 15, 1964. Professor R. A Schapery - In Charge)

5.1.1 Nonlinear Viscoelastic Behavior of Highly Filled Propellants

The first phase of this program is concerned with the development of realistic stress-strain equations which include the effects of strain induced anistropy, but are sufficiently simple to permit easy application to idealized motor problems in the second phase of the research. Work during the first quarter dealt primarily with the evaluation of existing theories of nonlinear constitutive equations for use in solid propellant applications Nonlinear equations range from extremely general forms for viscoelastic behavior[1] to piecewise linear approximations for elastic response [2] In the former case, a considerable number of mathematically (rather than physically) motivated assumptions must be made to put the equations in a practically useful form. On the other hand, the latter equations of piecewise linear elasticity, with coefficients depending on the state of stress or strain, seem to be useful engineering approximations for elastic behavior, however, it is not at all clear how these equations can be generalized to viscoelasticity, except by trial and error, along with considerable experimentation.

In another paper,[3] the role of thermodynamics in nonlinear viscoelasticity was investigated, and it was shown that thermodynamic principles can be used to develop relatively general (but simple) stress-strain equations. Although Ref. 3 gives only a one-dimensional illustration, we have recently made the generalization to three dimensional behavior; the thermodynamic basis permitted a straightforward generalization. Briefly, this theory makes use of the first and second laws of thermodynamics and Onsager's principle. Also, it is assumed that the material behaves thermodynamically as a linear viscoelastic body, but with nonlinear measures of deformation in place of the classical linear strains The stress-strain equations so developed contain a natural generalization of the Boltzman superposition principle. Moreover, the equations appear to be consistent with existing propellant data, and, for example, yield a relaxation modulus which has the commonly observed form in which strain and time dependence appear as separate factors.

---

[1] See, for example, A. E. Green and R S. Rivlin, Archive for Rational Mechanics and Analysis, Vol. 1, pp 1-2', 1957.

[2] S. B. Dong, L. R Herrmann, K S Pister, R. L Taylor, Studies Relating to Structural Analysis of Solid Propellants, Institute of Engineering Research, University of California, Berkeley, 1962.

[3] R. A. Schapery, Journal of Applied Physics, Vol. 35, No. 5, pp 1451-1465, 1964.

Current efforts are directed at application of the equations to the mechanical property test geometries used by LPC in order to evaluate the relatively few unknown functions and to determine the limits of validity of the theory.

5.1.2 Thermomechanical Response Studies of Solid Propellants Subjected to Cyclic and Random Loading

A report on the first-quarter work has been prepared jointly with Dalton Cantey of LPC, and for presentation at the AIAA 6th Solid Propellant Rocket Conference to be held February 1-3, 1965. Briefly, it contains an extension of previous theoretical studies on heat generation to random loading, provides solutions to the thermal and mechanical response of specimens being tested by LPC, compares theory with experimental data (with reasonably good agreement found), and draws certain practical conclusions concerning the engineering usefulness of the two limit cases of adiabatic and steady-state thermal behavior.

Future theoretical investigations will study the thermomechanical behavior of a cantilever beam with and without inertial loading. Also, we shall attempt to improve the method used to predict heat generation by taking into account nonlinearities in the stress-strain law.

5.2 UNIVERSITY OF WASHINGTON

The following outlines the objectives of the work to be performed at the University of Washington under the direction of Professors R.J.H. Ballard and E.H. Dill.

(1) To obtain quantitative data, from direct observation in the photoviscoelastic bench, of the effect of local stress concentrations under dynamic loadings with small strains and constant strain rate tests.

(2) To investigate experimentally some of the facets of the nonlinear theory for viscoelastic materials which has been proposed by Coleman and Noll (Foundations of Linear Viscoelasticity, Rev. Mod. Phys., Vol. 33(1961), pp. 239-249) and investigated further by G. Lianis in previous LPC work. With consideration of incompressible fluids, it has been hypothesized that some of the material constants employed in the nonlinear constitutive relations (large strains) can be determined either from simple dynamic modulii tests at small strains or creeptests to large strains. If the same result can be shown to be true in the case of viscoelastic solids it would be of great importance to the definition of future testing programs for the characterization of solid propellant materials in the nonlinear range of deformation. Since the same line of reasoning which led to the hypothesis concerning the constitutive relation can be applied to the relation of the dielectric tensor to strain, this relation could be checked by simple photoviscoelastic observation. This experimental verification of the above stated hypothesis will be undertaken, employing the optical bench and materials now available.

Progress during the reporting period was as follows. The photoelastic bench has been modified to accept a double-lap shear specimen of viscoelastic birefringent plastic and to provide variable frequency sinusoidal strain inputs of varying amplitude. Qualitative observations of the effect of the stress concentrations are being made.

Theoretical studies of viscoelastic solids have been carried out and have raised the question as to whether or not the nonlinear constitutive laws can be obtained from either simple dynamic moduli tests at small strains or from creep tests to large strains. These theoretical studies are near completion and will be reported in the near future.

5.2 UNIVERSITY OF WASHINGTON

The following outlines the objectives of the work to be performed at the University of Washington under the direction of Professors R.J.H. Ballard and E.H. Dill.

(1) To obtain quantitative data, from direct observation in the photoviscoelastic bench, of the effect of local stress concentrations under dynamic loadings with small strains and constant strain rate tests.

(2) To investigate experimentally some of the facets of the nonlinear theory for viscoelastic materials which has been proposed by Coleman and Noll (Foundations of Linear Viscoelasticity, Rev. Mod. Phys., Vol. 33(1961), pp. 239-249) and investigated further by G. Lianis in previous LPC work. With consideration of incompressible fluids, it has been hypothesized that some of the material constants employed in the nonlinear constitutive relations (large strains) can be determined either from simple dynamic modulii tests at small strains or creep tests to large strains. If the same result can be shown to be true in the case of viscoelastic solids it would be of great importance to the definition of future testing programs for the characterization of solid propellant materials in the nonlinear range of deformation. Since the same line of reasoning which led to the hypothesis concerning the constitutive relation can be applied to the relation of the dielectric tensor to strain, this relation could be checked by simple photoviscoelastic observation. This experimental verification of the above stated hypothesis will be undertaken, employing the optical bench and materials now available.

Progress during the reporting period was as follows. The photoelastic bench has been modified to accept a double-lap shear specimen of viscoelastic birefringent plastic and to provide variable frequency sinusoidal strain inputs of varying amplitude. Qualitative observations of the effect of the stress concentrations are being made.

Theoretical studies of viscoelastic solids have been carried out and have raised the question as to whether or not the nonlinear constitutive laws can be obtained from either simple dynamic moduli tests at small strains or from creep tests to large strains. These theoretical studies are near completion and will be reported in the near future.

Section 6

FUTURE PROGRAM

Technical objectives of the third quarter program are listed below.

- Completion of the viscoelastic response and multiaxial failure investigation of the remaining group of high solids formulation variations (80 percent complete).
- Extension of multiaxial failure testing and investigation of propellant failure surfaces in stress space (30 percent complete).
- Determination of bulk moduli of propellant compositions as a function of applied hydrostatic pressure and temperature (in progress).
- Experimental investigation of nonlinearity effects in propellants under various types of test for development of realistic nonlinear stress-strain equations

Section 7

REFERENCES

1. Lockheed Propulsion Company, Solid Propellant Structural Integrity Investigations: Dynamic Response and Failure Mechanisms, Technical Documentary Report No. AFRPL-TR-64-148, Volume I, LPC Report No. 667-Q-1, 14 October 1964

2. Chemical Propulsion Information Agency, ICRPG Solid Propellant Mechanical Behavior Manual, CPIA Publication 21, September 1963

3. Williams, M. L., et al., Fundamental Studies Relating to Systems Analysis of Solid Propellants, GALCIT SM 61-5, California Institute of Technology, 1961

4. Ko, W. L., Application of Finite Elastic Theory to the Behavior of Rubber-Like Materials, PhD. thesis, California Institute of Technology, 1963

5. Sharma, M. G., personal communication.

6. Sharma, M. G., and Lin, C. K., Mechanical Properties of Solid Propellant for Combined States of Stress at Various Temperatures, Report No. ABL FLASHX-114, Pennsylvania State University, 1963

7. Jones, J. W., "Propellant Failure Criteria," Bulletin of the 3rd ICRPG Working Group on Mechanical Behavior, CPIA Pub. No. 61U, 1964

8. Majerus, J. N., "A Unified Approach to Failure and Its Application to Solid Propellant Materials," ibid, 1964

9. Lockheed Propulsion Company, Structural Integrity of Large Solid Propellant Grains, LPC Report No. 642-F, 1964

10. Herrmann, L. R., "Bilinear Elasticity with Application to Thickwalled Cylinders," Studies Relating to Structural Analysis of Solid Propellants, from the Institute of Engineering Research, University of California, Berkeley, 1962

11. Tschebotarioff, Gregory P., Soil Mechanics, Foundations and Earth Structures, McGraw-Hill, 1951

12. Nadai, A., Theory of Flow and Fracture of Solids, McGraw-Hill, 1950

13. Griffith, A. A., 1921, "The Phenomena of Rupture and Flow in Solids," Philo. Trans. Roy Soc. (London), Ser. A, Vol. 221. See also: "The Theory of Rupture," Proc. of The First International Congress for Applied Mechanics, 1924

14. Rivlin, R. S., Thomas, A. G., "Rupture of Rubber. I. Characteristic Energy for Tearing," Jour. of Polymer Sci., Vol. 10, No. 3, 1953

15. Greensmith, H. W., "Rupture of Rubber. VII. Effect of Rate of Extension in Tensile Tests," Jour. Appl. Polymer Sci., Vol. 3, No. 8, 1960

16. Greensmith, H. W., "Rupture of Rubber. VIII. Comparison of Tear and Tensile Rupture Measurements," Jour. Appl. Polymer Sci., Vol. 3, No. 8, 1960

17. Thomas, A. G., "Rupture of Rubber. II. The Strain Concentration at an Incision," Jour. of Polymer Sci., Vol. 18, 1955

18. Greensmith, H. W., Thomas, A. G., "Rupture of Rubber. III. Determination of Tear Properties," Jour Polymer Sci., Vol. 18, 1955

19. Williams, M. L., et al; Fundamental Studies Relating to Systems Analysis of Solid Propellants, GALCIT SM-61-5, California Institute of Technology, 1961

20. Williams, M. L., "Fracture of Viscoelastic Materials," Fracture of Solids, edited by Drucker and Gilman, Interscience, 1962

21. Lockheed Propulsion Company, Solid Propellant Structural Integrity Investigations: Dynamic Response and Failure Mechanisms, RPL-TDR-64-32, LPC Report No. 618-F, 17 April 1964

22. Jones, J. W., "Propellant Failure Mechanisms," Bulletin of the 3rd Meeting, ICRPG Working Group on Mechanical Behavior, November 1964

DISTRIBUTION LIST

	Copies
U.S. Department of the Interior Bureau of Mines 4800 Forbes Avenue Pittsburgh 13, Penn. 15213 Attn: M.M Dolinar, Reports Librarian Explosives Research Lab. CP-3	1
Central Intelligence Agency 2430 E. Street, N.W. Washington, D.C. 20505 Attn: OCD, Standard Dist. CP-6	1
Office of the Director of Defense Research and Engineering Washington, D.C. 20301 Attn: W.E. Sheehan Office of Assistant Director Chemical Technology CP-7	1
National Aeronautics & Space Admin. Lewis Research Center 21000 Brookpark Road Cleveland 35, Ohio 44135 Attn: Library CP-8	1
John F. Kennedy Space Center, NASA Cocoa Beach, Florida 32931 Attn: Library CP-9	1
National Aeronautics & Space Admin. Manned Spacecraft Center P.O. Box 1537 Houston 1, Texas 77001 Attn: Library CP-10	1
National Aeronautics & Space Admin. George C. Marshall Space Flight Center Huntsville, Alabama 35800 Attn: Library CP-11	1
National Aeronautics & Space Admin. Langley Research Center Langley Air Force Base Virginia 23365 Attn: Library CP-12	3
National Aeronautics & Space Admin. Washington, D.C. 20546 Attn: Office of Technical Info & Educational Programs, Code ETL CP-13	1
Scientific and Tech. Info. Facility P.O. Box 5700 CP-14 Bethesda, Maryland 20014 Attn: NASA Representative	2
National Aeronautics & Space Admin. Washington, D.C. 20546 CP-209 Attn: R.W. Ziem RPS	1
National Aeronautics & Space Admin. Goddard Space Flight Center Greenbelt, Maryland 20771 CP-210 Attn: Library	1
Arnold Eng. Development Center Air Force Systems Command Tullahoma, Tennessee 37389 Attn: ABOIM CP-59	1
Defense Documentation Center Cameron Station Alexandria, Virginia 22314 CP-61	20
Air Force Rocket Propulsion Lab. RPR Edwards, California 93523 CP-64	1
Air Force Rocket Propulsion Lab. RPM Edwards, California 93523 CP-65	1
Air Force Flight Test Center FTAT-2 Edwards Air Force Base, California 93523 CP-66	1
Office of Research Analysis Holloman Air Force Base New Mexico 88330 Attn: RRRT DAR CP-69	1
Bolling Air Force Base RTD RTNP CP-58 Washington, D.C. 20332	1
Wright-Patterson AFB Ohio 45433 Attn: AFML MAAE CP-78	1
Commanding Officer Ballistic Research Laboratories Aberdeen Proving Ground Maryland 21005 Attn: AMXBR-1 CP-15	2
U.S. Army Missile Command Redstone Scientific Information Center Redstone Arsenal, Alabama 35808 Attn: Chief, Document Section CP-29	4
Commanding Officer Army Research Office Durham Box CM, Duke Station Durham, North Carolina 27706 CP-21	1
Commanding Officer Frankford Arsenal Philadelphia 37, Penn. 19137 Attn: Propellant and Explosives Section, 1331 CP-23	1
Commanding Officer Picatinny Arsenal Dover, New Jersey 07801 Attn: Library CP-25	2

Commanding Officer 2
Picatinny Arsenal
Liquid Rocket Propulsion Laboratory
Dover, New Jersey 07801
Attn: Technical Library CP-26

Commanding General 1
White Sands Missile Range
New Mexico 88002
Attn: Technical Library CP-30

Bureau of Naval Weapons 2
Department of the Navy
Washington, D.C. 20360
Attn: DLI-3 CP-34

Bureau of Naval Weapons 2
Department of the Navy
Washington, D.C. 20360
Attn: RMMP-2 CP-35

Bureau of Naval Weapons 1
Department of the Navy
Washington, D.C. 20360
Attn: RMMP-3 CP-36

Bureau of Naval Weapons 1
Department of the Navy
Washington, D.C. 20360
Attn: RMMP-4 CP-37

Bureau of Naval Weapons 1
Department of the Navy
Washington, D.C. 20360
Attn: RRRE-6 CP-38

Commander 2
U.S. Naval Missile Center
Point Mugu, California 93041
Attn: Technical Library CP-40

Commander 2
U.S. Naval Ordnance Laboratory
White Oak
Silver Spring, Maryland 20910
Attn: Library CP-42

Commander 5
U.S. Naval Ordnance Test Station
China Lake, California 93557
Attn: Code 45 CP-43

Commander 1
U.S. Naval Ordnance Test Station
China Lake, California 93557
Attn: Technical Library
Branch CP-44

Superintendent 1
U.S. Naval Postgraduate School
Naval Academy
Monterey, Calif. 93900 CP-45

Commanding Officer 2
U.S. Naval Propellant Plant
Indian Head, Maryland 20640
Attn: Technical Library CP-46

Commanding Officer 1
Office of Naval Research
1030 E. Green Street
Pasadena 1, Calif. 91101 CP-51

Director Code 6180 1
U.S. Naval Research Laboratory
Washington, D.C. 20390
Attn: H.W. Carhart CP-53

Director 1
Special Projects Office
Department of the Navy
Washington, D.C. 20360 CP-55

Commanding Officer 1
U.S. Naval Underwater Ordrance Sta.
Newport, Rhode Island 02844
Attn: W.W. Bartlett CP-56

Aerojet-General Corporation 1
P.O. Box 296
Azusa, California 91703
Attn: F.M. West,
Chief Librarian CP-83

Aerojet-General Corporation 1
11711 South Woodruff Avenue
Downey, California 90241
Attn: Florence Walsh,
Librarian CP-84

Aerojet-General Corporation 3
P.O. Box 1947
Sacramento, California 95809
Attn: Technical Information
Office CP-85

Aerospace Corporation 2
P.O. Box 95085
Los Angeles 45, California 90045
Attn: Library - Documents CP-88

Allied Chemical Corporation 1
General Chemical Division
Research Laboratory
P.O. Box 405
Morristown, New Jersey 07960
Attn: L.J. Wiltrakis,
Security Officer CP-91

Amcel Propulsion Company 1
Box 3049, Asheville,
North Carolina 28802 CP-92

American Cyanamid Company 1
1937 W. Main Street
Stamford, Connecticut 06902
Attn: Security Officer CP-93

IIT Research Institute 1
Technology Center
Chicago, Illinois 60616
Attn: C.K. Hersh,
Chemistry Division CP-98

ARO, Inc 1
Arnold Engineering Develop Center
Arnold AF Station, Tenn. 37389
Attn: Dr. B.H. Goethert
Director of Engineering CP-99

Atlantic Research Corporation 2
Shirley Highway and Edsall Road
Alexandria, Virginia 22314
Attn: Security Officer for
Library CP-101

	Copies	
Atlantic Research Corporation Western Division 48-506 Easy Street El Monte, California 91731 Attn: H. Niederman	1	CP-102
Battelle Memorial Institute 505 King Avenue Columbus, Ohio 43201 Attn: Report Library, Room 6A	1	CP-103
The Boeing Company Aero Space Division P.O. Box 3707 Seattle 24, Washington 98124 Attn: R.R. Barber, Lib. UT. CH.	1	CP-108
Chemical Propulsion Information Agency Applied Physics Laboratory 8621 Georgia Avenue 20910 Silver Spring, Maryland	3	CP-114
Douglas Aircraft Co., Inc. Santa Monica Division 3000 Ocean Park Boulevard Santa Monica, Calif. 90405 Attn: Mr. J.L. Waisman	1	CP-122
The Dow Chemical Company Security Section Box 31 Midland, Michigan 48641 Attn: Dr. R.S. Karpiuk 1710 Bldg.	1	CP-123
E.I. DuPont Denemours and Company Eastern Laboratory Gibbstown, New Jersey 08027 Attn: Mrs. Alice R. Steward	1	CP-125
Esso Research and Engineering Co. Special Projects Unit P.O. Box 8 Linden, New Jersey 07036 Attn: Mr. D.L. Baeder	1	CP-126
General Electric Company Flight Propulsion Division Evendale Cincinnati, Ohio 45215	1	CP-134
Hercules Powder Company Allegany Ballistics Laboratory P.O. Box 210 Cumberland, Maryland 21501 Attn: Library	1	CP-138
Hercules Powder Company Kenvil, New Jersey 07847 Attn: Library	1	CP-139
Hercules Powder Company Research Center Wilmington, Delaware 19899 Attn: Dr. Herman Skolnik, Manager Technical Information Div.	1	CP-142
Institute For Defense Analysis Research & Engineering Support Division Attn: Technical Information Office 1825 Connecticut Avenue Washington, D.C. 20009	1	CP-146
Jet Propulsion Laboratory 4800 Oak Grove Drive Pasadena, California 91103 Attn: Library TDS Mr. N.E. Devereux	1	CP-147
Martin Company Baltimore 3, Maryland 21203 Attn: Science-Technology Library - Mail 398	1	CP-156
Martin Company Advanced Technology Library P.O. Box 1176 Denver, Colorado 80201	1	CP-157
Martin Company Orlando, Florida 32800 Attn: Library	1	CP-158
Minnesota Mining & Manufacturing Co. 900 Bush Avenue St. Paul, Minnesota 55106 Attn: Code 0013 R & D Via H.C. Zeman Security Administrator	2	CP-159
Monsanto Research Corporation Boston Labs., Everett Station Chemical Lane Boston, Mass. 02149 Attn: Library	1	CP-161
New York University Research Building No. 3 233 Fordham Landing Road University Heights, N.Y. 10468 Attn: Document Control - CJM	1	CP-164
North American Aviation, Inc. Space & Information Systems Div. 12214 Lakewood Boulevard Downey, California 90242 Attn: W.H. Morita	1	CP-166
Rocketdyne 6633 Canoga Avenue Canoga Park, California 91304 Attn: Library Dept. 596-306	3	CP-180

DISTRIBUTION LIST (cont'd)

	Copies
Rohm & Haas Company Redstone Arsenal Research Division Huntsville, Alabama 35808 Attn: Librarian CP-182	1
Texaco Experiment Incorporated P.O. Box 1-T Richmond 2, Virginia 23202 Attn: Librarian CP-187	1
Thiokol Chemical Corporation Elkton Division Elkton, Maryland 21921 Attn: Librarian CP-192	1
Thiokol Chemical Corporation Reaction Motors Division Denville New Jersey 07834 Attn: Librarian CP-193	1
Thiokol Chemical Corporation Rocket Operations Center P.O. Box 1640 Ogden, Utah 84401 Attn: Librarian CP-194	1
Thiokol Chemical Corporation Wasatch Division P.O. Box 524 Brigham City, Utah 84302 Attn: Library Section CP-195	2
Thompson Ramo Wooldridge 23555 Euclid Avenue Cleveland 17, Ohio 44117 Attn: Librarian CP-196	2
British Defence Staff British Embassy 3100 Massachusetts Ave. Washington, D.C. Attn: Scientific Information Officer	4*
Defence Research Member Canadian Joint Staff (W) 2150 Massachusetts Ave. Washington, D.C.	4*

* Transmitted via:
Headquarters
Air Force Systems Command
Andrews AFB
Washington, D.C.
Attn: SCS-41(3-1833)

	Copies
Space Technology Laboratory, Inc. 1 Space Park Redondo Beach, California 90200 Attn: STL Tech. Library Document Acquisitions CP-185	2
United Aircraft Corporation Corporation Library 400 Main Street East Hartford, Connecticut 06118 Attn: Dr. David Rix CP-201	1
United Aircraft Corporation Pratt & Whitney Fla. Res. & Dev. Ct. P.O. Box 2691 W. Palm Beach, Florida 33402 Attn: Library CP-202	1
United Technology Center P.O. Box 358 Sunnyvale, California 94088 Attn: Librarian CP-204	1
Commanding Officer U. S. Naval Air Development Center Johnsville, Penn. 18974 CP-31	1
General Electric Company Apollo Support Department P.O. Box 2500 Daytona Beach, Florida 32015 Attn: C. Day CP-211	1
Defense Metals Information Center Battelle Memorial Institute 505 King Avenue Columbus, Ohio 43201 CP-120	1
Arthur D. Little, Inc. 15 Acorn Park Cambridge, Mass. 02140 Attn: V. H. Varley CP-150	1
Air Force Office of Scientific Research Washington, D.C. 20333 Attn: SREP, Dr. J. F. Masi CP-71	1

DISTRIBUTION LIST (cont'd)

	Copies
Commanding Officer Ammunition Procurement & Supply Agency Joliet, Illinois Attn, Engr. Library	1
American Machine & Foundry Co. Mechanics Research Department 7501 North Natchez Avenue Niles, Illinois Attn: Phil Rosenberg	1
Hercules Powder Company Bacchus Works Magna, Utah Attn: Librarian	1
Callery Chemical Company Research and Development Callery, Pennsylvania Attn: Document Control	1
Thiokol Chemical Corporation CP-190 Space Booster Division Brunswick, Georgia 31520 Attn: Librarian	1
Walter Kidde Company 675 Main Street Belleville, New Jersey Attn: Security Librarian	1
Olin Mathieson Chemical Corp. Box 508 Marion, Illinois Attn: Research Library	1
Olin Mathieson Chemical Corp. Research Library 1-K-3 275 Winchester Avenue New Haven, Connecticut Attn: Mail Control Room Miss Laura M. Kajuti	1
Pennsalt Chemicals Corp. Technological Center 900 First Avenue King of Prussia, Pennsylvania	1
Rocketdyne, A Division of North American Aviation, Inc. Solid Propulsion Operations P.O. Box 548 McGregor, Texas Attn: Library	1
Thiokol Chemical Corp. P. O. Box 27 Bristol, Pennsylvania Attn: R. Morris	1
Los Alamos Scientific Laboratory University of California P. O. Box 1663 Los Alamos, New Mexico	1
AFRPL RPCS Edwards, California	1
Purdue University Lafayette, Indiana Attn: M. J. Zucrow	1
Clevite Corporation CP-117 Mechanical Research Division 540 East 105th Street Cleveland, Ohio 44108 Attn: N. C. Beesell	1

Air Force Rocket Propulsion Laboratory, Edwards, Calif. Report No. AFRPL-TR-65-20, "SOLID PROPELLANT STRUCTURAL INTEGRITY INVESTIGATIONS: DYNAMIC RESPONSE AND FAILURE MECHANISMS," Quarterly Progress Report No. 2. 15 January 1965. Period Covered: 15 September through 15 December 1964. 84 pages, including 32 illustrations, 4 tables and 22 references.

Unclassified Report

The results of an investigation of viscoelastic and failure properties of highly filled PBAA and PBAN propellants as a function of solids loading are recorded. Studies of failure surface, and the relation between crack propagation velocity and propellant physical characteristics are discussed. Propellant dynamic shear and bulk properties were investigated with small deformation piezoelectric devices. An experimental investigation of propellant thermomechanical response to sustained cyclic inertial loading was completed, and the results compare favorably with theory. Transient thermoviscoelastic response of propellant under constant cyclic strain amplitude and inertial loading are also discussed.

Unclassified Abstract

1. Solid Rocket Propellants
2. Mechanical Properties

I. AF Program Structure No. 750G Project No. 3059

II. Contract No. AF 04(611)-9953

III. Prepared by Lockheed Propulsion Company, Redlands, California

IV. LPC Report No. 667-Q-2

V. In DDC Collection

Air Force Rocket Propulsion Laboratory, Edwards, Calif. Report No. AFRPL-TR-65-20, "SOLID PROPELLANT STRUCTURAL INTEGRITY INVESTIGATIONS: DYNAMIC RESPONSE AND FAILURE MECHANISMS," Quarterly Progress Report No. 2. 15 January 1965. Period Covered: 15 September through 15 December 1964. 84 pages, including 32 illustrations, 4 tables and 22 references.

Unclassified Report

The results of an investigation of viscoelastic and failure properties of highly filled PBAA and PBAN propellants as a function of solids loading are recorded. Studies of failure surface, and the relation between crack propagation velocity and propellant physical characteristics are discussed. Propellant dynamic shear and bulk properties were investigated with small deformation piezoelectric devices. An experimental investigation of propellant thermomechanical response to sustained cyclic inertial loading was completed, and the results compare favorably with theory. Transient thermoviscoelastic response of propellant under constant cyclic strain amplitude and inertial loading are also discussed.

Unclassified Abstract

1. Solid Rocket Propellants
2. Mechanical Properties

I. AF Program Structure No. 750G Project No. 3059

II. Contract No. AF 04(611)-9953

III. Prepared by Lockheed Propulsion Company, Redlands, California

IV. LPC Report No. 667-Q-2

V. In DDC Collection

Air Force Rocket Propulsion Laboratory, Edwards, Calif. Report No. AFRPL-TR-65-20, "SOLID PROPELLANT STRUCTURAL INTEGRITY INVESTIGATIONS: DYNAMIC RESPONSE AND FAILURE MECHANISMS," Quarterly Progress Report No. 2. 15 January 1965. Period Covered: 15 September through 15 December 1964. 84 pages, including 32 illustrations, 4 tables and 22 references.

Unclassified Report

The results of an investigation of viscoelastic and failure properties of highly filled PBAA and PBAN propellants as a function of solids loading are recorded. Studies of failure surface, and the relation between crack propagation velocity and propellant physical characteristics are discussed. Propellant dynamic shear and bulk properties were investigated with small deformation piezoelectric devices. An experimental investigation of propellant thermomechanical response to sustained cyclic inertial loading was completed, and the results compare favorably with theory. Transient thermoviscoelastic response of propellant under constant cyclic strain amplitude and inertial loading are also discussed.

Unclassified Abstract

1. Solid Rocket Propellants
2. Mechanical Properties

I. AF Program Structure No. 750G Project No. 3059

II. Contract No. AF 04(611)-9953

III. Prepared by Lockheed Propulsion Company, Redlands, California

IV. LPC Report No. 667-Q-2

V. In DDC Collection

Air Force Rocket Propulsion Laboratory, Edwards, Calif. Report No. AFRPL-TR-65-20, "SOLID PROPELLANT STRUCTURAL INTEGRITY INVESTIGATIONS: DYNAMIC RESPONSE AND FAILURE MECHANISMS," Quarterly Progress Report No. 2. 15 January 1965. Period Covered: 15 September through 15 December 1964. 84 pages, including 32 illustrations, 4 tables and 22 references.

Unclassified Report

The results of an investigation of viscoelastic and failure properties of highly filled PBAA and PBAN propellants as a function of solids loading are recorded. Studies of failure surface, and the relation between crack propagation velocity and propellant physical characteristics are discussed. Propellant dynamic shear and bulk properties were investigated with small deformation piezoelectric devices. An experimental investigation of propellant thermomechanical response to sustained cyclic inertial loading was completed, and the results compare favorably with theory. Transient thermoviscoelastic response of propellant under constant cyclic strain amplitude and inertial loading are also discussed.

Unclassified Abstract

1. Solid Rocket Propellants
2. Mechanical Properties

I. AF Program Structure No. 750G Project No. 3059

II. Contract No. AF 04(611)-9953

III. Prepared by Lockheed Propulsion Company, Redlands, California

IV. LPC Report No. 667-Q-2

V. In DDC Collection

Best Available Copy